Published for SISSA by Springer

Received: *May 7, 2026*
Revised: *August 26, 2026*
Accepted: *August 27, 2026*
Published: *October 5, 2026*

Differential measurements of $\gamma\gamma \to \tau\tau$ and constraints on τ-lepton electromagnetic moments in Pb+Pb collisions at $\sqrt{s_{\mathrm{NN}}} = 5.02$ TeV with ATLAS



The ATLAS collaboration

Full author list at the end of the paper

E-mail: atlas.publications@cern.ch

Abstract: This paper presents the first differential fiducial measurements of $\gamma\gamma \to \tau\tau$ using 1.93 nb^{-1} of Pb+Pb data at $\sqrt{s_{\mathrm{NN}}} = 5.02$ TeV recorded by the ATLAS detector. Events in which one of the τ-leptons decays into a muon and two neutrinos $\tau \to \nu_\tau \bar{\nu}_\mu \mu$ are selected and are categorized into three regions by the presence of an electron or either one or three charged-particle track(s) from the second τ-lepton decay. The measurement is performed in events where both Pb ions remain intact and no neutrons are emitted. Differential cross-sections are measured for seven variables in three fiducial regions at particle level. The measurements are compared to theory predictions with different photon flux models and spin correlation effects. For the fiducial region with one muon and one electron in the final state, comparisons to next-to-leading-order electroweak predictions are also made. The transverse momentum (p_{T}) of the decay muon, the p_{T} of the visible decay particles of the other τ-lepton, the total p_{T}, invariant mass, and pseudorapidity of the visible particles from the di-τ system, and the rapidity and acoplanarity of the visible decay particles from either τ-lepton are measured. A maximum-likelihood fit to the muon transverse-momentum distributions in the three regions before unfolding is performed to extract the τ-lepton anomalous magnetic moment a_τ and electric dipole moment d_τ, the latter for the first time in heavy ion collisions. The observed 95% confidence level intervals are $-0.057 < a_\tau < 0.035$ and $|d_\tau| < 2.7 \times 10^{-16}$ $e$cm.

Keywords: Heavy Ion Experiments

ArXiv ePrint: 2605.04584

Open Access, Copyright CERN,
for the benefit of the ATLAS Collaboration.
Article funded by SCOAP^3.

https://doi.org/10.1007/JHEP10(2026)053

JHEP10(2026)053

Contents

1 Introduction 1

2 ATLAS detector 3

3 Data and Monte Carlo samples 4

4 Object definition 6

5 Event selection 7

6 Background estimate 10

7 Data unfolding 15

8 Systematic uncertainties 18

9 Differential fiducial cross-sections 19

10 Determination of the τ-lepton's electromagnetic moments 21

11 Conclusion 28

A Event-level reweighting for non-zero a_τ and d_τ predictions 30

The ATLAS collaboration 39

JHEP10(2026)053

1 Introduction

Photon-induced processes occur in ultra-relativistic heavy-ion collisions at the LHC, in which the ion beams can be described as being accompanied by a large equivalent photon flux [1–3]. For photons that are emitted coherently by an entire nucleus, the flux at matrix-element level is enhanced by a factor of Z compared with the emission from a proton, resulting in a cross-section enhancement by Z^2 for single-photon processes, and Z^4 for di-photon processes, where Z is the atomic number and $Z = 82$ for lead. Depending on the closest distance of approach between the two nuclear centers-of-mass, defined as the impact parameter, photon-induced processes can become the dominant interaction mechanism. This is realized for impact parameters above twice the nuclear radius where hadronic interactions are suppressed. These events, referred to as ultra-peripheral collisions (UPC), can be used to study photon-photon and photonuclear interactions [4]. They typically have features such as regions of pseudorapidity devoid of produced particles (typically referred-to as "rapidity gaps"), the absence of neutrons in one or both beam directions, and low particle multiplicity or exclusive final states. These make them qualitatively different from typical high multiplicity inelastic nuclear collisions, where hadronic interactions occur [5, 6].

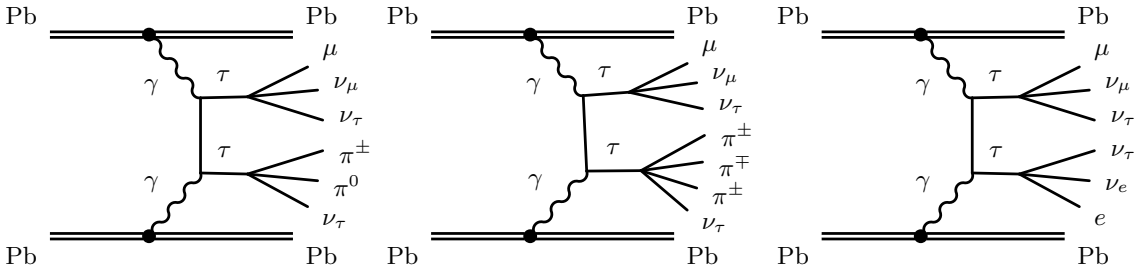


Figure 1. Schematic diagrams of $\gamma\gamma \to \tau\tau$ production in UPC Pb+Pb collisions, with the τ-leptons decaying into (left) one muon, one charged pion $\pi^{\pm}$, one neutral pion π^0 and neutrinos, (middle) one muon, three charged pions $\pi^{\pm}$ and neutrinos and (right) one muon, one electron and neutrinos.

Photon-induced processes can give rise to the production of oppositely-charged τ-lepton pairs, denoted by $\gamma\gamma \to \tau\tau$ [7, 8]. In the Standard Model (SM) of particle physics, this process can be calculated using purely quantum electrodynamics (QED) at leading-order, and enables the measurement of electromagnetic properties of τ-leptons. Leading-order diagrams for $\gamma\gamma \to \tau\tau$ production and decay in lead-lead (Pb+Pb) collisions, as considered in this analysis, are shown in figure 1. The presence of $\gamma\tau\tau$ vertices in these diagrams provides sensitivity to the electromagnetic moments of the τ-lepton, corresponding to the τ anomalous magnetic moment $a_\tau = \frac{1}{2}(g_\tau - 2)$, where g_τ is the τ-lepton g-factor, and electric dipole moment d_τ. In the SM, small non-zero values are predicted for a_τ and d_τ due to higher order corrections to the calculations, resulting in a predicted value of $a_\tau = 0.001\,177\,21\ (5)$ [9] and a limit on $|d_\tau| \lesssim 10^{-37} e\text{cm}$ [10]. Measuring these moments with improved precision fundamentally tests the SM and can be sensitive to physics beyond the Standard Model (BSM). Some BSM models relate coupling strengths to the mass of the respective lepton, suggesting that their impact could be largest for the τ-lepton, compared to muons and electrons. A value of d_τ larger than predicted by the SM could indicate a new source of symmetry violation under charge-parity (CP) conjugation, in this case in the leptonic sector, which is of great interest for explaining the matter-antimatter-asymmetry in the universe [11]. Models involving unparticles [12] or leptoquarks [13] could produce enhancements to a_τ or d_τ, or both.

At the LHC, the $\gamma\gamma \to \tau\tau$ process was first observed in Pb+Pb collisions by the ATLAS [14] and CMS [15] Collaborations and in proton-proton (pp) collisions by the CMS Collaboration [16]. The integrated $\gamma\gamma \to \tau\tau$ fiducial cross-section was measured by the CMS Collaboration in Pb+Pb collisions [15] and pp collisions [16], and by the DELPHI [17] and L3 [18, 19] Collaborations in electron-positron (e^+e^-) collisions at the Large Electron Positron (LEP) collider. Both ATLAS and CMS set constraints on a_τ using Pb+Pb collisions [14, 15] and the CMS Collaboration set constraints on a_τ and d_τ using pp collisions [16]. Most recently, ATLAS tested BSM contributions to the photon-τ-lepton interaction, using an effective field theory (EFT) approach in Drell-Yan (DY) production, $pp \to \gamma^*/Z \to \tau\tau$ [20]. However, this does not directly probe the SM a_τ component, and the SM d_τ component is far beyond current measurement sensitivities. At LEP, the DELPHI [17], OPAL [21] and L3 [19, 22] Collaborations set constraints on a_τ and d_τ. For d_τ, constraints have also been set by the Belle [23] and ARGUS Collaborations [24].

JHEP10(2026)053

Various strategies to measure $\gamma\gamma \to \tau\tau$ production using the high photon fluxes generated at the LHC have been proposed for Pb+Pb collisions [25–33], and pp collisions [34, 35]. In general, the structure and energy of the emitting particles, as well as the impact parameter between them influence the kinematics of the interaction. Measurements of $\gamma\gamma \to \tau\tau$ production in LHC Pb+Pb collisions cover a complementary phase space to LHC pp collisions. The Pb+Pb measurements provide sensitivity in the low di-τ mass region, below ∼50 GeV, due to the coherent photon-flux enhancement and lower trigger thresholds, resulting in a larger cross-section, and enabling greater precision on the cross-section measurement in that region. For the extraction of the electromagnetic moments, the phase space of $\gamma\gamma \to \tau\tau$ production is typically restricted to ensure photon virtualities $q^2 \sim 0$ GeV^2, since the electromagnetic moments are formally defined in the limit $q^2 \to 0$ GeV^2. Alternative approaches for extracting a_τ and d_τ, not using $\gamma\gamma \to \tau\tau$, have been proposed for pp collisions [36–38], e^+e^- collisions [39–41], and for fixed target experiments with bent crystals [42, 43]. Some of these have $q^2 \gg 0$ GeV^2, e.g. in DY production, which means that the SM form factors are suppressed. Different processes and beam types typically provide statistically independent datasets with interesting future opportunities for combining their respective constraints on τ-lepton electromagnetic moments.

This paper presents differential fiducial cross-section measurements of photon-induced τ-lepton pair production $\gamma\gamma \to \tau\tau$ as well as constraints on the τ-lepton a_τ and d_τ. The results are obtained using UPC lead-lead collisions recorded in 2015 and 2018 at $\sqrt{s_{\mathrm{NN}}} = 5.02$ TeV. The dataset corresponds to an integrated luminosity of 1.93 nb^{-1}. Events are categorized into three regions using topologies with one of the τ-leptons decaying into a muon and two neutrinos and by the presence of one electron, or either one or three charged-particle track(s) from the second τ-lepton decay. Events without forward neutron emissions are used to suppress photonuclear backgrounds and to reduce contributions from dissociative processes which typically have larger initial-state photon virtuality. The data are corrected for detector-related effects through an iterative Bayesian unfolding procedure, obtaining differential fiducial cross-sections at particle-level for seven kinematic variables of the visible τ-lepton decay products for each of the three considered regions. Electromagnetic moments of the τ-lepton are extracted from maximum-likelihood fits to the muon transverse-momentum distributions in the three regions before unfolding is performed.

2 ATLAS detector

The ATLAS experiment [44–46] at the LHC is a multipurpose particle detector with a forward-backward symmetric cylindrical geometry.[1] It consists of an inner tracking detector (ID) surrounded by a thin superconducting solenoid providing a 2 T axial magnetic field, electromagnetic and hadronic calorimeters, and a muon spectrometer (MS). The inner tracking

[1] ATLAS uses a right-handed coordinate system with its origin at the nominal interaction point (IP) in the center of the detector and the z-axis along the beam pipe. The x-axis points from the IP to the center of the LHC ring, and the y-axis points upwards. Polar coordinates (r, ϕ) are used in the transverse plane, ϕ being the azimuthal angle around the z-axis. The pseudorapidity is defined in terms of the polar angle θ as $\eta = -\ln\tan(\theta/2)$ and is equal to the rapidity $y = \frac{1}{2}\ln\left(\frac{E+p_z}{E-p_z}\right)$ in the relativistic limit. Angular distance is measured in units of $\Delta R \equiv \sqrt{(\Delta y)^2 + (\Delta\phi)^2}$.

JHEP10(2026)053

detector covers the pseudorapidity range $|\eta| < 2.5$. It consists of silicon pixel, silicon microstrip, and transition radiation tracking detectors. Lead/liquid-argon (LAr) sampling calorimeters provide electromagnetic (EM) energy measurements with high granularity within the region $|\eta| < 3.2$. A steel/scintillator-tile hadronic calorimeter covers the central pseudorapidity range ($|\eta| < 1.7$). The endcap and forward regions are instrumented with LAr calorimeters for EM and hadronic energy measurements up to $|\eta| = 4.9$. The muon spectrometer surrounds the calorimeters and is based on three large superconducting air-core toroidal magnets with eight coils each. The field integral of the toroids ranges between 2.0 and 6.0 T m across most of the detector. The muon spectrometer includes a system of precision tracking chambers up to $|\eta| = 2.7$ and fast detectors for triggering up to $|\eta| = 2.4$. For heavy-ion data taking, Zero Degree Calorimeters (ZDCs) [47] are installed at $z = \pm 140$ m from the interaction point. The ZDCs detect neutral particles in the forward region (approximately $|\eta| > 8.3$), such as forward neutrons. Each ZDC detector consists of four modules, each with tungsten absorber read out by layers of vertical quartz rods. Minimum-bias Trigger Scintillators (MBTS) detectors situated at $z = \pm 3.56$ m detect charged particles in the pseudorapidity range $2.07 < |\eta| < 3.86$. These detectors comprise two rings with azimuthal scintillator counters for the inner and outer rings. The luminosity is measured mainly by the LUCID-2 [48] detector, which is located close to the beam pipe, complemented with calorimeter and beam conditions systems for stability monitoring.

A two-level trigger system is used to select events [49, 50]. The first-level trigger is implemented in hardware and uses a subset of the detector information to accept events. This is followed by a software-based trigger that reduces the accepted rate of complete events.

A software suite [51] is used in the simulation of collision events, in the reconstruction and analysis of real and simulated data, in detector operations, and in the trigger and data acquisition systems of the experiment.

3 Data and Monte Carlo samples

This analysis uses Pb+Pb data recorded at a center-of-mass energy of $\sqrt{s_{\mathrm{NN}}} = 5.02$ TeV during LHC Run 2. The data were recorded in 2015 and 2018, with an integrated luminosity of 0.49 nb^{-1} and 1.44 nb^{-1}, respectively. The average number of hadronic interactions per bunch crossing was 0.0022 in 2015 and 0.003 in 2018. Only data that satisfy standard data-quality requirements [52] are included.

Monte Carlo (MC) simulated signal events $\gamma\gamma \to \tau\tau$ were generated at leading-order in QED using the STARLIGHT 2.0 [53] generator, interfaced with PYTHIA 8.245 [54] to simulate final-state radiation (FSR) from the τ-leptons, TAUOLA [55, 56] to handle τ-lepton decays and PHOTOS++ 3.61 [57] to simulate FSR from the charged decay products of τ-leptons (STARLIGHT + PYTHIA 8 + TAUOLA). The signal samples interfaced with TAUOLA are used as the nominal samples, and alternative signal samples employing PYTHIA 8.245 itself, instead of TAUOLA, for τ-lepton decays (STARLIGHT + PYTHIA 8) are used to estimate a systematic uncertainty from the modeling of τ-lepton decays. For the nominal and alternative signal samples, the di-τ invariant mass is required to be above 4 GeV and the p_{T} of the τ-leptons is required to be above 2 GeV at generator-level. A generator-level filter is also applied to select events with at least one charged particle with p_{T} above 3 GeV within $|\eta| < 2.6$.

JHEP10(2026)053

For the $\gamma\gamma \to \tau\tau$ process, it was shown in ref. [58] that the inclusion of full spin correlation effects in the τ-lepton pair production and decay can impact the kinematic distributions of the decay products at the level of a few percent, with the corresponding theoretical calculations being present in TauSpinner 2.1.2 [59, 60]. The signal MC samples described above lack full spin correlation effects. The effect of full spin correlations in the $\gamma\gamma \to \tau\tau$ predictions was therefore evaluated using a generator-level $\gamma\gamma \to \tau\tau$ sample produced at leading-order in QED using gamma-UPC 1.0 [61] to simulate the photon flux with the charged form factor approach, combined with MadGraph5_aMC@NLO 3.5.1 [62] to simulate the hard interaction process of $\gamma\gamma \to \tau\tau$. This was interfaced with Tauola to handle the τ-lepton decays. The TauSpinner 2.1.2 package was then used to compute spin-weights on an event-by-event basis. Spin correlation bin-by-bin correction factors are then derived by taking the ratio of kinematic distributions of τ-lepton decay products with and without applying the spin-weights. The correction factors are computed for all fiducial regions and measured observables, and are found to be significant only for the one muon plus one track fiducial region μ1T-FR defined in section 7. The spin-weights applied for events in μ1T-FR are normalized to the average spin-weight in that fiducial region, to remove the event selection bias on the spin-weight. The distribution of event-by-event spin-weights after normalization is approximately Gaussian, with a mean of 1.0 and standard deviation ≈ 0.2. The resulting bin-by-bin spin correlation correction factors are typically within 5% of unity, with maximum deviations of up to 10% observed only in a few bins.

One of the main sources of background is the $\gamma\gamma \to \mu\mu(\gamma)$ process [63]. MC samples for this process are generated using the STARlight generator, interfaced to Pythia 8 to model FSR from the muons. If the FSR photon with the highest transverse momentum has $p_{\mathrm{T}} > 2$ GeV, a dedicated Next-to-Leading-Order (NLO) QED $\gamma\gamma \to \mu\mu\gamma$ MC sample generated using MadGraph5_aMC@NLO 2.9 [62] interfaced to Pythia 8 is used, instead of STARlight interfaced to Pythia 8. This additional sample improves the modeling of high-p_{T} FSR photon emissions for cases where $p_{\mathrm{T}}^{\gamma} \gtrsim p_{\mathrm{T}}^{\mu}$. Since the version of MadGraph5_aMC@NLO used only generates initial-state photons from protons, the photon flux of this sample is reweighted to the one from STARlight in Pb+Pb interactions. The reweighting is performed differentially in generator-level di-muon invariant mass and rapidity.

For the $\gamma\gamma \to \tau\tau$ and $\gamma\gamma \to \mu\mu(\gamma)$ samples, the photon flux distribution is (further) reweighted to match that of SuperChic 3.05 [64]. In this case, SuperChic is indicated in the sample name, e.g., for the nominal signal sample as STARlight/SuperChic + Pythia 8 + Tauola. This reweighting is motivated as STARlight is known to underpredict the photon flux compared with previous measurements in refs. [63, 65]. The reweighting is performed differentially in generator-level di-τ or di-muon invariant mass and rapidity. In STARlight, the photon flux is approximated using the Weizsäcker-Williams method [66–70], which approximates the electromagnetic field of a relativistic point charge as a cloud of virtual photons. To avoid interactions inside a nucleus that would lead to its breakup, the photon flux description in STARlight is restricted to distances from the nucleus center larger than the geometric nuclear radius. To avoid physical collisions of the nuclei where hadronic interactions would dominate, the impact parameter of the collision is required to be larger than twice the geometric nuclear radius of the lead nuclei [53, 71]. In contrast,

JHEP10(2026)053

SuperChic uses a nucleus charge form factor based on the Woods-Saxon distribution and a survival factor considering nucleon-nucleon interactions, where the survival factor is the probability of the large rapidity gaps in $\gamma\gamma \to X$ surviving the nucleus-nucleus interaction. Thus, for SuperChic the photon flux validity and impact parameter does not need to be restricted in this explicit way [64]. For STARlight and SuperChic MC samples, all possible configurations for Coulomb breakup of either nucleus (none, one or both), i.e., through additional electromagnetic interaction, is included.

Simulated samples for the $\gamma\gamma \to ee$ process were generated using the STARlight generator and Pythia 8 to model FSR from the electrons. Dijet samples from the $\gamma\gamma \to q\bar{q}$ process with $q = u, d, s, c, b$ were generated using Pythia 8. Non-diffractive photonuclear events ($\gamma\mathrm{A} \to X$) were generated using STARlight interfaced with Dpmjet-III [72].

All MC samples described in this section which are not explicitly referred to as generator-level, were processed with a full detector simulation based on Geant4 [73, 74].

4 Object definition

Events that contain one τ-lepton decaying into a muon and two neutrinos and one τ-lepton decaying into a lepton or charged pion(s) or kaon(s) require the reconstruction of muons, electrons and charged-particle tracks from the detector signals. Additionally, photons and calorimeter topoclusters, defined below, are used to identify FSR and to reject hadronic backgrounds, respectively.

Muons are reconstructed from tracks in the ID and the MS. The muons must satisfy the dedicated "LowPt" [75] identification criteria that are optimized for increased efficiency and fake-rejection for muons with $p_{\mathrm{T}} < 5$ GeV. In addition, they are required to have transverse momentum $p_{\mathrm{T}} > 4$ GeV, $|\eta| < 2.4$ and a transverse impact parameter relative to the measured beam-line position of $|d_0| < 0.3$ mm.

Electrons are reconstructed from tracks in the ID matched with EM clusters in the calorimeter. The EM clusters must be of good quality, meaning EM clusters with a large amount of energy from poorly functioning calorimeter cells are removed [76], and a timing requirement is used to reject out-of-time candidates [77]. The electrons must satisfy the "Loose" [76] likelihood-based identification criteria, based on shower-shape and track-quality variables. They must also satisfy $p_{\mathrm{T}} > 4$ GeV, $|\eta| < 2.47$, with the calorimeter transition region $1.37 < |\eta| < 1.52$ excluded, and $|d_0| < 0.5$ mm.

Photons are reconstructed from EM clusters in the calorimeter, and tracks in the ID to identify photon conversions to e^+e^- pairs. The EM clusters and the reconstructed photons must both be of good quality. The photons must satisfy dedicated identification criteria defined in ref. [77], which are based on a neural network approach and are optimized for low-E_T photons ($E_{\mathrm{T}} < 20$ GeV). They must also satisfy $E_{\mathrm{T}} > 1.5$ GeV and $|\eta| < 2.37$ with the calorimeter transition region $1.37 < |\eta| < 1.52$ excluded.

Charged-particle tracks are reconstructed from hit information in the ID [78, 79]. The tracks must satisfy the "Loose Primary" criteria [80–82], and must satisfy $p_{\mathrm{T}} > 100$ MeV, $|\eta| < 2.5$ and $|d_0| < 1.5$ mm. When calculating track four-vectors and derived variables for tracks not associated with muons, electrons or photons, the particle is assumed to be a charged pion.

JHEP10(2026)053

Three-dimensional collections of topologically connected calorimeter cells ("topoclusters") [83] are formed and must satisfy the energy significance criteria for individual cells described in ref. [84]. The topoclusters must satisfy $|\eta| < 4.9$, $p_{\mathrm{T}} > 1$ GeV for $|\eta| < 2.5$ and $p_{\mathrm{T}} > 0.1$ GeV for $2.5 < |\eta| < 4.9$. Additionally, topoclusters arising from noise bursts in the calorimeters or malfunctioning calorimeter cells are removed. The data-driven removal procedure involves studying two dimensional distributions of topocluster activity in η and ϕ for each calorimeter layer. When calculating topocluster-related variables, the topoclusters are considered to be massless.

5 Event selection

In 2015, candidate events were recorded by triggers that require a muon track in the muon spectrometer (with no minimum p_{T} requirement) and a total transverse energy below 50 GeV in the entire calorimeter. Additionally, in 2015 events were rejected if more than one hit was registered in the inner ring of the MBTS detectors on either side, and a well-reconstructed track with $p_{\mathrm{T}} > 200$ MeV was required in the ID. In 2018, the trigger required at least one muon with $p_{\mathrm{T}} > 4$ GeV, a total transverse energy below 50 GeV in the entire calorimeter and a total transverse energy below 3 GeV in the forward calorimeter on each side [85]. On average, muons lose roughly 3 GeV of their energy while passing through the calorimeter system [75]. To correct for differences between simulation and data, the reconstruction and identification efficiencies for electrons and muons and the trigger efficiencies for muons are measured using tag-and-probe methods that are similar to those described in refs. [63, 77, 86]. The efficiency of the threshold of 50 GeV on the maximum total transverse energy accepted in the entire calorimeter is studied using a data-driven approach, and is found to be 100%. Moreover, the trigger efficiency associated with the selection of the activity in the forward direction (MBTS in 2015 or the forward calorimeter in 2018) is evaluated in ref. [77], and is found to be above 98%. The small inefficiency is accounted for in the analysis, along with its uncertainty. The triggers select $\sim 6\%$ of the signal events which pass the generator-level requirements including the filter requirements, described in section 3.

Three mutually exclusive $\gamma\gamma \to \tau\tau$ signal regions (SR) are defined. All SRs require exactly one muon, targeting events where one of the τ-leptons decays into a muon and two neutrinos, i.e., as $\tau \to \nu_\tau \bar{\nu}_\mu \mu$. This requirement reduces dilepton and hadronic backgrounds. The events are then categorized according to the signature of the other τ-lepton decay. A summary of the SR selections is given in table 1.

The μ1T-SR requires exactly one muon and exactly one track separated by $\Delta R > 0.1$ from the muon and with opposite charge to the muon. This SR targets cases where the second τ-lepton decays into one charged hadron, or leptonically, where the lepton has a p_{T} below the electron and muon p_{T} thresholds. To further reject $\gamma\gamma \to \mu\mu/ee$ backgrounds, the event must contain zero electrons and no additional baseline muons that satisfy looser criteria (muons from matched ID and MS tracks with $p_{\mathrm{T}} > 2$ GeV and $|\eta| < 2.5$). The p_{T} of the muon-track system must be above 1 GeV. This suppresses p_{T}-balanced backgrounds, for example $\gamma\gamma \to \mu\mu$, while retaining signal events that are generally more p_{T}-imbalanced due to the presence of neutrinos. Additional system p_{T} selections are performed to reject backgrounds with FSR emissions, for example $\gamma\gamma \to \mu\mu(\gamma)$. Low-$p_{\mathrm{T}}$ photons or topoclusters

JHEP10(2026)053

Region	μ1T-SR	μ3T-SR	μe-SR
Trigger	Single-muon based		
$0n0n$ topology	$E_{\mathrm{ZDC}}^{A,C} < 1$ TeV for data, $0n0n$ weights for MC		
$N_{\mu}^{\mathrm{baseline}}$	$= 1$	$= 1$	—
N_{μ}	$= 1$	$= 1$	$= 1$
N_{e}	$= 0$	$= 0$	$= 1$
$N_{\mathrm{trk}}(\Delta R > 0.1$ from $\mu)$	$= 1$	$= 3$	—
$N_{\mathrm{trk}}(\Delta R > 0.1$ from $\ell)$	—	—	$= 0$
$N_{\mathrm{topoclusters}}^{\mathrm{unmatched}}$	$= 0$	$= 0$	—
$\Sigma_{\mu,\mathrm{trk(s)\ or\ }e}$ charge	$= 0$	$= 0$	$= 0$
p_{T} of muon and track	> 1 GeV	—	—
p_{T} of muon, track and photon	> 1 GeV	—	—
p_{T} of muon, track and topocluster	> 1 GeV	—	—
m_{trks}	—	< 1.7 GeV	—
$A_{\phi}^{\mu,\mathrm{trk(s)}}$	< 0.4	< 0.2	—

Table 1. Summary of the signal region definitions. The $0n0n$ weights include the contribution from EM pileup. The notation trk(s) indicates a single track for the μ1T-SR and the three track-system for the μ3T-SR. The system p_{T} selections are not mutually exclusive, meaning an event may satisfy either one or both requirements.

are used to recover energy lost to FSR and compute a three-body system p_{T}. If a photon is found within $\Delta R < 1$ of the track, the p_{T} of the muon-track-photon system must be above 1 GeV. If multiple photons meet these criteria, the highest-p_{T} photon is used. Furthermore, if a topocluster with $p_{\mathrm{T}} > 2$ GeV is found within $\Delta R < 1$ of the track but not directly associated with it, the p_{T} of the muon-track-topocluster system must be above 1 GeV. A topocluster is considered to originate from the track if it lies within $\Delta R < 0.1$ of the track's extrapolation to the calorimeter for a track with $p_{\mathrm{T}} > 0.7$ GeV, since lower-p_{T} tracks are unlikely to deposit significant energy in the calorimeter. If multiple topoclusters meet these criteria, the highest-p_{T} topocluster is used. These system p_{T} selections are not mutually exclusive, meaning an event may satisfy either one or both requirements.

The μ3T-SR requires exactly one muon and exactly three tracks separated by $\Delta R > 0.1$ from the muon, targeting cases where the second τ-lepton decays into three charged hadrons. The total charge of the muon and tracks must sum to zero. The event must contain no electrons and there must be no additional baseline muons. To ensure that the three tracks are compatible with a single 3-prong hadronic τ-lepton decay, while also suppressing background from exclusive ρ-meson production which coincides with $\gamma\gamma \to \mu\mu$ events, the mass of the three-track system m_{trks} must be less than 1.7 GeV.

The μe-SR requires exactly one muon and exactly one electron with opposite charge to the muon, targeting cases where both τ-leptons decay leptonically. The event must have no additional tracks with $\Delta R > 0.1$ from the electron and the muon.

To reject hadronic backgrounds, for example photonuclear processes, a topocluster veto is applied for μ1T-SR and μ3T-SR. This veto requires zero topoclusters located outside the proximity of the muon, with $\Delta R > 0.3$, and the track (for μ1T-SR) or three-track system (for

JHEP10(2026)053

μ3T-SR) with $\Delta R > 1.0$, referred to as 'unmatched topoclusters' in the following. For the SRs that use the topocluster veto, a small correction of ∼2% is applied to the MC to account for differences between the number of topoclusters in data and MC. Further selections are imposed on the acoplanarity, which is defined as $A_{\phi}^{\mu,\mathrm{trk(s)}} = 1 - |\Delta\phi(\mu, \mathrm{trk(s)})|/\pi$, to reduce photonuclear backgrounds. For the μ1T-SR, the acoplanarity between the muon and the track must be less than 0.4, whereas for the μ3T-SR, the acoplanarity between the muon and the track system is required to be less than 0.2. This requirement favors back-to-back production of the muon and the track(s).

For all signal regions, the energy recorded by the ZDC detectors must be less than 1 TeV on both sides of the interaction point. This selects a $0n0n$ topology where no neutrons are detected in both ion directions. This suppresses dissociative processes which typically have larger initial-state photon virtuality, thus, this requirement helps to ensure that the initial-state photons have near-zero virtuality $q^2 \sim 0$ GeV^2. It also significantly reduces photonuclear backgrounds, which often involve nuclear dissociation leading to ion break up. Ion break up can, however, also arise in parallel to $\gamma\gamma \to \tau\tau$ or $\gamma\gamma \to \mu\mu(\gamma)$ processes due to soft Coulomb exchanges. These exchanges typically excite one or both nuclei e.g., via a giant dipole resonance, inducing the emission of one or more neutrons. These neutrons, on average, carry the full per-nucleon beam energy [63].

The ZDC selection is applied only to data, as the ZDC response is not simulated in the MC samples, nor are forward neutrons typically produced by the generators. The $\gamma\gamma \to \tau\tau$ and $\gamma\gamma \to \mu\mu(\gamma)$ MC samples utilized here do not distinguish among neutron topologies, requiring a data-driven correction to be applied to specifically account for the probability of having a $0n0n$ topology. The probability of an event being $0n0n$ is extracted from data using $\gamma\gamma \to \mu\mu(\gamma)$ candidate events by measuring the ratio of $0n0n$ events to all events (without any ZDC requirements). The $\gamma\gamma \to \mu\mu(\gamma)$ candidate events are selected by requiring exactly two muons and no additional charged-particle tracks, the di-muon system must have $p_{\mathrm{T}} <$ 1 GeV and acoplanarity < 0.01 to suppress backgrounds. Probabilities are extracted as a function of di-muon invariant mass in four rapidity intervals: $|y_{\mu\mu}| < 0.5$, $0.5 < |y_{\mu\mu}| < 1.0$, $1.0 < |y_{\mu\mu}| < 1.5$, and $|y_{\mu\mu}| > 1.5$. For the most forward rapidity bin, $|y_{\mu\mu}| > 1.5$, there are very few data events at high di-muon mass, typically up to ∼5 events, and even fewer di-τ events so this region has a negligible impact. The $0n0n$ probabilities are then applied in the simulation as a weight depending on the generator-level di-muon or di-τ mass and rapidity for both $\gamma\gamma \to \mu\mu(\gamma)$ and $\gamma\gamma \to \tau\tau$ events, which requires the measured probabilities to be corrected for migrations between measured bins and generator-level bins. Pileup from simultaneous electromagnetic interactions within the same LHC bunch crossing (EM pileup) can lead to additional neutrons generated, which are not associated with the observed di-muon pair. These neutrons can be detected in one or both ZDC arms, artificially lowering the $0n0n$ fraction. An additional correction is therefore determined to remove effects due to EM pileup, separately for 2015 and 2018, using a similar procedure to refs. [63, 65]. Following the EM pileup correction, the 2015 and 2018 $0n0n$ probabilities are combined. The combined $0n0n$ probabilities after EM pileup correction (filled markers) are shown in figure 2. The error bars include data statistical uncertainties and statistical and systematic uncertainties in the exclusive single and double EM dissociation cross-sections measured by the ALICE

JHEP10(2026)053

Collaboration [87], and their extrapolation from $\sqrt{s_{\mathrm{NN}}} = 2.76$ TeV to $\sqrt{s_{\mathrm{NN}}} = 5.02$ TeV, as described in ref. [63].

To smooth statistical fluctuations, the $0n0n$ probabilities are fit with an exponential function $e^{p_0+p_1\times m_{\mu\mu}}$, which determines the nominal $0n0n$ weights. The nominal fit to the combined EM-pileup-corrected points is displayed in figure 2, together with its 68% Confidence Level (CL) uncertainty, which is considered as the statistical uncertainty in the $0n0n$ probability. A second fit with the functional form $e^{p_0+p_1\times m_{\mu\mu}} + p_2$ is also shown and is referred to as the alternative fit. The difference between the alternative fit and the nominal one serves as a systematic uncertainty in the $0n0n$ probability. In addition, a systematic uncertainty arising from the choice of binning is also applied. In the alternative version of the binning, three rapidity bins are utilized instead of four and coarser mass bins are utilized. The same fitting procedure and uncertainty treatment is also performed for non-EM-pileup-corrected points separately for 2015 and 2018 data. The parameterized probabilities are subsequently used to reweight the MC samples as a function of the generator-level di-muon or di-τ mass and rapidity. For MC simulation compared directly to data, the fits to the non-EM-pileup-corrected points are used, i.e., the MC then includes contributions from EM pileup, in line with measured data. The application of the $0n0n$ weights reduces the nominal signal yield by ∼62% relative to the after-trigger yield. For MC simulation compared with measured cross-sections, the fits to the EM-pileup-corrected points are used, i.e., the MC then excludes contributions from EM pileup. Using this approach for the MC-based unfolding inputs, the unfolding procedure described in section 7 automatically extrapolates the data from the $0n0n$ phase space including EM pileup to the $0n0n$ phase space with EM pileup subtracted. Additionally, statistical uncertainties and systematic uncertainties from using the alternative fit parameterization and from using the alternative binning for the nominal fit are also provided for use when applying the provided parameterized $0n0n$ probabilities.

In principle, the $0n0n$ probabilities should also be corrected for a potential ZDC inefficiency in detecting the emitted neutrons. As reported in ref. [63], the overall ZDC efficiency was, however, estimated to be over 99%. The small inefficiency is therefore addressed in the systematic uncertainties, by varying the $0n0n$ probabilities applied to the MC simulation, when compared with measured data, by ±1%.

6 Background estimate

After applying the event selection, there are two main sources of background, $\gamma\gamma \to \mu\mu(\gamma)$ and photonuclear events with low activity in the ATLAS detector.

Photon-induced di-muon production with the emission of a FSR photon ($\gamma\gamma \to \mu\mu\gamma$) is especially likely to mimic the $\gamma\gamma \to \tau\tau$ signal as the FSR photon can cause a momentum imbalance between the muons, making the event more likely to satisfy the μ1T-SR selection. It can also cause additional particle production, for example due to photon conversions that can produce two additional tracks, making the event more likely to satisfy the μ3T-SR requirements, or the FSR photon could fake an electron which is pertinent for the μe-SR. The background from the $\gamma\gamma \to \mu\mu(\gamma)$ processes is estimated by using the combination of MC samples discussed in section 3. The modeling of the $\gamma\gamma \to \mu\mu(\gamma)$ background is checked and corrected using a dedicated control region 2μ-CR. The 2μ-CR requires exactly two

JHEP10(2026)053

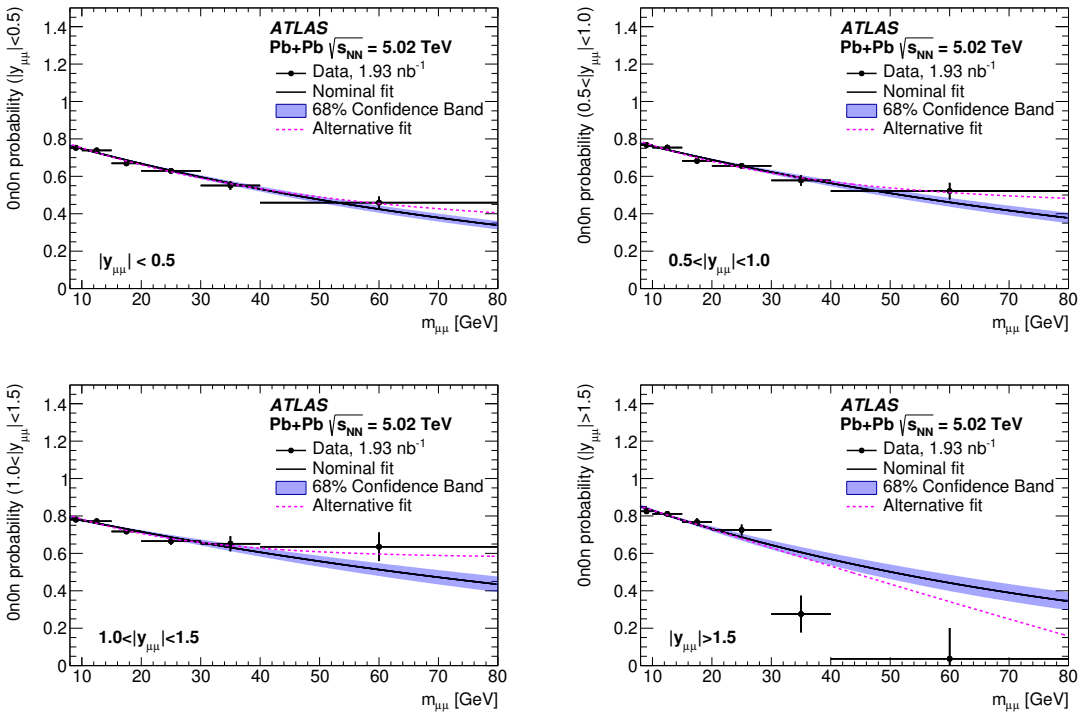


Figure 2. Probabilities of $0n0n$ events extracted from 2015 and 2018 data using the $\gamma\gamma \to \mu\mu(\gamma)$ candidate events in the di-muon rapidity region (top-left) $|y_{\mu\mu}| < 0.5$, (top-right) $0.5 < |y_{\mu\mu}| < 1.0$, (bottom-left) $1.0 < |y_{\mu\mu}| < 1.5$ and (bottom-right) $|y_{\mu\mu}| > 1.5$. Probabilities after correction for EM pileup (filled markers) are displayed. The error bars include statistical uncertainties and uncertainties in the exclusive single and double EM dissociation cross-sections measured by the ALICE Collaboration [87], and their extrapolation to $\sqrt{s_{\mathrm{NN}}} = 5.02$ TeV as described in ref. [63]. To smooth statistical fluctuations, the corrected points are fitted using an exponential function (solid lines) with a shaded uncertainty band or an exponential function with an additional constant parameter (dashed lines).

muons with a di-muon invariant mass $m_{\mu\mu}$ greater than 11 GeV to reject low mass di-muon resonances. Additionally, no extra tracks with $\Delta R > 0.1$ from the muons are allowed. Similar to the SRs, the 2μ-CR requires a $0n0n$ topology.

A summary of the selection requirements is given in table 2. The $\gamma\gamma \to \tau\tau$ signal contamination in the 2μ-CR is below 0.1% of the total signal plus background prediction for both 2015 and 2018 data, and is thus neglected. Figure 3 (left) shows the data-to-MC agreement for 2μ-CR before any corrections are applied. Reasonable agreement in shape is found, however, there is an offset in the normalization which has also been observed in the ATLAS $\gamma\gamma \to ee$ analysis in ref. [65]. The residual offset between the $\gamma\gamma \to \mu\mu(\gamma)$ prediction and the data is considered to result from inadequacies in the photon flux description [63]. A data-driven normalization correction factor, referred to as the Global Residual Flux Factor (GRFF), is thus extracted from the 2μ-CR and is applied to the $\gamma\gamma \to \mu\mu(\gamma)$ background and the nominal $\gamma\gamma \to \tau\tau$ signal predictions. The GRFF is extracted using a profile likelihood fit [88] to the highest-p_{T} (leading) muon p_{T} distribution in the 2μ-CR.

JHEP10(2026)053

Region	2μ-CR	μ2T-CR	μ4T-CR
0n0n topology	As in SRs	$E_{\mathrm{ZDC}} < 1$ TeV for side A and/or C	
$N_{\mu}^{\mathrm{baseline}}$	—	$= 1$	$= 1$
N_{μ}	$= 2$	$= 1$	$= 1$
$N_{\mathrm{trk}}(\Delta R > 0.1$ from $\mu)$	$= 0$	$= 2$	$= 4$
p_{T} of lowest-p_{T} trk	—	< 500 MeV	< 500 MeV
$N_{\mathrm{topoclusters}}^{\mathrm{unmatched}}$	—	≤ 8	≤ 8
$\Sigma_{\mu,\text{highest-}p_{\mathrm{T}}\text{ trk}}$ charge	—	$= 0$	—
m_{trks} (or $A_{\phi}^{\mu,\text{highest-}p_{\mathrm{T}}\text{ trk}}$)	—	> 1 GeV (or > 0.2)	< 1.7 GeV
$m_{\mu\mu}$	> 11 GeV	—	—

Table 2. Summary of the control region definitions. The 2μ-CR is used to improve the photon flux modeling and μ2T-CR and μ4T-CR are used to obtain templates for estimating the photonuclear background.

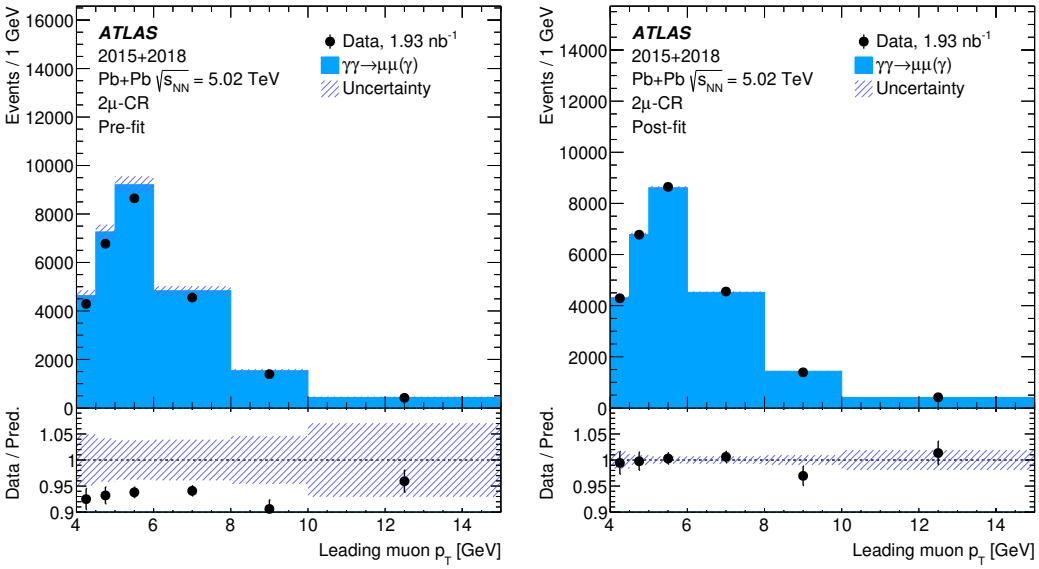


Figure 3. Leading muon p_{T} distribution in the 2μ-CR category for the combined 2015 and 2018 data, pre-fit (left) and post-fit (right). The data (filled markers) are compared with the $\gamma\gamma \to \mu\mu(\gamma)$ background. The hatched band indicates the total uncertainties in the prediction. The error bars on the data points indicate the statistical uncertainty in the data. Event counts are shown normalized by bin width. The bottom panel displays the ratio of the data to the predictions.

Nuisance parameters representing systematic uncertainties, described in section 8, are included in the fit. The extracted value of the GRFF from the fit is $0.935^{+0.035}_{-0.033}$. After the GRFF is applied as an overall scale factor, the data-to-MC agreement is significantly improved, as shown in figure 3 (right).

Diffractive photonuclear processes also constitute a non-negligible background and can mimic the $\gamma\gamma \to \tau\tau$ signal due to their characteristic low particle activity. These interactions involve the exchange of a colorless object, known as a pomeron, which can result in one-sided rapidity gaps being partially filled by pomeron remnants [89, 90]. The diffractive photonuclear

JHEP10(2026)053

background in the μe-SR is negligible in both 2015 and 2018 data, due to the very high purity of this region. The diffractive photonuclear background in μ1T-SR and μ3T-SR is estimated by using a fully data-driven method, exploiting the fact that the photonuclear events are often accompanied by extra particle production. Template distributions are built using control regions, which are similar to the signal regions but require an additional low-p_{T} track with $p_{\mathrm{T}} < 500$ MeV. The control regions are referred to as μ2T-CR and μ4T-CR, related to the μ1T-SR and μ3T-SR, respectively. Aside from modifying the requirement on the number of tracks, for μ2T-CR and μ4T-CR the $0n0n$ topology requirement is loosened to require that the energy recorded by the ZDC detectors is less than 1 TeV on one or both sides of the interaction point. Loosening the $0n0n$ topology requirement enhances statistics, given that photonuclear events are often accompanied by break up of one of the ions. Additionally, the topocluster veto is relaxed to require less than or equal to eight unmatched topoclusters instead of zero. For the μ2T-CR, the mass of the two-track-system is required to be above 1 GeV or the acoplanarity between the muon and the highest-p_{T} track must be above 0.2, to reduce $\gamma\gamma \to \tau\tau$ signal contamination. For the μ4T-CR, the requirement of zero net charge summing over the muon and tracks is removed. The other selections remain the same as those of μ3T-SR. The contributions from $\gamma\gamma \to \tau\tau$ and $\gamma\gamma \to \mu\mu(\gamma)$ were checked for the μ2T-CR and μ3T-CR using simulation and were found to be negligible as no event passes the criteria for either region. A summary of the selection criteria is given in table 2. The measured kinematic distributions in the μ2T-CR and μ4T-CR are used as diffractive photonuclear template distributions. The normalization of the templates is performed using the ratio of the integrated data distribution and the integrated photonuclear background distribution, in a region where the SR selections are applied except for the topocluster veto, and instead $4 \leq N_{\text{topoclusters}}^{\text{unmatched}} \leq 8$ is required. The fully reconstructed MC samples demonstrate that this region has no contribution from the $\gamma\gamma \to \tau\tau$ signal or the $\gamma\gamma \to \mu\mu(\gamma)$ background. For 2015 data, the diffractive photonuclear background is negligible in the μ3T-SR, compared with 3.2 ± 2.1 events for 2018 data.

All other considered background sources are negligible. The backgrounds from $\gamma\gamma \to ee$ production and non-diffractive photonuclear processes were estimated by using simulation and were found to be negligible as no event passes any of the three SR criteria. The contribution from $\gamma\gamma \to q\bar{q}$ is estimated with simulation and found to be negligible. The same is found for resolved $\gamma\gamma$ interactions where at least one of the photons fluctuates into a hadronic state of a $q\bar{q}$ pair, which is modeled in Pythia 8 [91]. The contribution due to the simultaneous production of $\gamma\gamma \to \mu\mu$ or $\gamma\gamma \to \tau\tau$ and exclusive ρ^0-meson production $\gamma P \to \rho^0 \to \pi\pi$ in the same ion-ion interaction [92] is estimated by using a fully data-driven method [14] and is negligible.

Figure 4 shows the detector-level muon p_{T} distributions for μ1T-SR, μ3T-SR and μe-SR for the combined 2015 and 2018 data. The observed data yields after all event selections for the combined 2015 and 2018 data, compared with the expected background events, are listed in table 3, demonstrating the very low background levels. The predicted signal-plus-background yields in table 3 assume $a_\tau = d_\tau = 0$ for the signal and are compatible with the observed data yields.

JHEP10(2026)053

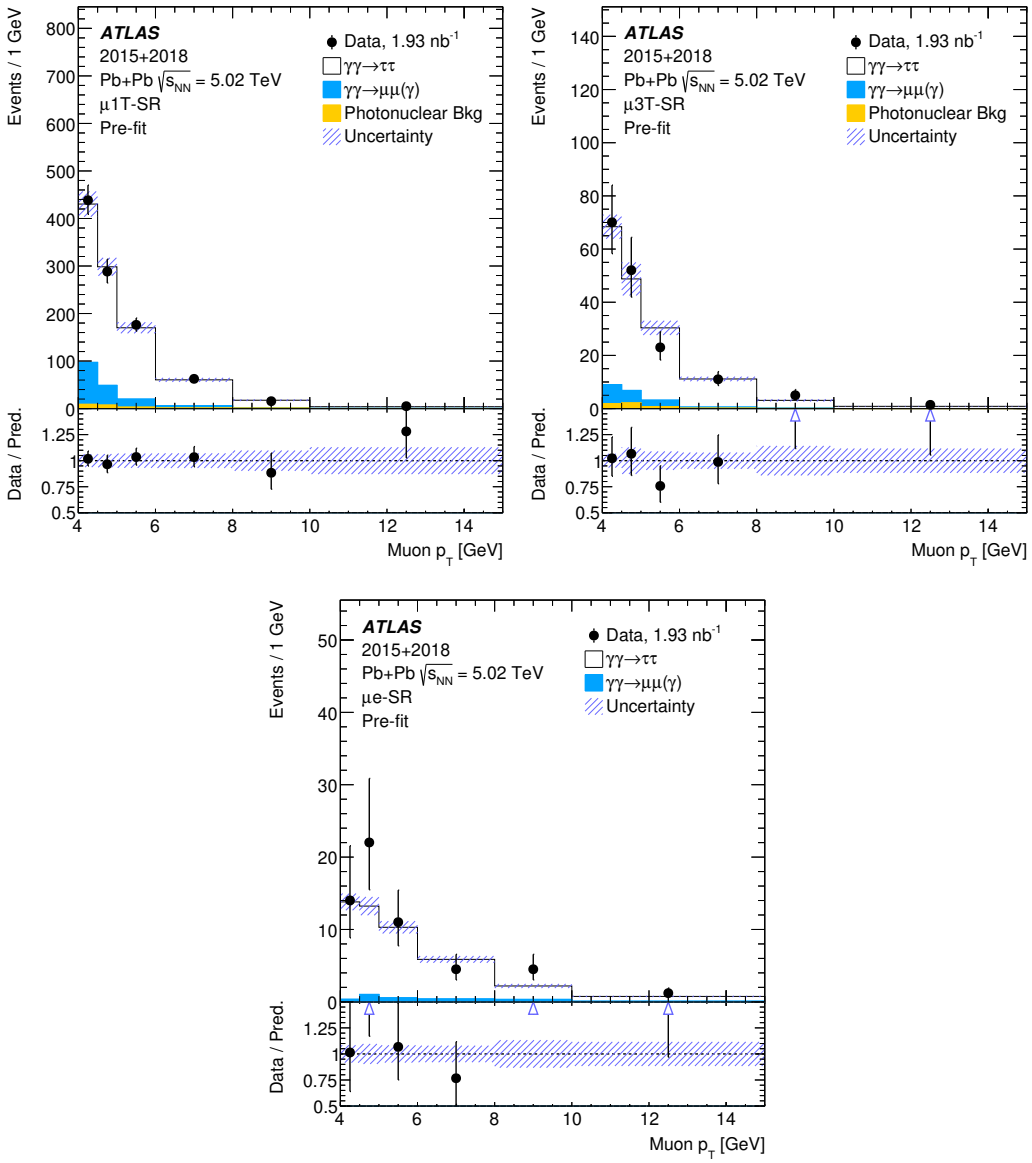


Figure 4. Muon p_{T} distributions in the (top left) μ1T-SR, (top right) μ3T-SR, (bottom) μe-SR categories for the combined 2015 and 2018 data. The data (filled markers) are compared with the stacked histograms showing $\gamma\gamma \to \tau\tau$ signal with $a_\tau = d_\tau = 0$, the $\gamma\gamma \to \mu\mu(\gamma)$ background and the photonuclear background. The hatched band indicates the total uncertainties in the prediction. The error bars on the data points indicate the statistical uncertainty in the data. Event counts are shown normalized by bin width. The bottom panel displays the ratio of the data to the predictions; arrows in this panel denote a data point that is outside the displayed range.

JHEP10(2026)053

Region	μ1T-SR	μ3T-SR	μe-SR
$\gamma\gamma \to \tau\tau$ signal	598.4 ± 39.2	109.0 ± 9.1	40.6 ± 3.3
$\gamma\gamma \to \tau\tau$ contribution [%]	84.3% ± 5.5%	89.6% ± 7.5%	92.7% ± 7.5%
$\gamma\gamma \to \mu\mu(\gamma)$ background	95.8 ± 8.1	9.4 ± 1.0	3.2 ± 0.5
$\gamma\gamma \to \mu\mu(\gamma)$ contribution [%]	13.5% ± 1.1%	7.7% ± 0.8%	7.3% ± 1.1%
Photonuclear background	15.6 ± 11.4	3.2 ± 2.1	—
Photonuclear contribution [%]	2.2% ± 1.6%	2.6% ± 1.7%	—
Combined background	111.4 ± 14.0	12.6 ± 2.3	3.2 ± 0.5
Combined background contribution [%]	15.7% ± 2.0%	10.4% ± 1.9%	7.3% ± 1.1%
Combined signal+background	709.7 ± 46.2	121.6 ± 9.9	43.8 ± 3.6
Data	723	124	53

Table 3. Signal and background yields in the three SRs, together with the observed event counts in data. Negligible contributions are indicated by —. Uncertainties in the predictions are the total uncertainties in the respective prediction. Percentages, including the uncertainty values, use the total signal-plus-background prediction as denominator.

7 Data unfolding

Differential cross-sections are measured for seven variables in each of the three fiducial regions. The fiducial regions (FRs) referred to as μ1T-FR, μ3T-FR, and μe-FR (defined at particle-level) correspond to μ1T-SR, μ3T-SR, and μe-SR (defined at detector-level), respectively. The FR selections are defined in table 4 and each FR is statistically independent to the others. The definition of the FRs only considers final-state particles with lifetimes greater than 30 ps, which are considered 'stable' — this is also referred to as "particle-level" in the simulation and for cross-section measurements. The definitions of the variables in each FR are given in table 5.

To determine the yield of $\gamma\gamma \to \tau\tau$ events in data, the estimated background contributions described in section 6 are subtracted from the data in each bin of the studied variable. Following the background subtraction, the data are corrected for detector effects ("unfolded") using simulation, where the data and background estimates are considered to be at detector-level, and are unfolded to particle-level. The unfolding is performed using the iterative Bayesian unfolding (IBU) method [93–95], implemented using the D'Agostini iterative scheme within RooUnfold [96] with the generated signal distribution used as the initial prior. The relationships between the generated signal distribution and the corresponding reconstructed one are obtained from the nominal $\gamma\gamma \to \tau\tau$ signal sample (STARLIGHT/SUPERCHIC + PYTHIA 8 + TAUOLA), and are summarized in the migration matrix. Events used to populate the matrix are required to satisfy both the SR (detector-level) and FR (particle-level) selections. Migrations between detector-level and particle-level bins are considered via this matrix. Typical off-diagonal contributions to the matrix are in the range ∼5–10%, up to a maximum of ∼20% for some variables and fiducial regions. The fraction of events that fall into the SR and originate from the FR, referred to as the fiducial fraction, is 0.63 for μ1T-FR, 0.91 for μ3T-FR, and 0.88 for μe-FR. The fraction of events that originate from the FR and

JHEP10(2026)053

Object	Requirements		
Leptons (e,μ)	$p_{\mathrm{T}} > 4$ GeV and $\lvert\eta\rvert < 2.5$		
Charged hadrons	$p_{\mathrm{T}} > 100$ MeV and $\lvert\eta\rvert < 2.5$		
Low-p_{T} Leptons	100 MeV $< p_{\mathrm{T}} < 4$ GeV and $\lvert\eta\rvert < 2.5$		
Track particles (trk)	Charged hadron or low-p_{T} lepton		
Region	μ1T-FR	μ3T-FR	μe-FR
$0n0n$ topology	$0n0n$ weights for MC		
N_{μ}	$= 1$	$= 1$	$= 1$
N_{e}	$= 0$	$= 0$	$= 1$
$N_{\mathrm{trk}}(\Delta R > 0.1$ from μ or $e)$	$= 1$	$= 3$	$= 0$
$\Sigma_{\mu,\mathrm{trk(s)\ or\ }e}$ charge	$= 0$	$= 0$	$= 0$
p_{T} of muon and track	> 1 GeV	—	—
m_{trks}	—	< 1.7 GeV	—
$A_{\phi}^{\mu,\mathrm{trk}(s)}$	< 0.4	< 0.2	—

Table 4. Summary of fiducial object requirements and fiducial region definitions. The $0n0n$ weights here exclude the contribution from EM pileup. The notation trk(s) indicates a single track for the μ1T-FR and the three track-system for the μ3T-FR.

Variable	μ1T-FR	μ3T-FR	μe-FR
Muon p_{T}	p_{T}^{μ}	p_{T}^{μ}	p_{T}^{μ}
Track(s)/Electron p_{T}	$p_{\mathrm{T}}^{\mathrm{trk}}$	$p_{\mathrm{T}}(\mathbf{p}_{\mathrm{trks}})$	p_{T}^{e}
$p_{\mathrm{T}}\,(\mu, \mathrm{trk(s)}/e)$	$p_{\mathrm{T}}(\mathbf{p}_{\mu} + \mathbf{p}_{\mathrm{trk}})$	$p_{\mathrm{T}}(\mathbf{p}_{\mu} + \mathbf{p}_{\mathrm{trks}})$	$p_{\mathrm{T}}(\mathbf{p}_{\mu} + \mathbf{p}_{e})$
$m_{\mathrm{inv}}(\mu, \mathrm{trk(s)}/e)$	$m_{\mathrm{inv}}(\mathbf{p}_{\mu} + \mathbf{p}_{\mathrm{trk}})$	$m_{\mathrm{inv}}(\mathbf{p}_{\mu} + \mathbf{p}_{\mathrm{trks}})$	$m_{\mathrm{inv}}(\mathbf{p}_{\mu} + \mathbf{p}_{e})$
$\eta(\mu, \mathrm{trk(s)}/e)$	$\eta(\mathbf{p}_{\mu} + \mathbf{p}_{\mathrm{trk}})$	$\eta(\mathbf{p}_{\mu} + \mathbf{p}_{\mathrm{trks}})$	$\eta(\mathbf{p}_{\mu} + \mathbf{p}_{e})$
$\Delta\eta\,(\mu, \mathrm{trk(s)}/e)$	$\eta_{\mu} - \eta_{\mathrm{trk}}$	$\eta_{\mu} - \eta(\mathbf{p}_{\mathrm{trks}})$	$\eta_{\mu} - \eta_{e}$
$A_{\phi}^{\mu,\mathrm{trk(s)}/e}$	$1 - \lvert\phi_{\mu} - \phi_{\mathrm{trk}}\rvert / \pi$	$1 - \lvert\phi_{\mu} - \phi(\mathbf{p}_{\mathrm{trks}})\rvert / \pi$	$1 - \lvert\phi_{\mu} - \phi_{e}\rvert / \pi$

Table 5. Definition of variables measured in each FR. The notation $\mathbf{p}$ indicates the four-vector of the related particles. The four-vector sum of the three selected tracks in the μ3T-FR is indicated as $\mathbf{p}_{\mathrm{trks}}$, i.e., $\mathbf{p}_{\mathrm{trks}} = \sum_{i=1}^{3} \mathbf{p}_{\mathrm{trk},i}$. If a variable is derived from a sum of four-vectors, the definition of that four-vector sum is provided in parentheses. Otherwise, the related particle is indicated as sub- or superscript.

are reconstructed in the SR, referred to as efficiency, is 0.34 for μ1T-FR, 0.33 for μ3T-FR, and 0.36 for μe-FR. The fiducial fractions are corrected for before unfolding by multiplying the background-subtracted data in each bin with the fiducial fraction corresponding to that particular bin. The efficiencies are corrected for in the application of the IBU method. The number of iterations in the IBU method is optimized to correspond to the minimal number where the χ^2-difference between unfolded data and the generated signal distribution does not change by more than 1% with further iterations. The resulting numbers of iterations are between one and four iterations depending on the considered distribution. The effect of systematic uncertainties on the background estimate, detector-level and particle-level inputs to the unfolding are described in section 8 and the uncertainties related to the unfolding procedure itself are described in this section.

JHEP10(2026)053

A bootstrap method [97] is used to propagate the statistical uncertainties of the data through the unfolding, allowing to determine the correlations between bins of the same unfolded distribution, and between different unfolded distributions in the same FR. Bootstrap replicas are constructed by assigning each data event a random weight based on a Poisson distribution with mean of one, and employing this to generate varied copies of the measured data distributions. The unfolding procedure is repeated for each bootstrap replica. The statistical covariance between two bins is defined relative to the mean bin content over all replicas. The statistical uncertainty in the unfolded data distribution is given by the square-root of the diagonal entries in the covariance matrix. To determine the statistical covariance matrix, 10 000 replicas were generated.

The statistical uncertainty in the background estimate is propagated with pseudo-experiments through the unfolding. For this purpose, the background predictions are varied randomly in each bin, assuming a Gaussian probability distribution centered on the nominal content with standard deviation corresponding to the background statistical uncertainty in this bin. The unfolding is repeated with the varied background estimates, and the covariance matrix is calculated as previously, with only correlations within the same distribution being accessible. To propagate the statistical uncertainty in the background prediction, 10 000 pseudo-experiments were used. The propagated statistical uncertainties in the background estimate are considered to be systematic uncertainties in the cross-section distributions.

The statistical uncertainty in the signal MC-based unfolding inputs is considered as further systematic uncertainty in the unfolding. It is determined with a simpler and faster unfolding method: a variant of bin-by-bin unfolding that accounts for correlations between detector-level and particle-level. The statistical uncertainties in the bin-by-bin weights, which are the ratios of the generated vs. reconstructed events per bin, are determined through error propagation [98], properly taking the statistical overlap of events in the numerator and denominator of the weights into account.

A data-driven non-closure uncertainty is determined to cover potential biases in the unfolding procedure arising from the potential mismodeling of the data by the nominal signal MC simulation, employed to produce the MC-based unfolding inputs. The uncertainty is determined using pseudodata generated from MC distributions that were re-weighted based on comparisons with data [99, 100]. More specifically, for each unfolded variable, a pseudodata generated signal distribution and — through folding with the correspondingly adjusted migration matrix — the related pseudodata signal reconstructed distribution is produced. The pseudodata reconstructed distribution is unfolded with the original (non-adjusted) signal MC unfolding inputs and the result compared with the pseudodata generated distribution. The difference between the two is considered as systematic uncertainty. The same numbers of iterations are used for the unfolding of the pseudodata reconstructed distribution as used in the unfolding of data. To reduce sensitivity to statistical fluctuations, six differently smoothed data-driven weights are tested to determine the pseudodata generated distribution, and the average over the unfolded results from these variations is used to provide the non-closure systematic uncertainty for each considered observable.

JHEP10(2026)053

8 Systematic uncertainties

The leading sources of uncertainty for this measurement are the statistical uncertainties of the data. In addition to these and the unfolding uncertainties, which are described in section 7, several sources of systematic uncertainties also affect this measurement. These include those arising from the trigger efficiency, object reconstruction and calibration, luminosity and the modeling of signal and background.

The uncertainties associated with the muon trigger efficiency include both statistical and systematic contributions and are applied to the muon trigger data-to-MC correction factors used to correct the simulated samples. The uncertainties associated with muon reconstruction and identification efficiency are applied to the muon reconstruction and identification correction factors. The systematic uncertainties in the muon trigger, reconstruction and identification efficiency correction factors are derived by varying selection requirements in the $\gamma\gamma \to \mu\mu$ tag-and-probe analysis used to derive the correction factors. Systematic uncertainties associated with the muon momentum scale and resolution corrections are determined following ref. [101]. The uncertainties associated with the electron and photon reconstruction and identification efficiency and energy scale and resolution corrections are derived following ref. [77].

The systematic uncertainty associated with the track reconstruction efficiency is determined using alternative MC samples that vary the detector material budget or the physics model for particle interactions in the detector material employed in the GEANT4 simulation. The tracking efficiency is studied as a function of the charged particle p_{T} and η, separately for charged pions, electrons, and muons. The impact of systematic variations in the tracking efficiency is propagated by randomly removing tracks in the nominal MC samples, according to the varied track efficiency in bins of p_{T} and $|\eta|$.

The uncertainty in the topocluster reconstruction efficiency and energy calibration is determined using $\gamma\gamma \to ee$ events in which one of the electrons emits a hard bremsstrahlung photon due to its interaction with the ID material. No data-to-MC correction factors are applied for the topocluster reconstruction efficiency but a global systematic uncertainty of 2% is assigned to cover small data-to-MC discrepancies. The uncertainty in topocluster energy calibration is assessed by applying additional corrections (shifts) to the reconstructed topocluster p_{T}, based on small data-to-MC discrepancies [77].

The estimate of the diffractive photonuclear background is impacted by both statistical and systematic uncertainties. The statistical uncertainty arises due to the limited number of events in the photonuclear background normalization region $4 \leq N^{\mathrm{unmatched}}_{\mathrm{topoclusters}} \leq 8$. The systematic uncertainty is estimated by using alternative control regions to construct diffractive photonuclear background templates. The control regions have the same event selections as the μ2T-CR and μ4T-CR, except that the net electric charge of the muon and the track/three-track system must be non-zero. The uncertainty is given by the difference between the diffractive photonuclear background estimate determined using the nominal control regions and that obtained using the alternative control regions.

To estimate the uncertainty arising from the modeling of the photon flux, parameters describing the proton and neutron densities are varied by their experimental uncertainties using the SUPERCHIC3 generator. In particular, the parameters $R_p = 6.68 \pm 0.02\,\mathrm{fm}$,

JHEP10(2026)053

$R_n = 6.69 \pm 0.03\,\text{fm}$, $a_p = 0.447 \pm 0.01\,\text{fm}$ and $a_n = 0.560 \pm 0.03\,\text{fm}$ are varied by their uncertainties, where $R_{p,n}$ and $a_{p,n}$ are the radius and skin depth of the proton and neutron densities, respectively [102–104]. The average of the largest absolute up and down deviations in the $\gamma\gamma \to \mu\mu$ cross-section, inclusive in forward neutron topologies, in bins of $m_{\mu\mu}$ and $|y_{\mu\mu}|$ is taken and symmetrized. Since the photon flux depends only on the invariant mass and rapidity of the centrally produced system (when $s \gg m_X^2$), the uncertainty computed using $\gamma\gamma \to \mu\mu$ events is also valid for $\gamma\gamma \to \tau\tau$ events. The uncertainty is of order 0.5% in bins with the largest number of observed $\gamma\gamma \to \tau\tau$ events i.e., $m_{\mu\mu} \lesssim 50$ GeV and $|y_{\mu\mu}| \lesssim 2.0$. In addition, a flat 2.5% uncertainty is assigned on the theoretical modeling of the survival factor [105]. The photon flux uncertainties are applied to both the $\gamma\gamma \to \tau\tau$ and $\gamma\gamma \to \mu\mu(\gamma)$ samples. The uncertainty in the GRFF is described in section 6. Potential correlations between the nuisance parameters in the fit to extract the GRFF and in the fits performed to extract the τ-lepton electromagnetic dipole moments, described in section 10, are not retained as the fits are performed independently to ensure that the GRFF extraction is free from any influence of signal. The uncertainties related to the modeling of τ-lepton decays are evaluated using alternative signal samples, which use Pythia 8 instead of Tauola to model τ-lepton decays. The uncertainty in the modeling of spin correlation effects is defined as the size of the bin-by-bin correction factor. The uncertainty in the $0n0n$ reweighting and the efficiency of the ZDC detectors are described in section 5.

The luminosity uncertainty for the combined 2015 and 2018 data is 1.5%. It is derived using beam-separation scans, following a similar method to ref. [106], and using LUCID-2 for the baseline luminosity measurements.

For presentation purposes, the systematic uncertainties in the cross-sections are grouped into categories. The impact of each group of systematic uncertainties for the unfolded muon p_{T} distribution in μ1T-FR, μ3T-FR and μe-FR for the combined 2015 and 2018 data are shown in figure 5. "Muon" includes all systematic uncertainties related to muon reconstruction, identification and calibration, "Trigger" includes muon trigger scale factor systematic uncertainties, "EGamma" includes electron and photon reconstruction, identification, energy scale and resolution systematic uncertainties, and topocluster systematic uncertainties. "Track" includes uncertainties in the track reconstruction efficiency, "Modeling" includes the $0n0n$ systematic uncertainties, photon flux, GRFF, spin correlation and τ-lepton decay systematic uncertainties. Finally, "Other" includes luminosity, background and unfolding uncertainties. Data statistical uncertainties are not shown as they are much larger than the systematic uncertainties. The largest uncertainty contributions in many bins come from the "Trigger", "Modeling", and "Other" categories.

9 Differential fiducial cross-sections

The differential fiducial cross-sections are measured in the FRs combining the 2015 and 2018 data before unfolding, and treating systematic uncertainties as correlated between the two data samples. The consistency of the 2015 and 2018 data was verified beforehand, and the two datasets were found to agree within uncertainties. The cross-sections per-bin are estimated by dividing the unfolded number of events by the bin width and the central value of the 2015 and 2018 luminosity. The last bin of the measured cross-sections is normalized by the bin

JHEP10(2026)053

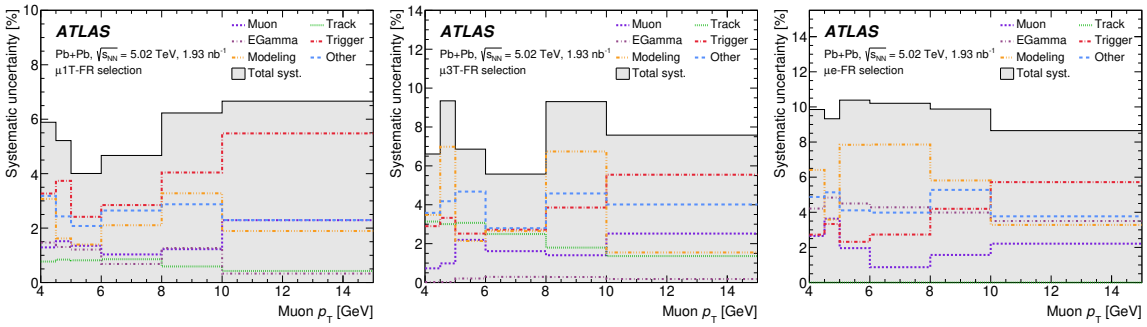


Figure 5. Grouped systematic uncertainties in the cross-sections per bin of leading muon p_{T} for μ1T-FR (left), μ3T-FR (middle) and μe-FR (right) for the combined 2015 and 2018 data. The contents of the various categories are explained in the text.

width of the last detector-level bin. Figures 6, 7 and 8 show the measured differential fiducial cross-sections for the μ1T-FR, μ3T-FR, and μe-FR, respectively. Beyond enabling constraints on τ-lepton electromagnetic dipole moments a_τ and d_τ, these measurements probe initial-state and final-state dynamics including photon-flux modeling and the underlying nuclear form factors, as well as spin-correlation effects and higher-order electroweak corrections.

The measured differential cross-sections are compared with several SM signal predictions. The nominal $\gamma\gamma \to \tau\tau$ signal sample with the application of the GRFF, STARLIGHT/SUPERCHIC (GRFF) + PYTHIA 8 + TAUOLA (short form SL/SC(GRFF) + PY8 + T) is shown, and with the application of the GRFF and spin-correlation corrections, STARLIGHT/SUPERCHIC (GRFF) + PYTHIA 8 + TAUOLA + Spin-correlations (short form SL/SC(GRFF) + PY8 + T + **S**-corr) for μ1T-FR. In addition, predictions removing the reweighting to the SUPERCHIC photon flux, i.e., utilizing the original STARLIGHT photon flux STARLIGHT + PYTHIA 8 + TAUOLA (short form SL + PY8 + T) are shown. For the above listed predictions PHOTOS++ was used to simulate FSR from the charged decay products of the τ-leptons.

Predictions using the GAMMA-UPC 1.0 generator integrated with MADGRAPH 3.5.1 and using PYTHIA 8.245 to handle τ-lepton decays and FSR from the τ-leptons and PHOTOS++ 3.61 [57] to simulate FSR from the charged decay products of τ-leptons are also displayed. Two different assumptions on the modeling of the ion nucleus form factor, and hence the photon flux, are shown. The electric dipole form factor approach (short form γUPC(EDFF) + MG5 + PY8) assumes a point-like distribution for the Pb charge, but restricts the impact parameter integration range to distances from the nucleus center larger than the geometric nuclear radius, similarly to STARLIGHT. The charged form factor approach (short form γUPC(CHFF) + MG5 + PY8) assumes a 3-parameter Woods-Saxon distribution for the Pb charge, with no restriction on the impact parameter integration range, similarly to SUPERCHIC.

For the μe-FR, NLO electroweak (EW) predictions based on the results of ref. [107] are shown (short form JHEP08(2025)051 (NLO)). The authors do the full matrix element calculation for the $\gamma\gamma \to \tau^+\tau^- \to e^+\mu^- 4\nu$ process instead of splitting the calculation between the τ-lepton pair production and decay, thereby retaining full spin correlation effects. A mixed EW input parameter scheme is utilized and the GAMMA-UPC charged form factor

JHEP10(2026)053

photon flux is used for the initial state, so the predictions are at a similar scale as the γUPC(CHFF) + MG5 + Py8 predictions. The NLO predictions shown in figure 8 were prepared by the authors of ref. [107] including applying an additional weighting factor for the combined EM-pileup-corrected $0n0n$ weights, since the results of ref. [107] are nominally presented for the case where no requirement on forward neutron activity is imposed.

Overall, reasonable agreement is observed between the measured differential fiducial cross-sections and the SM predictions in most of the bins. The p_{T} of the visible di-τ system ($p_{\mathrm{T}}(\mu, \mathrm{trk})$, $p_{\mathrm{T}}(\mu, \mathrm{trks})$, $p_{\mathrm{T}}(\mu, e)$ in μ1T-FR, μ3T-FR and μe-FR, respectively) shows a slope in the ratio of the nominal prediction to data, though in opposite directions in μ1T-FR vs. μ3T-FR and μe-FR. For the nominal sample, the GRFF and spin-correlation corrections improve the agreement with the unfolded data. The predictions using the STARlight photon flux (STARlight + Pythia 8 + Tauola) and the gamma-UPC electric dipole form factor photon flux (γUPC(EDFF) + MG5 + Py8) shows poorer agreement with the data for most bins across the various distributions in all FRs.

The difference between the photon flux description in SuperChic and STARlight has the largest impact on the predictions where predictions with the photon flux from STARlight are typically below the ones from Superchic. The difference between the two predictions is typically in the range of 10% and 30%. The NLO EW predictions shown for the μe-FR are typically ∼1–2% lower than the corresponding leading-order prediction. The overall measurement precision ranges typically between 12% and 45%, depending on the bin, the observable and the FR.

10 Determination of the τ-lepton's electromagnetic moments

The values of the electromagnetic moments of the τ-lepton (a_τ and d_τ) can influence the interaction probabilities for $\gamma\gamma \to \tau\tau$ production and modify the expected event yields and the shape of differential distributions. To extract the values of a_τ and d_τ best describing the data, predictions for a range of a_τ and d_τ values are required. An event-level reweighting procedure, using generator-level τ-lepton kinematics and SM tree-level (i.e., $a_\tau = d_\tau = 0$) QED matrix element calculations of the $\gamma\gamma \to \tau\tau$ process, was employed to obtain these templates. In this procedure, the $\gamma\tau\tau$ vertex function is parameterized, depending on the momentum transfer, q, as follows:

$$i\Gamma_{\mu}^{(\gamma\tau\tau)}(q) = -ie\left[\gamma_\mu F_1(q^2) + \frac{i}{2m_\tau}\sigma_{\mu\nu}q^\nu F_2(q^2) + \frac{1}{2m_\tau}\gamma^5\sigma_{\mu\nu}q^\nu F_3(q^2)\right], \tag{10.1}$$

where $F_1(q^2)$ and $F_2(q^2)$ are the Dirac and Pauli form factors, $F_3(q^2)$ is the electric dipole form factor and $\sigma_{\mu\nu} = i[\gamma_\mu, \gamma_\nu]/2$ denotes the spin tensor, proportional to the commutator of the gamma matrices. In the limit $q^2 \to 0$ GeV^2, the asymptotic values of the form factors describe the electromagnetic properties of the τ-lepton, with:

$$F_1(0) = 1\,,\ F_2(0) = a_\tau\,,\ \text{ and } F_3(0) = d_\tau\frac{2m_\tau}{e}\,. \tag{10.2}$$

Since the photon virtualities in UPC Pb+Pb collisions at the LHC are near-zero, this asymptotic condition is well satisfied. A similar parameterization was employed in previous

JHEP10(2026)053

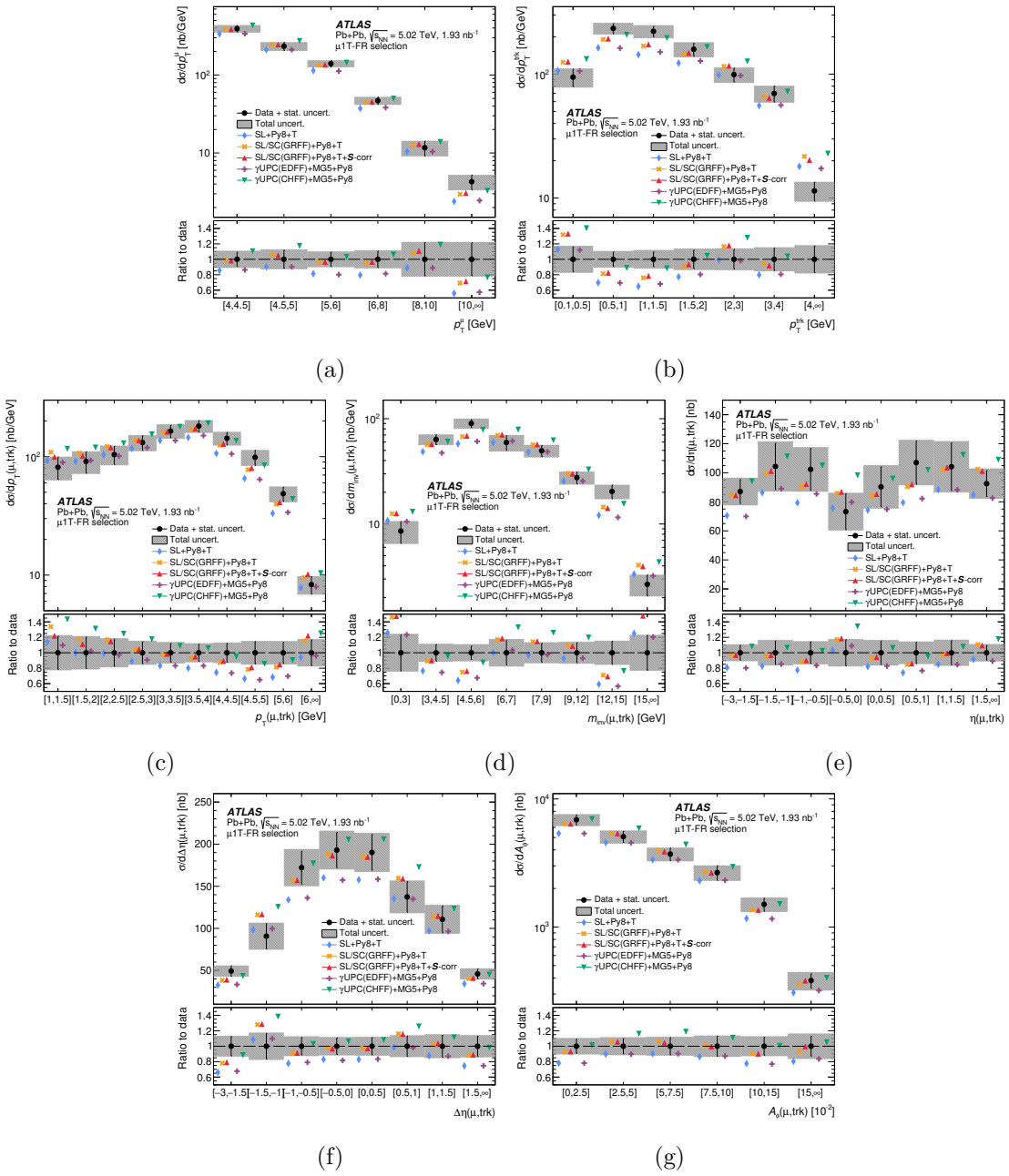


Figure 6. Differential fiducial cross-sections at particle-level for the variables (a) muon p_{T}, (b) track p_{T}, (c) $p_{\mathrm{T}}\,(\mu,\mathrm{trk})$, (d) $m(\mu,\mathrm{trk})$, (e) $\eta(\mu,\mathrm{trk})$, (f) $\Delta\eta\,(\mu,\mathrm{trk})$, and (g) $A_{\phi}^{\mu,\mathrm{trk}}$, in the μ1T-FR, using combined 2015 and 2018 data. The statistical uncertainty in the data (error bars) and the total uncertainty (hatched band) are shown. The cross-sections are compared with several SM $\gamma\gamma \to \tau\tau$ predictions: nominal with GRFF (SL/SC(GRFF) + Py8 + T), nominal with GRFF and spin correlations (SL/SC(GRFF) + Py8 + T + **S**-corr), varied photon-flux modeling (SL + Py8 + T), gamma-UPC predictions with the electric dipole form factor photon-flux (γUPC(EDFF) + MG5 + Py8) and the charged form factor photon-flux (γUPC(CHFF) + MG5 + Py8). The error bars on the leading-order predictions are the statistical uncertainty. The lower panel displays the ratio of these predictions to data. The respective bin sizes are indicated in square brackets on the x-axis. Infinity is used to represent the upper boundary of the fiducial region, within the definitions given in table 5.

JHEP10(2026)053

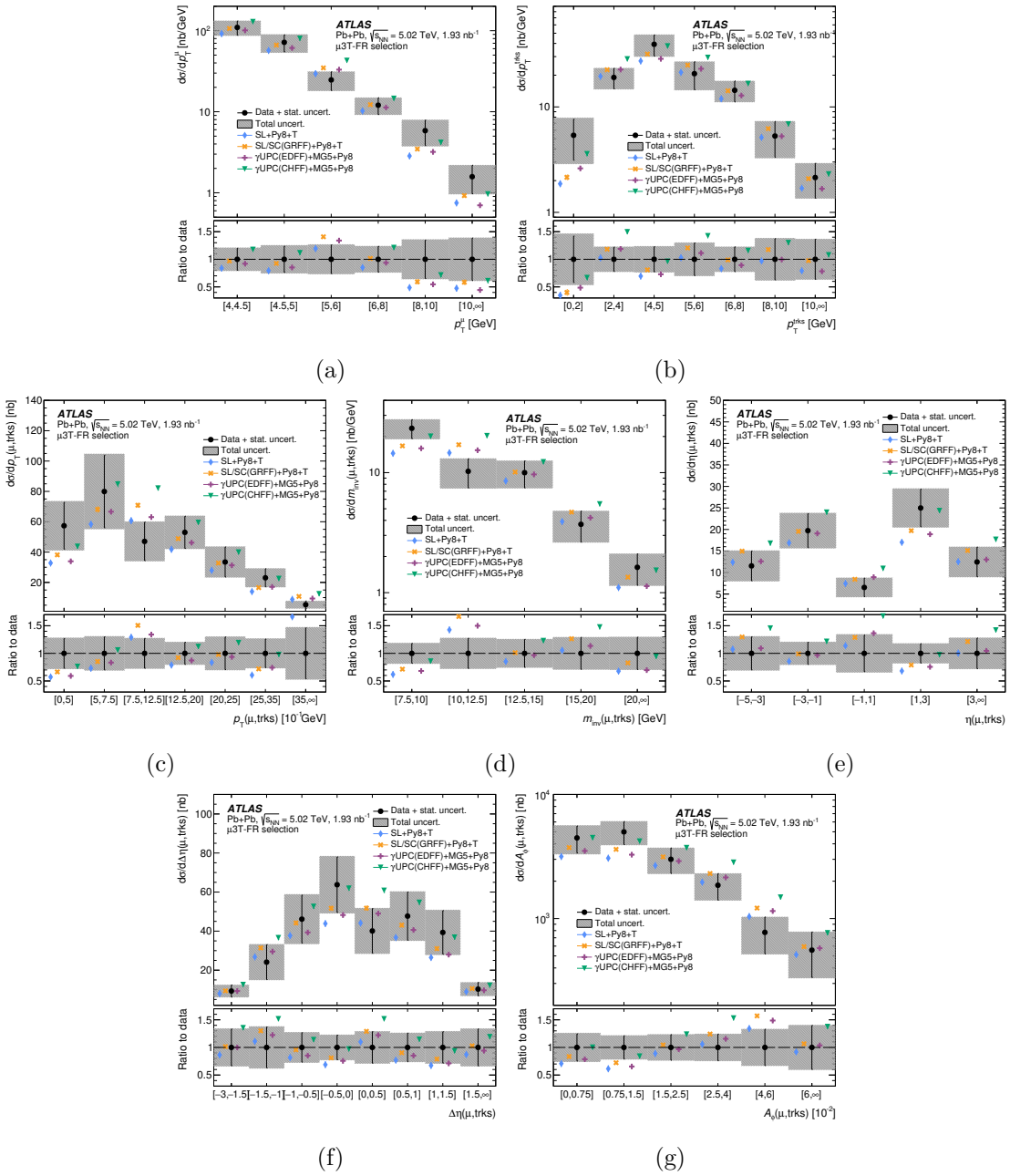


Figure 7. Differential fiducial cross-sections at particle-level for the variables (a) muon p_{T}, (b) p_{T} (trks), (c) p_{T} (μ, trks), (d) $m(\mu, \mathrm{trks})$, (e) $\eta(\mu, \mathrm{trks})$, (f) $\Delta\eta\,(\mu, \mathrm{trks})$, and (g) $A_{\phi}^{\mu,\mathrm{trks}}$, in the μ3T-FR, using combined 2015 and 2018 data. The statistical uncertainty in the data (error bars) and the total uncertainty (hatched band) are shown. The cross-sections are compared with several SM $\gamma\gamma \to \tau\tau$ predictions: nominal with GRFF (SL/SC(GRFF) + Py8 + T), varied photon-flux modeling (SL + Py8 + T), gamma-UPC predictions with the electric dipole form factor photon-flux (γUPC(EDFF) + MG5 + Py8) and the charged form factor photon-flux (γUPC(CHFF) + MG5 + Py8). The error bars on the leading-order predictions are the statistical uncertainty. The lower panel displays the ratio of these predictions to data. The respective bin sizes are indicated in square brackets on the x-axis. Infinity is used to represent the upper boundary of the fiducial region, within the definitions given in table 5.

JHEP10(2026)053

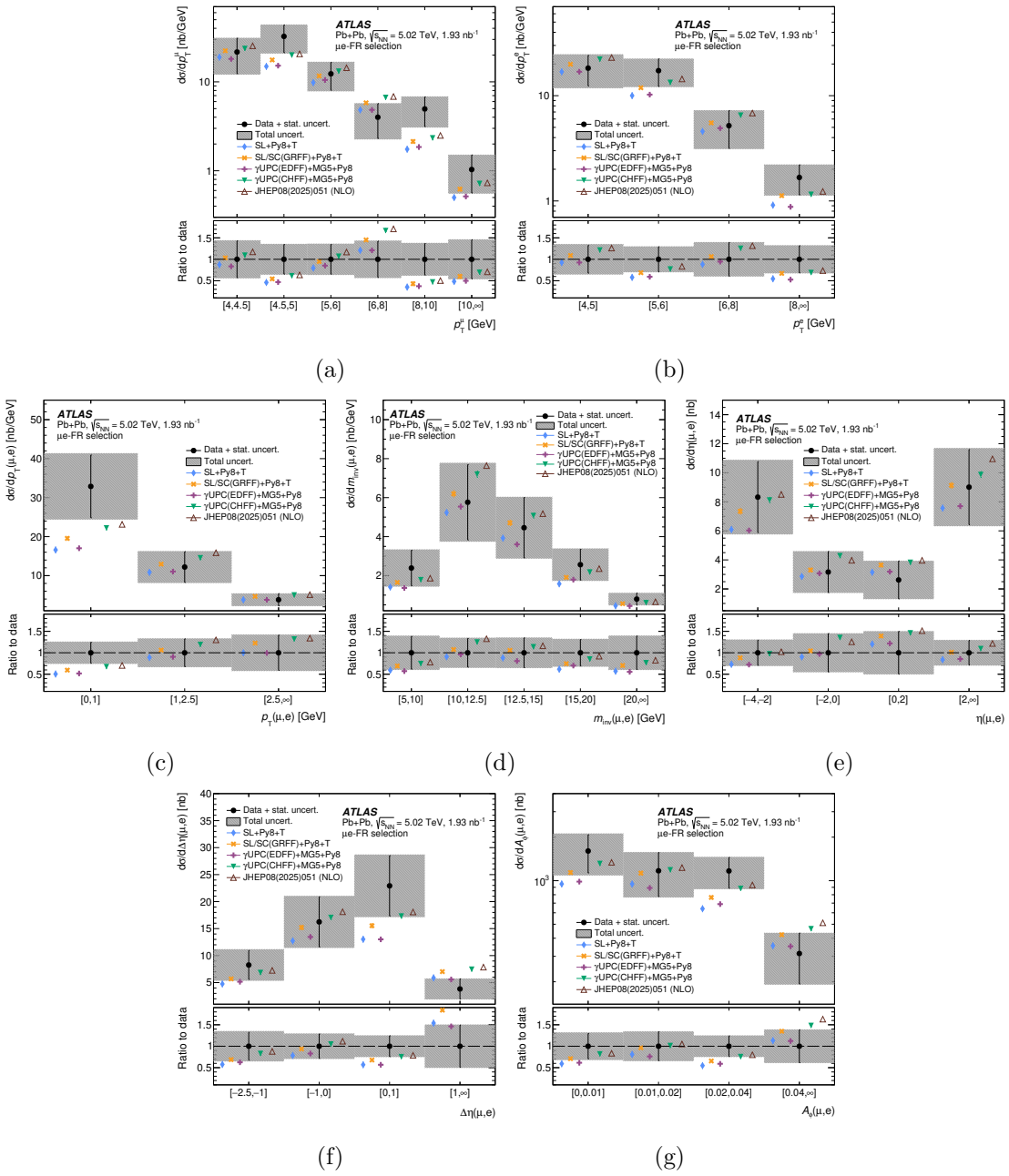


Figure 8. Differential fiducial cross-sections at particle-level for the variables (a) muon p_{T}, (b) electron p_{T}, (c) $p_{\mathrm{T}}\,(e,\mu)$, (d) $m(e,\mu)$, (e) $\eta(e,\mu)$, (f) $\Delta\eta\,(e,\mu)$, and (g) $A_{\phi}^{e,\mu}$, in the μe-FR, using combined 2015 and 2018 data. The statistical uncertainty in the data (error bars) and the total uncertainty (hatched band) are shown. The cross-sections are compared with several SM $\gamma\gamma \to \tau\tau$ predictions: nominal with GRFF (SL/SC(GRFF) + Py8 + T), varied photon-flux modeling (SL + Py8 + T), gamma-UPC predictions with the electric dipole form factor photon-flux (γUPC(EDFF) + MG5 + Py8) and the charged form factor photon-flux (γUPC(CHFF) + MG5 + Py8), and NLO predictions (JHEP08(2025)051 (NLO)). The error bars on the leading-order predictions are the statistical uncertainty. The lower panel displays the ratio of these predictions to data. The respective bin sizes are indicated in square brackets on the x-axis. Infinity is used to represent the upper boundary of the fiducial region, within the definitions given in table 5.

JHEP10(2026)053

ATLAS and LEP results [14, 17, 21, 22]. More details on the event-level reweighting procedure are provided in appendix A. To extract the best-fit a_τ and d_τ values, 76 templates were produced for each a_τ and $F_3\,(0)$ with a spacing of 0.002 for $|a_\tau$ or $F_3\,(0)\,| < 0.06$ and a spacing of 0.005 for $0.06 < |a_\tau$ or $F_3\,(0)\,| < 0.10$. The weights are applied to the nominal STARLIGHT/SUPERCHIC + PYTHIA 8 + TAUOLA signal MC simulation. Furthermore, the GRFF is also applied for both the $\gamma\gamma \to \tau\tau$ MC simulation, and the $\gamma\gamma \to \mu\mu(\gamma)$ background simulation. Effects of spin correlations between the two produced τ-leptons in $\gamma\gamma \to \tau\tau$ production, and their propagation to the τ-lepton decay products are included for μ1T-SR via bin-by-bin correction factors.

The values of a_τ and d_τ best describing the data are extracted using a maximum-likelihood fit [88, 108, 109] of the detector-level muon p_{T} distributions in the three SRs, μ1T-SR, μ3T-SR, and μe-SR, as muon p_{T} was found to be the most sensitive variable from a set of tested variables. The fits are performed independently, assuming the tree-level SM value for a_τ, i.e., zero, in the d_τ fit and vice versa. The likelihood $\mathcal{L}$ for the parameter of interest (POI) a_τ or d_τ is given as the product of the Poisson probability distributions of the observed event count in data n_i given the expected values ν_i for each bin i of these distributions:

$$\mathcal{L}(a_\tau) = \prod_{i \in \text{ bins}} P\left(n_i | \nu_i\left(a_\tau \text{ or } d_\tau, \boldsymbol{\theta}\right)\right) \times \prod_{j \in \text{ NPs}} G(\theta_j) \tag{10.3}$$

The expected values ν_i include the $\gamma\gamma \to \tau\tau$ signal prediction as a function of a_τ or d_τ and the background estimates. Systematic uncertainties $\boldsymbol{\theta}$ are added as nuisance parameters (NPs) in the fit, including additional terms with Gaussian probability distributions $G(\theta_j)$ centered at zero with standard deviations corresponding to the respective systematic uncertainty θ_j. In this way, large shifts in the nuisance parameters are penalized through a reduction of the overall likelihood, while small shifts are possible if the agreement with data is improved in this way. Statistical uncertainties in the background predictions are included as separate nuisance parameters for each bin. Statistical uncertainties in the signal MC prediction largely fall below a minimal-size threshold of 0.3% and those that do fall below this threshold are neglected in the fit to improve numerical stability. In the fit, the value of a_τ or d_τ that minimizes the negative log-likelihood (NLL) is extracted.

The data are compared with the post-fit expectations for the a_τ and d_τ fits, shown in figure 9. The best-fit predictions agree better with data, compared with the pre-fit predictions shown in figure 4, as expected. In particular, at high muon p_{T} the small pre-fit data excess is reduced.

A pseudodata-derived correction is used to obtain the Confidence Intervals (CIs) for a_τ and d_τ since the typically used asymptotic assumption relies on Wilk's Theorem [110]. Wilk's Theorem may not be valid for cases where the parameters of interest involve a quadratic cross-section dependence [111], which is the case for both a_τ and d_τ. Observed and expected NLL scan curves for a_τ and d_τ combined fits to all SRs (the latter in units of $F_3(0)$), normalized to their minimum ΔNLL, are shown in figure 10. The 68% and 95% coverage lines, under the asymptotic assumption, are shown by the dotted lines. The 68% and 95% coverage points, calculated using pseudodata, are also shown. These points are calculated following the approach presented in ref. [112]. Rather than assuming a χ^2 distribution of the profile-likelihood-ratio (PLR), pseudodata are used to directly generate the PLR distribution of

JHEP10(2026)053

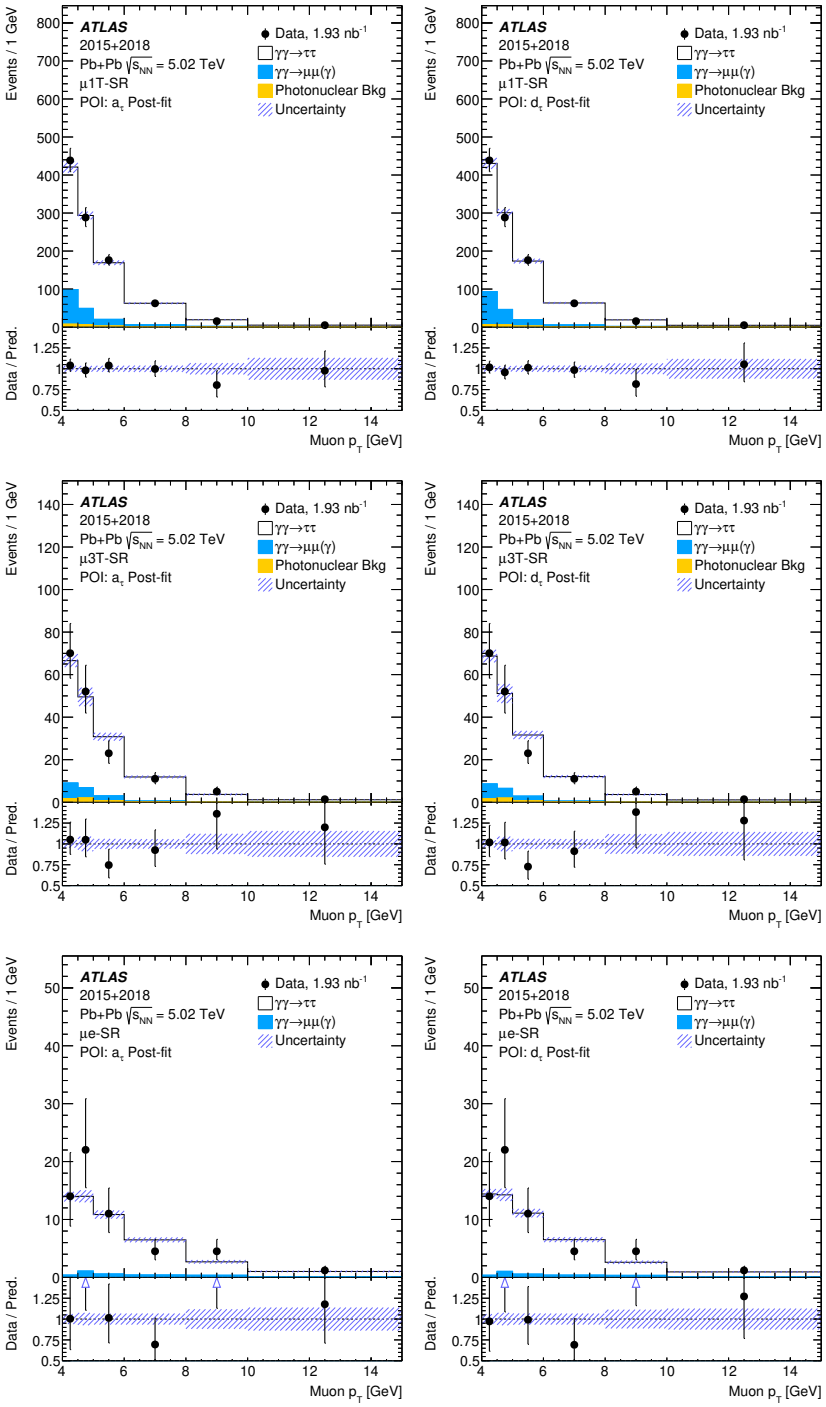


Figure 9. Muon p_{T} distributions in the (top) μ1T-SR, (middle) μ3T-SR, (bottom) μe-SR. Data (filled markers) are compared with the post-fit predictions for the a_τ fit (left) and d_τ fit (right) summing signal and background contributions (stacked histograms). Event counts are shown normalized by bin width. The bottom panel displays the ratio of the data to post-fit predictions. Uncertainties from the finite number of data events (filled markers) and $\pm 1\sigma$ systematic uncertainties of the prediction with the constraints from the fit applied (hatched bands) are indicated to better judge variations between data and predictions. Arrows in the ratio panel denote a data point outside the displayed range.

JHEP10(2026)053

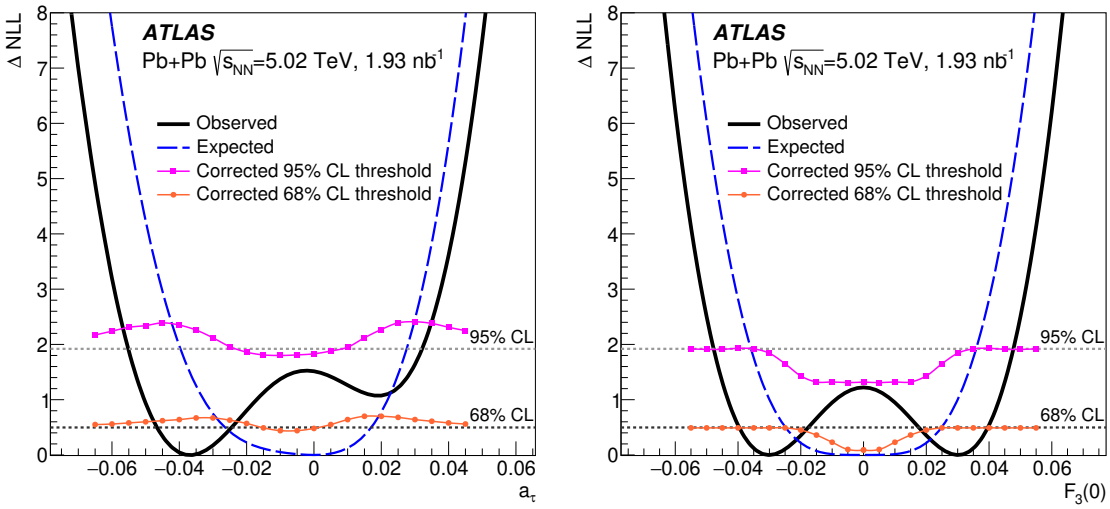


Figure 10. Observed and expected NLL curves for the combined fit to all SRs, normalized to its minimum ΔNLL, as a function of a_τ (left) and $F_3(0)$ (right). The coverage-corrected threshold points, calculated via pseudoexperiments [112], and interpolated lines for 68% and 95% coverage are shown.

many pseudoexperiments, and NLL thresholds with correct coverage are calculated. Coverage lines are then obtained by interpolating between the points. CIs are calculated by determining the intersections between the NLL-scan curves and the coverage-corrected lines.

The measured best-fit value for a_τ from the combined fit is $a_\tau = -0.037$ and the CIs are $(-0.048, -0.023)$ and $(-0.057, 0.035)$ at 68% and 95% CL, respectively. The measured best-fit value for d_τ from the combined fit is $|d_\tau| = 1.7 \times 10^{-16}$ $e$cm. The CIs for d_τ are $(-1.1, -2.2) \times 10^{-16}$ $e$cm and $(1.1, 2.2) \times 10^{-16}$ $e$cm at 68% CL and $|d_\tau| < 2.7 \times 10^{-16}$ $e$cm at 95% CL. The higher-than-expected observed yields lead to the highly asymmetric 68% CL interval for a_τ and the double minima for d_τ. This arises from the nearly quadratic signal cross-section dependence on a_τ and the quadratic dependence on d_τ, caused by the interference of the SM and BSM amplitudes [21, 22, 27, 35]. Figure 11 shows the obtained constraints on a_τ and d_τ for the combined fit together with a selection of the most precise existing constraints from pp and Pb+Pb collisions at the LHC [14–16] and e^+e^- collisions at LEP [17, 21, 22]. Only constraints for which $q^2 \sim 0$ GeV^2 are shown. The current strongest constraints on a_τ and d_τ are set by CMS using pp collisions. The constraints on a_τ obtained by this analysis using Pb+Pb collisions are of similar sensitivity to previous constraints obtained using Pb+Pb collisions and e^+e^- collisions at LEP. For $|d_\tau|$ the presented results are the first constraints obtained using Pb+Pb collisions and they are competitive with constraints from DELPHI, OPAL and L3.

JHEP10(2026)053

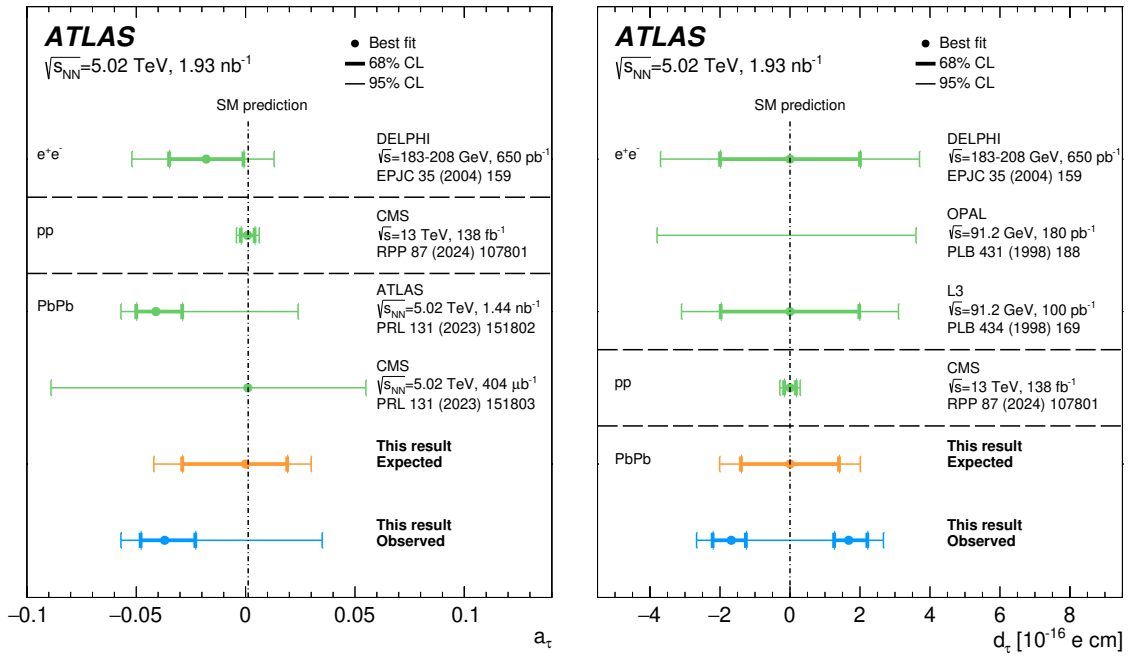


Figure 11. Constraints on a_τ (left) and d_τ (right) from the combined fit to the three SRs. The observed confidence intervals obtained from the combined fit to data are displayed together with the best-fit value, at 68% and 95% confidence level. The observed 68% CL interval is highly asymmetric for a_τ and has double minima for d_τ due to the higher-than-expected observed yields. The expected interval from the combined fit, representing the median sensitivity assuming only SM processes occur, is also shown. The obtained results are compared with a selection of the most precise previous measurements from the OPAL, L3 and DELPHI experiments at LEP, and from ATLAS and CMS at the LHC.

11 Conclusion

This paper presents the first differential fiducial measurements of photon-induced τ-lepton pair production in ultra-peripheral Pb+Pb collisions. The measurement uses the full Run 2 Pb+Pb data sample recorded by the ATLAS experiment at the LHC at $\sqrt{s_{\mathrm{NN}}} = 5.02$ TeV with an integrated luminosity of 1.93 nb^{-1}. The phase space of the measurement is chosen to suppress breakup of the lead ions by selecting events without forward neutron emission. This ensures that both initial photons are almost on-shell with virtuality $q^2 \sim 0$ GeV^2. Fiducial cross-sections are measured as a function of seven different kinematic variables for three different final state configurations from the τ-lepton decays. The cross-sections are compared with several leading-order SM theoretical predictions and with a NLO electroweak prediction for the one muon plus one electron fiducial region. For the predictions, several different photon flux models are compared. The measured cross-sections are found to be largely compatible with the theoretical predictions within measurement uncertainties. The precision of the measurements is limited by statistical uncertainties. A fit to the detector-level muon-p_{T} distributions in each of the three SRs is used to set constraints on the τ-lepton electromagnetic dipole moments. A data-driven correction is applied to the photon flux for the $\gamma\gamma \to \tau\tau$ and $\gamma\gamma \to \mu\mu(\gamma)$ predictions used in the fit. The correction is derived using a dedicated di-muon control region, exploiting the process independence of the initial-state

JHEP10(2026)053

photon flux. The observed 95% CL intervals from the combined fit to the three SRs are $-0.057 < a_\tau < 0.035$ and $|d_\tau| < 2.7 \times 10^{-16}$ $e$cm. For a_τ the achieved constraints are of similar precision to existing lepton-collider and Pb+Pb constraints. For d_τ the achieved precision is competitive with existing lepton-collider precision and the presented results are the first constraints obtained using Pb+Pb data.

Acknowledgments

We thank CERN for the very successful operation of the LHC and its injectors, as well as the support staff at CERN and at our institutions worldwide without whom ATLAS could not be operated efficiently.

The crucial computing support from all WLCG partners is acknowledged gratefully, in particular from CERN, the ATLAS Tier-1 facilities at TRIUMF/SFU (Canada), NDGF (Denmark, Norway, Sweden), CC-IN2P3 (France), KIT/GridKA (Germany), INFN-CNAF (Italy), NL-T1 (Netherlands), PIC (Spain), RAL (U.K.) and BNL (U.S.A.), the Tier-2 facilities worldwide and large non-WLCG resource providers. Major contributors of computing resources are listed in ref. [113].

We gratefully acknowledge the support of ANPCyT, Argentina; YerPhI, Armenia; ARC, Australia; BMWFW and FWF, Austria; ANAS, Azerbaijan; CNPq and FAPESP, Brazil; NSERC, NRC and CFI, Canada; CERN; ANID, Chile; CAS, MOST, NSFC and FRFCU, China; Minciencias, Colombia; MEYS CR, Czech Republic; DNRF and DNSRC, Denmark; IN2P3-CNRS and CEA-DRF/IRFU, France; SRNSFG, Georgia; BMFTR, HGF and MPG, Germany; GSRI, Greece; RGC and Hong Kong SAR, China; ICHEP and Academy of Sciences and Humanities, Israel; INFN, Italy; MEXT and JSPS, Japan; CNRST, Morocco; NWO, Netherlands; RCN, Norway; MNiSW, Poland; FCT, Portugal; MNE/IFA, Romania; MSTDI, Serbia; MSSR, Slovakia; ARIS and MVZI, Slovenia; DSI/NRF, South Africa; MICIU/AEI, Spain; SRC and Wallenberg Foundation, Sweden; SERI, SNSF and Cantons of Bern and Geneva, Switzerland; NSTC, Taipei; TENMAK, Türkiye; STFC/UKRI, United Kingdom; DOE and NSF, United States of America.

Individual groups and members have received support from BCKDF, CANARIE, CRC and DRAC, Canada; CERN-CZ, FORTE and PRIMUS, Czech Republic; COST, ERC, ERDF, Horizon 2020 and Marie Skłodowska-Curie Actions, European Union; Investissements d'Avenir Labex, Investissements d'Avenir Idex and ANR, France; DFG and AvH Foundation, Germany; Herakleitos, Thales and Aristeia programmes co-financed by EU-ESF and the Greek NSRF, Greece; BSF-NSF and MINERVA, Israel; NCN and NAWA, Poland; La Caixa Banking Foundation, CERCA and AGAUR programs from Generalitat de Catalunya and PROMETEO and GenT Programmes Generalitat Valenciana, Spain; Göran Gustafssons Stiftelse, Sweden; The Royal Society and Leverhulme Trust, United Kingdom; Eric and Wendy Schmidt Fund for Strategic Innovation, United States of America.

In addition, individual members wish to acknowledge support from Chile: Agencia Nacional de Investigación y Desarrollo (ANID FONDECYT reg. 1230987, FONDECYT 1230812, FONDECYT 1240864, Fondecyt 3240661, Fondecyt Regular 1240721); China: Fundamental Research Funds for the Central Universities (010-63263105), Chinese Ministry of Science and Technology (MOST-2023YFA1605700, MOST-2023YFA1609300), National

JHEP10(2026)053

Natural Science Foundation of China (NSFC 12275265, NSFC-W2543005); Czech Republic: Czech Science Foundation (GACR — 24-11373S), Ministry of Education Youth and Sports (ERC-CZ-LL2327, FORTE CZ.02.01.01/00/22_008/0004632); EU: H2020 European Research Council (ERC — 101002463); European Union: European Research Council (BARD No. 101116429, ERC — 101219398, ERC 101089007), European Regional Development Fund (HE COFUND GA No.101081355, ERDF), Marie Sklodowska-Curie Actions (GAP-101168829); France: Agence Nationale de la Recherche (ANR-21-CE31-0013, ANR-22-EDIR-0002, ANR-24-CE31-0504-01); Germany: Deutsche Forschungsgemeinschaft (DFG — 469666862); China: Research Grants Council (GRF); Italy: Istituto Nazionale di Fisica Nucleare (LHC-MIUR — 28003/2025), Ministero dell'Università e della Ricerca (NextGenEU I53D23000820006 M4C2.1.1, SOE2024_0000023); Japan: Japan Society for the Promotion of Science (JSPS KAKENHI JP25H0063, JSPS KAKENHI JP22H04944, JSPS KAKENHI JP24K23939, JSPS KAKENHI JP24KK0251, JSPS KAKENHI JP25H00650, JSPS KAKENHI JP25H01291, JSPS KAKENHI JP25K01011, JSPS KAKENHI JP25K01023, JSPS KAKENHI JP25KK0047); Poland: Polish National Science Centre (NCN 2021/42/E/ST2/00350, NCN OPUS 2023/51/B/ST2/02507, NCN OPUS nr 2022/47/B/ST2/03059, NCN UMO-2019/34/E/ST2/00393, UMO-2022/47/O/ST2/00148, UMO-2023/49/B/ST2/04085, UMO-2023/51/B/ST2/00920, UMO-2024/53/N/ST2/00869); Spain: Agència de Gestió d'Ajuts Universitaris i de Recerca. (AGAUR — 2023 BP 00141), Ministry of Science and Innovation (RYC2019-028510-I, RYC2020-030254-I, RYC2021-031273-I, RYC2022-038164-I), Ministerio de Ciencia, Innovación y Universidades/Agencia Estatal de Investigación (EU NextGenerationEU (PRTR-C17.I1), PID2022-142604OB-C22); Sweden: Carl Trygger Foundation (Carl Trygger Foundation CTS 22:2312), Swedish Research Council (Swedish Research Council 2023-04654, VR 2021-03651, VR 2022-03845, VR 2022-04683, VR 2023-03403, VR 2024-05451, VR 2025-05940), Knut and Alice Wallenberg Foundation (KAW 2023.0366); United Kingdom: The Binks Trust, Royal Society (NIF-R1-231091); United States of America: U.S. Department of Energy (ECA DE-AC02-76SF00515), John Templeton Foundation (John Templeton Foundation 63206), Neubauer Family Foundation.

JHEP10(2026)053

A Event-level reweighting for non-zero a_τ and d_τ predictions

Predictions with non-zero a_τ or d_τ values are obtained through an event-level reweighting procedure, applied to the nominal signal MC prediction. In this procedure, the photon-lepton vertex is parameterized using form factors $F_2\left(q^2\right)$ and $F_3\left(q^2\right)$ as shown in eq. (10.1) in section 10, where the asymptotic form factor values for the squared momentum transfer $q^2 \to 0$ GeV^2 are related to a_τ and d_τ, respectively. The event-level reweighting procedure provides predictions both for non-zero a_τ and non-zero d_τ values.

The event-level weights are determined from tree-level QED matrix element calculations of the $\gamma\gamma \to \tau\tau$ process. For this, the four-momenta of the particles are defined as follows:

$$p^\mu_{\gamma_1} = (E, E\hat{z})\,, \qquad p^\mu_{\tau^+} = (E, \vec{p})\,, \tag{A.1}$$

$$p^\mu_{\gamma_2} = (E, -E\hat{z})\,, \qquad p^\mu_{\tau^-} = (E, -\vec{p})\,, \tag{A.2}$$

where $\vec{p} = (0, \beta E \sin\theta, \beta E \cos\theta)$ is the 3-momentum of the τ-leptons with $\beta = \sqrt{1 - \frac{m_\tau^2}{E^2}}$ being the boost and θ being the longitudinal angle. Since the physics of interest in this

$2 \to 2$ process is invariant under coordinate transformations, the kinematics are defined in the center-of-mass frame with $p_x = 0$ for convenience. By definition, the virtuality of the photons in the initial-state is $q^2 = 0$ GeV^2.

The matrix element of the $\gamma\gamma \to \tau\tau$ process is calculated using spin-polarization sums, and factorized in the form factors $F_{2,3}(0)$ as:

$$|\mathcal{M}(\beta, \theta, F_2(0), F_3(0))|^2 = \sum_{i,j=0}^{4} [F_2(0)]^i [F_3(0)]^j C_{ij} \tag{A.3}$$

where the non-zero parts of C_{ij} are:

$$C_{00} = \frac{-\beta^4 (\sin^4\theta + 1) + 2\beta^2 \sin^2\theta + 1}{(\beta^2 \cos^2\theta - 1)^2} \tag{A.4}$$

$$C_{10} = -\frac{4}{\beta^2 \cos^2\theta - 1} \tag{A.5}$$

$$C_{20} = \frac{2(-2\beta^2 \cos 2\theta - 3\beta^2 + 5)}{(\beta^2 - 1)(\beta^2 \cos 2\theta + \beta^2 - 2)} \tag{A.6}$$

$$C_{30} = \frac{4(-\beta^2 \cos 2\theta + 1)}{(\beta^2 - 1)(\beta^2 \cos 2\theta + \beta^2 - 2)} \tag{A.7}$$

$$C_{40} = \frac{\beta^4 (-\cos^4\theta - 2\cos^2\theta + 2) + 2\beta^2 \cos 2\theta - 1}{4(\beta^2 - 1)^2 (\beta^2 \cos^2\theta - 1)} \tag{A.8}$$

$$C_{02} = \frac{2(-2\beta^2 \cos 2\theta - \beta^2 + 3)}{(\beta^2 - 1)(\beta^2 \cos 2\theta + \beta^2 - 2)} \tag{A.9}$$

$$C_{12} = \frac{4(-\beta^2 \cos 2\theta + 1)}{(\beta^2 - 1)(\beta^2 \cos 2\theta + \beta^2 - 2)} \tag{A.10}$$

$$C_{22} = \frac{\beta^4 (-\cos^4\theta - 2\cos^2\theta + 2) + 2\beta^2 \cos 2\theta - 1}{2(\beta^2 - 1)^2 (\beta^2 \cos^2\theta - 1)} \tag{A.11}$$

$$C_{04} = \frac{\beta^4 (-\cos^4\theta - 2\cos^2\theta + 2) + 2\beta^2 \cos 2\theta - 1}{4(\beta^2 - 1)^2 (\beta^2 \cos^2\theta - 1)} \tag{A.12}$$

The C_{00} term corresponds to the tree-level SM case (i.e., $a_\tau = d_\tau = 0$). The predicted small non-zero a_τ and d_τ values are neglected in the used leading-order SM signal samples. For d_τ, the approach above means that the linear dependence of the cross-section on d_τ is zero, and only the quadratic dependence on d_τ is non-zero. In the determination of the C_{ij} above, this is visible through $C_{01} = 0$.

The determined weights are applied based on the generator-level $\tau\tau$ kinematics. For this purpose, the four-vectors of the τ-leptons $p_{\tau^\pm}$ in event i in the simulation are found, and the system four-vector $p^\mu_{\text{system}} = p^\mu_{\tau^+} + p^\mu_{\tau^-}$ is calculated. The system is boosted back to the center-of-mass frame, and the boost β and longitudinal angle θ of the system are calculated. Weights are calculated as the ratio of the squared matrix elements:

$$w_i(\beta, \theta, F_2(0) = x, F_3(0) = y) = \frac{|\mathcal{M}_i(\beta, \theta, x, y)|^2}{|\mathcal{M}_i(\beta, \theta, 0, 0)|^2} \tag{A.13}$$

for chosen values of x and y for $F_2(0)$ and $F_3(0)$, respectively, and are multiplied to other MC signal weights.

JHEP10(2026)053

Data Availability Statement. The public release of data supporting the findings of this article will follow the CERN Open Data Policy [114]. The values of relevant plots and tables associated with this article are stored in HEPData (https://www.hepdata.net/record/172160 for this paper).

Code Availability Statement. The ATLAS collaboration's Athena software, including the configuration of the event generators, is open source (http://gitlab.cern.ch/atlas/athena).

Open Access. This article is distributed under the terms of the Creative Commons Attribution License (CC-BY4.0), which permits any use, distribution and reproduction in any medium, provided the original author(s) and source are credited.

JHEP10(2026)053

References

[1] G. Breit and J.A. Wheeler, *Collision of two light quanta*, *Phys. Rev.* **46** (1934) 1087 [INSPIRE].

[2] W. Heisenberg and H. Euler, *Consequences of Dirac's theory of positrons*, *Z. Phys.* **98** (1936) 714 [physics/0605038] [INSPIRE].

[3] J.S. Schwinger, *On gauge invariance and vacuum polarization*, *Phys. Rev.* **82** (1951) 664 [INSPIRE].

[4] S. Klein and P. Steinberg, *Photonuclear and two-photon interactions at high-energy nuclear colliders*, *Ann. Rev. Nucl. Part. Sci.* **70** (2020) 323 [arXiv:2005.01872] [INSPIRE].

[5] A.J. Baltz et al., *The physics of ultraperipheral collisions at the LHC*, *Phys. Rept.* **458** (2008) 1 [arXiv:0706.3356] [INSPIRE].

[6] J. de Favereau de Jeneret et al., *High energy photon interactions at the LHC*, arXiv:0908.2020 [INSPIRE].

[7] V.M. Budnev, I.F. Ginzburg, G.V. Meledin and V.G. Serbo, *The two photon particle production mechanism. Physical problems. Applications. Equivalent photon approximation*, *Phys. Rept.* **15** (1975) 181 [INSPIRE].

[8] M.-S. Chen, I.J. Muzinich, H. Terazawa and T.P. Cheng, *Lepton pair production from two-photon processes*, *Phys. Rev. D* **7** (1973) 3485 [INSPIRE].

[9] S. Eidelman and M. Passera, *Theory of the tau lepton anomalous magnetic moment*, *Mod. Phys. Lett. A* **22** (2007) 159 [hep-ph/0701260] [INSPIRE].

[10] Y. Yamaguchi and N. Yamanaka, *Large long-distance contributions to the electric dipole moments of charged leptons in the standard model*, *Phys. Rev. Lett.* **125** (2020) 241802 [arXiv:2003.08195] [INSPIRE].

[11] A.D. Sakharov, *Violation of CP invariance, C asymmetry, and baryon asymmetry of the universe*, *Pisma Zh. Eksp. Teor. Fiz.* **5** (1967) 32 [INSPIRE].

[12] A. Moyotl and G. Tavares-Velasco, *Weak properties of the tau lepton via a spin-0 unparticle*, *Phys. Rev. D* **86** (2012) 013014 [arXiv:1210.1994] [INSPIRE].

[13] S. Iguro and T. Kitahara, *Electric dipole moments as probes of the $R_{D^{(*)}}$ anomaly*, *Phys. Rev. D* **110** (2024) 075008 [arXiv:2307.11751] [INSPIRE].

[14] ATLAS collaboration, *Observation of the $\gamma\gamma \to \tau\tau$ process in Pb+Pb collisions and constraints on the τ-lepton anomalous magnetic moment with the ATLAS detector*, *Phys. Rev. Lett.* **131** (2023) 151802 [arXiv:2204.13478] [INSPIRE].

[15] CMS collaboration, *Observation of τ lepton pair production in ultraperipheral lead-lead collisions at $\sqrt{s_{\rm NN}} = 5.02$ TeV*, *Phys. Rev. Lett.* **131** (2023) 151803 [arXiv:2206.05192] [INSPIRE].

[16] CMS collaboration, *Observation of $\gamma\gamma \to \tau\tau$ in proton-proton collisions and limits on the anomalous electromagnetic moments of the τ lepton*, *Rept. Prog. Phys.* **87** (2024) 107801 [arXiv:2406.03975] [INSPIRE].

[17] DELPHI collaboration, *Study of tau-pair production in photon-photon collisions at LEP and limits on the anomalous electromagnetic moments of the tau lepton*, *Eur. Phys. J. C* **35** (2004) 159 [hep-ex/0406010] [INSPIRE].

[18] L3 collaboration, *Production of e, μ and τ pairs in untagged two photon collisions at LEP*, *Phys. Lett. B* **407** (1997) 341 [INSPIRE].

[19] L3 collaboration, *Muon pair and tau pair production in two photon collisions at LEP*, *Phys. Lett. B* **585** (2004) 53 [hep-ex/0402037] [INSPIRE].

[20] ATLAS collaboration, *A measurement of the high-mass $\tau\overline{\tau}$ production cross-section at $\sqrt{s} = 13$ TeV with the ATLAS detector and constraints on new particles and couplings*, *JHEP* **10** (2025) 054 [arXiv:2503.19836] [INSPIRE].

[21] OPAL collaboration, *An upper limit on the anomalous magnetic moment of the tau lepton*, *Phys. Lett. B* **431** (1998) 188 [hep-ex/9803020] [INSPIRE].

[22] L3 collaboration, *Measurement of the anomalous magnetic and electric dipole moments of the tau lepton*, *Phys. Lett. B* **434** (1998) 169 [INSPIRE].

[23] BELLE collaboration, *An improved search for the electric dipole moment of the τ lepton*, *JHEP* **04** (2022) 110 [arXiv:2108.11543] [INSPIRE].

[24] ARGUS collaboration, *A search for the electric dipole moment of the tau lepton*, *Phys. Lett. B* **485** (2000) 37 [hep-ex/0004031] [INSPIRE].

[25] F. del Aguila, F. Cornet and J.I. Illana, *The possibility of using a large heavy-ion collider for measuring the electromagnetic properties of the tau lepton*, *Phys. Lett. B* **271** (1991) 256 [INSPIRE].

[26] L. Beresford and J. Liu, *New physics and tau $g-2$ using LHC heavy ion collisions*, *Phys. Rev. D* **102** (2020) 113008 [*Erratum ibid.* **106** (2022) 039902] [arXiv:1908.05180] [INSPIRE].

[27] M. Dyndal, M. Klusek-Gawenda, M. Schott and A. Szczurek, *Anomalous electromagnetic moments of τ lepton in $\gamma\gamma \to \tau^+\tau^-$ reaction in Pb+Pb collisions at the LHC*, *Phys. Lett. B* **809** (2020) 135682 [arXiv:2002.05503] [INSPIRE].

[28] K. Bhide and V. Lang, *Probing optimal measurements of the electromagnetic dipole moments of the τ lepton*, arXiv:2410.23070 [INSPIRE].

[29] D. Shao, B. Yan, S.-R. Yuan and C. Zhang, *Spin asymmetry and dipole moments in τ-pair production with ultraperipheral heavy ion collisions*, *Sci. China Phys. Mech. Astron.* **67** (2024) 281062 [arXiv:2310.14153] [INSPIRE].

[30] N. Burmasov, E. Kryshen, P. Bühler and R. Lavicka, *Feasibility studies of tau-lepton anomalous magnetic moment measurements in ultraperipheral collisions at the LHC*, *Phys. Part. Nucl.* **54** (2023) 590 [INSPIRE].

JHEP10(2026)053

[31] M. Verducci, C. Roda, V. Cavasinni and N. Vignaroli, *A study of the measurement of the τ lepton anomalous magnetic moment in high energy lead-lead collisions at LHC*, *Phys. Rev. D* **110** (2024) 052001 [arXiv:2307.15160] [INSPIRE].

[32] N.A. Burmasov, *Search for new physics in ultraperipheral collisions at the Large Hadron Collider*, *Phys. Atom. Nucl.* **85** (2022) 942 [INSPIRE].

[33] V.P. Goncalves, D.E. Martins and M.S. Rangel, *Exclusive dilepton production at forward rapidities in PbPb collisions*, *Eur. Phys. J. C* **81** (2021) 220 [arXiv:2012.08923] [INSPIRE].

[34] S. Atag and A.A. Billur, *Possibility of determining τ lepton electromagnetic moments in $\gamma\gamma \to \tau^+\tau^-$ process at the CERN-LHC*, *JHEP* **11** (2010) 060 [arXiv:1005.2841] [INSPIRE].

[35] L. Beresford, S. Clawson and J. Liu, *Strategy to measure tau $g-2$ via photon fusion in LHC proton collisions*, *Phys. Rev. D* **110** (2024) 092016 [arXiv:2403.06336] [INSPIRE].

[36] U. Haisch, L. Schnell and J. Weiss, *LHC tau-pair production constraints on a_τ and d_τ*, *SciPost Phys.* **16** (2024) 048 [arXiv:2307.14133] [INSPIRE].

[37] I. Galon, A. Rajaraman and T.M.P. Tait, *$H \to \tau^+\tau^-\gamma$ as a probe of the τ magnetic dipole moment*, *JHEP* **12** (2016) 111 [arXiv:1610.01601] [INSPIRE].

[38] Q.-H. Cao et al., *Probing magnetic moment operators in production and rare decay*, *Chin. Phys. C* **45** (2021) 093108 [arXiv:2106.04143] [INSPIRE].

[39] J. Bernabeu, G.A. Gonzalez-Sprinberg, J. Papavassiliou and J. Vidal, *Tau anomalous magnetic moment form-factor at super B/flavor factories*, *Nucl. Phys. B* **790** (2008) 160 [arXiv:0707.2496] [INSPIRE].

[40] J. Bernabeu, G.A. Gonzalez-Sprinberg and J. Vidal, *Tau spin correlations and the anomalous magnetic moment*, *JHEP* **01** (2009) 062 [arXiv:0807.2366] [INSPIRE].

[41] S. Eidelman et al., *τ dipole moments via radiative leptonic τ decays*, *JHEP* **03** (2016) 140 [arXiv:1601.07987] [INSPIRE].

[42] A.S. Fomin et al., *Feasibility of τ-lepton electromagnetic dipole moments measurement using bent crystal at the LHC*, *JHEP* **03** (2019) 156 [arXiv:1810.06699] [INSPIRE].

[43] J. Fu et al., *Novel method for the direct measurement of the τ lepton dipole moments*, *Phys. Rev. Lett.* **123** (2019) 011801 [arXiv:1901.04003] [INSPIRE].

[44] ATLAS collaboration, *The ATLAS experiment at the CERN Large Hadron Collider*, 2008 *JINST* **3** S08003 [INSPIRE].

[45] ATLAS collaboration, *ATLAS Insertable B-Layer technical design report*, CERN-LHCC-2010-013 (2010) [INSPIRE].

[46] ATLAS IBL collaboration, *Production and integration of the ATLAS Insertable B-Layer*, 2018 *JINST* **13** T05008 [arXiv:1803.00844] [INSPIRE].

[47] ATLAS collaboration, *Zero degree calorimeters for ATLAS*, CERN-LHCC-2007-01 (2007) [INSPIRE].

[48] G. Avoni et al., *The new LUCID-2 detector for luminosity measurement and monitoring in ATLAS*, 2018 *JINST* **13** P07017 [INSPIRE].

[49] ATLAS collaboration, *Performance of the ATLAS trigger system in 2015*, *Eur. Phys. J. C* **77** (2017) 317 [arXiv:1611.09661] [INSPIRE].

[50] ATLAS collaboration, *Operation of the ATLAS trigger system in run 2*, 2020 *JINST* **15** P10004 [arXiv:2007.12539] [INSPIRE].

JHEP10(2026)053

[51] ATLAS collaboration, *The ATLAS collaboration software and firmware*, ATL-SOFT-PUB-2021-001 (2021) [INSPIRE].

[52] ATLAS collaboration, *ATLAS data quality operations and performance for 2015–2018 data-taking*, 2020 *JINST* **15** P04003 [arXiv:1911.04632] [INSPIRE].

[53] S.R. Klein et al., *STARlight: a Monte Carlo simulation program for ultra-peripheral collisions of relativistic ions*, *Comput. Phys. Commun.* **212** (2017) 258 [arXiv:1607.03838] [INSPIRE].

[54] T. Sjöstrand et al., *An introduction to PYTHIA 8.2*, *Comput. Phys. Commun.* **191** (2015) 159 [arXiv:1410.3012] [INSPIRE].

[55] S. Jadach, Z. Was, R. Decker and J.H. Kühn, *The tau decay library TAUOLA: version 2.4*, *Comput. Phys. Commun.* **76** (1993) 361 [INSPIRE].

[56] N. Davidson et al., *Universal interface of TAUOLA technical and physics documentation*, *Comput. Phys. Commun.* **183** (2012) 821 [arXiv:1002.0543] [INSPIRE].

[57] N. Davidson, T. Przedzinski and Z. Was, *PHOTOS interface in C++: technical and physics documentation*, *Comput. Phys. Commun.* **199** (2016) 86 [arXiv:1011.0937] [INSPIRE].

[58] A.Y. Korchin, E. Richter-Was and Z. Was, *TauSpinner algorithms for including spin and new physics effects in $\gamma\gamma \to \tau\tau$ process*, *Acta Phys. Polon. B* **56** (2025) 10 [arXiv:2506.15213] [INSPIRE].

[59] T. Przedzinski, E. Richter-Was and Z. Was, *Documentation of TauSpinner algorithms: program for simulating spin effects in τ-lepton production at LHC*, *Eur. Phys. J. C* **79** (2019) 91 [arXiv:1802.05459] [INSPIRE].

[60] Z. Czyczula, T. Przedzinski and Z. Was, *TauSpinner program for studies on spin effect in tau production at the LHC*, *Eur. Phys. J. C* **72** (2012) 1988 [arXiv:1201.0117] [INSPIRE].

[61] H.-S. Shao and D. d'Enterria, *gamma-UPC: automated generation of exclusive photon-photon processes in ultraperipheral proton and nuclear collisions with varying form factors*, *JHEP* **09** (2022) 248 [arXiv:2207.03012] [INSPIRE].

[62] J. Alwall et al., *The automated computation of tree-level and next-to-leading order differential cross sections, and their matching to parton shower simulations*, *JHEP* **07** (2014) 079 [arXiv:1405.0301] [INSPIRE].

[63] ATLAS collaboration, *Exclusive dimuon production in ultraperipheral Pb+Pb collisions at $\sqrt{s_{\rm NN}} = 5.02$ TeV with ATLAS*, *Phys. Rev. C* **104** (2021) 024906 [arXiv:2011.12211] [INSPIRE].

[64] L.A. Harland-Lang, V.A. Khoze and M.G. Ryskin, *Exclusive LHC physics with heavy ions: SuperChic 3*, *Eur. Phys. J. C* **79** (2019) 39 [arXiv:1810.06567] [INSPIRE].

[65] ATLAS collaboration, *Exclusive dielectron production in ultraperipheral Pb+Pb collisions at $\sqrt{s_{NN}} = 5.02$ TeV with ATLAS*, *JHEP* **06** (2023) 182 [arXiv:2207.12781] [INSPIRE].

[66] E. Fermi, *On the theory of the impact between atoms and electrically charged particles*, *Z. Phys.* **29** (1924) 315 [INSPIRE].

[67] E. Fermi, *On the theory of collisions between atoms and electrically charged particles*, *Nuovo Cim.* **2** (1925) 143 [hep-th/0205086] [INSPIRE].

[68] C.F. von Weizsacker, *Radiation emitted in collisions of very fast electrons*, *Z. Phys.* **88** (1934) 612 [INSPIRE].

[69] E.J. Williams, *Correlation of certain collision problems with radiation theory*, *Kong. Dan. Vid. Sel. Mat. Fys. Med.* **13N4** (1935) 1 [INSPIRE].

JHEP10(2026)053

[70] M.S. Zolotorev and K.T. McDonald, *Classical radiation processes in the Weizsacker-Williams approximation*, physics/0003096.

[71] A.J. Baltz, Y. Gorbunov, S.R. Klein and J. Nystrand, *Two-photon interactions with nuclear breakup in relativistic heavy ion collisions*, *Phys. Rev. C* **80** (2009) 044902 [arXiv:0907.1214] [INSPIRE].

[72] S. Roesler, R. Engel and J. Ranft, *The Monte Carlo event generator DPMJET-III*, in the proceedings of the *International Conference on Advanced Monte Carlo for Radiation Physics, Particle Transport Simulation and Applications (MC 2000)*, Lisbon, Portugal, 23–26 October 2000 [DOI:10.1007/978-3-642-18211-2_166] [hep-ph/0012252] [INSPIRE].

[73] GEANT4 collaboration, *GEANT4 — a simulation toolkit*, *Nucl. Instrum. Meth. A* **506** (2003) 250 [INSPIRE].

[74] ATLAS collaboration, *The ATLAS simulation infrastructure*, *Eur. Phys. J. C* **70** (2010) 823 [arXiv:1005.4568] [INSPIRE].

[75] ATLAS collaboration, *Muon reconstruction and identification efficiency in ATLAS using the full Run 2 pp collision data set at* $\sqrt{s} = 13$ *TeV*, *Eur. Phys. J. C* **81** (2021) 578 [arXiv:2012.00578] [INSPIRE].

[76] ATLAS collaboration, *Electron and photon performance measurements with the ATLAS detector using the 2015–2017 LHC proton-proton collision data*, 2019 *JINST* **14** P12006 [arXiv:1908.00005] [INSPIRE].

[77] ATLAS collaboration, *Measurement of light-by-light scattering and search for axion-like particles with 2.2* nb^{-1} *of Pb+Pb data with the ATLAS detector*, *JHEP* **03** (2021) 243 [*Erratum ibid.* **11** (2021) 050] [arXiv:2008.05355] [INSPIRE].

[78] F. Akesson et al., *ATLAS tracking event data model*, ATL-SOFT-PUB-2006-004 (2006) [INSPIRE].

[79] T.G. Cornelissen et al., *Updates of the ATLAS tracking event data model (release 13)*, ATL-SOFT-PUB-2007-003 (2007) [INSPIRE].

[80] ATLAS collaboration, *Early inner detector tracking performance in the 2015 data at* $\sqrt{s} = 13$ *TeV*, ATL-PHYS-PUB-2015-051 (2015) [INSPIRE].

[81] ATLAS collaboration, *Study of the material of the ATLAS inner detector for Run 2 of the LHC*, 2017 *JINST* **12** P12009 [arXiv:1707.02826] [INSPIRE].

[82] ATLAS collaboration, *Performance of the ATLAS track reconstruction algorithms in dense environments in LHC run 2*, *Eur. Phys. J. C* **77** (2017) 673 [arXiv:1704.07983] [INSPIRE].

[83] ATLAS collaboration, *Topological cell clustering in the ATLAS calorimeters and its performance in LHC run 1*, *Eur. Phys. J. C* **77** (2017) 490 [arXiv:1603.02934] [INSPIRE].

[84] ATLAS collaboration, *Rapidity gap cross sections measured with the ATLAS detector in pp collisions at* $\sqrt{s} = 7$ *TeV*, *Eur. Phys. J. C* **72** (2012) 1926 [arXiv:1201.2808] [INSPIRE].

[85] ATLAS collaboration, *Trigger menu in 2018*, ATL-DAQ-PUB-2019-001 (2019) [INSPIRE].

[86] ATLAS collaboration, *Performance of the ATLAS muon triggers in run 2*, 2020 *JINST* **15** P09015 [arXiv:2004.13447] [INSPIRE].

[87] ALICE collaboration, *Measurement of the cross section for electromagnetic dissociation with neutron emission in Pb-Pb collisions at* $\sqrt{s_{NN}} = 2.76$ *TeV*, *Phys. Rev. Lett.* **109** (2012) 252302 [arXiv:1203.2436] [INSPIRE].

JHEP10(2026)053

[88] ATLAS collaboration, *Trexfitter*, Zenodo (2026).

[89] I. Helenius and C.O. Rasmussen, *Hard diffraction in photoproduction with Pythia 8*, *Eur. Phys. J. C* **79** (2019) 413 [arXiv:1901.05261] [INSPIRE].

[90] W. Schäfer, *Photon induced processes: from ultraperipheral to semicentral heavy ion collisions*, *Eur. Phys. J. A* **56** (2020) 231 [INSPIRE].

[91] I. Helenius, *Photon-photon and photon-hadron processes in Pythia 8*, *CERN Proc.* **1** (2018) 119 [arXiv:1708.09759] [INSPIRE].

[92] ATLAS collaboration, *Measurement of coincident photon-initiated processes in ultra-peripheral Pb+Pb collisions with the ATLAS detector*, arXiv:2504.07795 [INSPIRE].

[93] G. D'Agostini, *A multidimensional unfolding method based on Bayes' theorem*, *Nucl. Instrum. Meth. A* **362** (1995) 487 [INSPIRE].

[94] G. D'Agostini, *Improved iterative Bayesian unfolding*, in the proceedings of the *Alliance Workshop on Unfolding and Data Correction*, Hamburg, Germany, 27–28 May 2010 [arXiv:1010.0632] [INSPIRE].

[95] ATLAS collaboration, *Experience with using unfolding procedures in ATLAS*, *EPJ Web Conf.* **137** (2017) 11002 [INSPIRE].

[96] T. Adye, *Unfolding algorithms and tests using RooUnfold*, in the proceedings of the *PHYSTAT 2011*, Geneva, Switzerland, 17–20 January 2011 [DOI:10.5170/CERN-2011-006.313] [arXiv:1105.1160] [INSPIRE].

[97] ATLAS collaboration, *Evaluating statistical uncertainties and correlations using the bootstrap method*, ATL-PHYS-PUB-2021-011 (2021) [INSPIRE].

[98] L. De Nardo, *On the propagation of statistical errors*, technical note 02-008, HERMES collaboration/PHENIX, March 2002.

[99] B. Malaescu, *An iterative, dynamically stabilized method of data unfolding*, arXiv:0907.3791 [INSPIRE].

[100] B. Malaescu, *An Iterative, Dynamically Stabilized (IDS) method of data unfolding*, in the proceedings of the *PHYSTAT 2011*, Geneva, Switzerland, 17–20 January 2011 [DOI:10.5170/CERN-2011-006.271] [arXiv:1106.3107] [INSPIRE].

[101] ATLAS collaboration, *Muon reconstruction performance of the ATLAS detector in proton–proton collision data at* $\sqrt{s} = 13$ *TeV*, *Eur. Phys. J. C* **76** (2016) 292 [arXiv:1603.05598] [INSPIRE].

[102] C. Loizides, J. Kamin and D. d'Enterria, *Improved Monte Carlo Glauber predictions at present and future nuclear colliders*, *Phys. Rev. C* **97** (2018) 054910 [*Erratum ibid.* **99** (2019) 019901] [arXiv:1710.07098] [INSPIRE].

[103] B. Klos et al., *Neutron density distributions from antiprotonic* ^{208}Pb *and* ^{209}Bi *atoms*, *Phys. Rev. C* **76** (2007) 014311 [nucl-ex/0702016] [INSPIRE].

[104] C.M. Tarbert et al., *Neutron skin of* ^{208}Pb *from coherent pion photoproduction*, *Phys. Rev. Lett.* **112** (2014) 242502 [arXiv:1311.0168] [INSPIRE].

[105] L.A. Harland-Lang, V.A. Khoze and M.G. Ryskin, *Elastic photon-initiated production at the LHC: the role of hadron-hadron interactions*, *SciPost Phys.* **11** (2021) 064 [arXiv:2104.13392] [INSPIRE].

[106] ATLAS collaboration, *Luminosity determination in pp collisions at* $\sqrt{s} = 13$ *TeV using the ATLAS detector at the LHC*, *Eur. Phys. J. C* **83** (2023) 982 [arXiv:2212.09379] [INSPIRE].

JHEP10(2026)053

[107] S. Dittmaier, T. Engel, J.L.H. Ariza and M. Pellen, *Electroweak corrections to $\tau^+\tau^-$ production in ultraperipheral heavy-ion collisions at the LHC*, *JHEP* **08** (2025) 051 [arXiv:2504.11391] [INSPIRE].

[108] G. Cowan, K. Cranmer, E. Gross and O. Vitells, *Asymptotic formulae for likelihood-based tests of new physics*, *Eur. Phys. J. C* **71** (2011) 1554 [*Erratum ibid.* **73** (2013) 2501] [arXiv:1007.1727] [INSPIRE].

[109] ROOT collaboration, *HistFactory: a tool for creating statistical models for use with RooFit and RooStats*, CERN-OPEN-2012-016 (2012) [INSPIRE].

[110] S.S. Wilks, *The large-sample distribution of the likelihood ratio for testing composite hypotheses*, *Annals Math. Statist.* **9** (1938) 60 [INSPIRE].

[111] F.U. Bernlochner, D.C. Fry, S.B. Menary and E. Persson, *Cover your bases: asymptotic distributions of the profile likelihood ratio when constraining effective field theories in high-energy physics*, *SciPost Phys. Core* **6** (2023) 013 [arXiv:2207.01350] [INSPIRE].

[112] ATLAS collaboration, *Measurement of high-mass $t\bar{t}\ell^+\ell^-$ production and lepton flavour universality-inspired effective field theory interpretations at $\sqrt{s} = 13$ TeV with the ATLAS detector*, *Eur. Phys. J. C* **85** (2025) 1434 [arXiv:2504.05919] [INSPIRE].

[113] ATLAS collaboration, *ATLAS computing acknowledgements*, ATL-SOFT-PUB-2026-001 (2026)

[114] ATLAS collaboration, *CERN Open Data Policy for the LHC experiments*, CERN-OPEN-2020-013 (2020).

[115] *ATLAS collaboration's Athena software*, http://gitlab.cern.ch/atlas/athena.

The ATLAS collaboration

G. Aad[102], E. Aakvaag[17], B. Abbott[121], S. Abdelhameed[83b], K. Abeling[54], N.J. Abicht[48], S.H. Abidi[30], M. Aboelela[44], A. Aboulhorma[36e], H. Abramowicz[154], B.S. Acharya[68a,68b,a], A. Ackermann[62a], J. Ackerschott[55], C. Adam Bourdarios[4], L. Adamczyk[85a], S.V. Addepalli[146], M. J. Addison[101], J. Adelman[117], A. Adiguzel[22c], T. Adye[135], A.A. Affolder[137], Y. Afik[39], M.N. Agaras[13], A. Aggarwal[100], C. Agheorghiesei[28c], A. Ahmad[83a], F. Ahmadov[38,b], S. Ahuja[165], X. Ai[113c], G. Aielli[75a,75b], A. Aikot[165], M. Ait Tamlihat[36e], T.P.A. Åkesson[98], D. Akiyama[170], N.N. Akolkar[25], S. Aktas[168], G.L. Alberghi[24b], J. Albert[167], U. Alberti[20], P. Albicocco[52], S. Alderweireldt[51], Z.L. Alegria[122], M. Aleksa[37], I.N. Aleksandrov[38], C. Alexa[28b], T. Alexopoulos[10], F. Alfonsi[24b], M. Algren[55], M. Alhroob[169], B. Ali[133], H. M. J. Ali[91,c], S. Ali[32], S.W. Alibocus[92], M. Aliev[34c], G. Alimonti[70a], C. Allaire[65], B.M.M. Allbrooke[149], D. R. Allen[122], J. S. Allen[101], J.F. Allen[51], C.S. Alley[1], E.R. Almazan[137], A. Aloisio[71a,71b], F. Alonso[90], C. Alpigiani[140], A. Alvarez Fernandez[100], M. Alves Cardoso[55], M.G. Alviggi[71a,71b], Y. Amaral Coutinho[81b], C. Amelung[37], M. Amerl[101], T. Amezza[128], B. Amini[53], K. Amirie[158], A. Amirkhanov[38], D. Amperiadou[155], C. Anastopoulos[142], T. Andeen[11], J.K. Anders[92], A. C. Anderson[58], A. Andreazza[70a,70b], S. Angelidakis[9], A. Angerami[41], A.V. Anisenkov[38], A. Annovi[73a], C. Antel[37], E. Antipov[148], M. Antonelli[52], F. Anulli[74a], M. Aoki[82], T. Aoki[156], M.A. Aparo[13], L. Aperio Bella[47], M. Apicella[31], C. Appelt[154], A. Apyan[27], M. Arampatzi[10], S. J. Arbiol Val[86], C. Arcangeletti[52], A.T.H. Arce[50], M. Arcuri[43b,43a], J-F. Arguin[108], S. Argyropoulos[155], J.-H. Arling[47], O. Arnaez[4], A.P. Arnold[94], H. Arnold[148], G. Artoni[74a,74b], H. Asada[111], S. Asatryan[175], N.A. Asbah[37], R. A. Ashby Pickering[169], A. M. Aslam[95], J. Assahsah[36d], K. Assamagan[30], R. Astalos[29a], K. S. V. Astrand[98], S. Atashi[162], R.J. Atkin[34a], H. Atmani[36f], P.A. Atmasiddha[129], K. Augsten[133], A.D. Auriol[40], V.A. Austrup[101], A.S. Avad[94], G. Avolio[37], A. Azzam[13], D. Babal[29b], H. Bachacou[136], K. Bachas[155,d], A. Bachiu[35], E. Bachmann[49], M. J. Backes[62a], A. Badea[39], T.M. Baer[106], M. Bahmani[19], D. Bahner[53], K. Bai[124], L. Baines[94], O.K. Baker[174], D. Bakshi Gupta[8], L.E. Balabram Filho[81b], V. Balakrishnan[121], R. Balasubramanian[4], P. Balek[85a], E. Ballabene[24b,24a], F. Balli[136], L.M. Baltes[62a], W.K. Balunas[127], I. Bamwidhi[83c], E. Banas[86], M. Bandieramonte[130], S. Bansal[25], L. Barak[154], M. Barakat[47], E.L. Barberio[105], D. Barberis[18b], M. Barbero[102], M. Z. Barel[116], T. Barillari[110], M-S. Barisits[37], T. Barklow[146], P. Baron[134], D.A. Baron Moreno[101], A. Baroncelli[61], A.J. Barr[127,e], J.D. Barr[96], F. Barreiro[99], J. Barreiro Guimarães da Costa[14], M.G. Barros Teixeira[131a], F. Bartels[37], R. Bartoldus[146], A.E. Barton[91], P. Bartos[29a], M. Baselga[48], S. Bashiri[86], A. Bassalat[65,f], M.J. Basso[159a], S. Bataju[44], R. Bate[166], R.L. Bates[58], M. Battaglia[137], D. Battulga[19], M. Bauce[74a,74b], L. Bauckhage[47], P. Bauer[25], L. T. Bayer[47], L.T. Bazzano Hurrell[31], T. Beau[128], J.Y. Beaucamp[90], S. Beauceron[128], P.H. Beauchemin[161], P. Bechtle[25], H.P. Beck[20,g], K. Becker[169], A.J. Beddall[80], V.A. Bednyakov[38], C.P. Bee[148], L.J. Beemster[16], M. Begalli[81d], M. Begel[30], J.K. Behr[47], J.F. Beirer[37], F. Beisiegel[25], I.B. Belean[28d], M. Belfkir[83c], G. Bella[154], L. Bellagamba[24b], A. Bellerive[35], C.D. Bellgraph[67], P. Bellos[21], I. Benaoumeur[21], D. Benchekroun[36a], F. Bendebba[36a],

JHEP10(2026)053

Y. Benhammou[154], K.C. Benkendorfer[167], L. Beresford[47], M. Beretta[52], E. Bergeaas Kuutmann[163], N. Berger[4], B. Bergmann[133], J. Beringer[18a], M. Berkat[136], G. Bernardi[5], C. Bernius[146], F.U. Bernlochner[25], A. Berrocal Guardia[13], T. Berry[95], P. Berta[134], A. Berti[131a], R. Bertrand[102], S. Bethke[110], A. Betti[74a,74b], T.F. Beumker[173], A.J. Bevan[94], L. Bezio[55], N.K. Bhalla[53], S. Bharthuar[110], S. Bhatta[148], P. Bhattarai[146], Z.M. Bhatti[118], K. D. Bhide[164], V.S. Bhopatkar[122], R.M. Bianchi[130], G. Bianco[24b,24a], O. Biebel[109], M. Biglietti[76a], P. Bijl[53], C. S. Billingsley[44], Y. Bimgdi[36f], M. Bindi[54], A. Bingham[173], A. Bingul[22b], C. Bini[74a,74b], M. Biros[134], S. Biryukov[149], T. Bisanz[48], E. Bisceglie[24b,24a], J.P. Biswal[135], D. Biswas[144], M. Biyabi[14], I. Bloch[47], A. Blue[58], U. Blumenschein[94], V.S. Bobrovnikov[38], L. Boccardo[56b,56a], M. Boehler[53], D. Bogavac[13], L. S. Boggia[128], V. Boisvert[95], P. Bokan[163], T. Bold[85a], M. Bomben[5], M. Bona[94], M. Boonekamp[136], A.G. Borbély[58], G. Borissov[91], A. Borkar[168], D. Bortoletto[127], M. Borysova[171], D. Boscherini[24b], M. Bosman[13], K. Bouaouda[36a], L. Boudet[136], J. Boudreau[130], E.V. Bouhova-Thacker[91], D. Boumediene[40], R. Bouquet[56b,56a], A. Boveia[120], D. Boye[30], I.R. Boyko[38], L. Bozianu[55], J. Bracinik[21], N. Brahimi[4], G. Brandt[173], O. Brandt[33], B. Brau[103], R. Brener[171], L. Brenner[116], R. Brenner[163], S. Bressler[171], M. Brettell[96], G. Brianti[116], D. Britton[58], D. Britzger[110], I. Brock[25], R. Brock[107], H. Bronson[129], G. Brooijmans[41], A.J. Brooks[67], E. M. Brooks[159b], E. Brost[30], L.M. Brown[167,159a], L.E. Bruce[60], T.L. Bruckler[127], P.A. Bruckman de Renstrom[86], B. Brüers[47], A. Bruni[24b], G. Bruni[24b], D. Brunner[46a,46b], M. Bruschi[24b], N. Bruscino[74a,74b], T. Buanes[17], Q. Buat[140], D. Buchin[110], A.G. Buckley[58], J. Bucko[134], M. Buhring[49], O. Bulekov[80], B.A. Bullard[146], T. O. Buratovich[90], S. Burdin[92], C.D. Burgard[48], A.M. Burger[89], B. Burghgrave[8], O. Burlayenko[53], J. Burleson[164], J.C. Burzynski[121], V. Büscher[100], P.J. Bussey[58], O. But[25], J.M. Butler[26], C.M. Buttar[58], J.M. Butterworth[96], P. Butti[37], W. Buttinger[135], C.J. Buxo Vazquez[107], A.R. Buzykaev[38], S. Cabrera Urbán[165], L. Cadamuro[65], H. Cai[37], Y. Cai[24b,112c,24a], Y. Cai[112a], M.A. Cairo[129], V.M.M. Cairo[37], O. Cakir[3a], N. Calace[37], P. Calafiura[18a], G. Calderini[128], P. Calfayan[35], L. Calic[98], G. Callea[58], L.P. Caloba[81b], D. Calvet[40], S. Calvet[40], R. Camacho Toro[128], S. Camarda[37], D. Camarero Munoz[27], P. Camarri[75a,75b], C. Camincher[37], M. Campanelli[96], A. Camplani[42], V. Canale[71a,71b], A.C. Canbay[3a], E. Canonero[95], J. Cantero[165], F. Capocasa[27], P. Cappelli[27], M. Capua[43b,43a], A. Carbone[70a,70b], R. Cardarelli[75a], J.C.J. Cardenas[8], M. P. Cardiff[27], G. Carducci[43b,43a], T. Carli[37], G. Carlino[71a], J.I. Carlotto[13], B.T. Carlson[130,h], E.M. Carlson[167], L. Carminati[70a,70b], A. Carnelli[4], M. Carnesale[37], S. Caron[115], E. Carquin[138g], I.B. Carr[105], S. Carrà[72a,72b], G. Carratta[24b,24a], C. Carrion Martinez[165], A.M. Carroll[124], N. Cartalade[40], M.P. Casado[13,i], P. Casolaro[71a,71b], M. Caspar[47], F. Cassinese[90], F. Castiglioni[73a,73b], W.R. Castiglioni[39], F.L. Castillo[4], V. Castillo Gimenez[165], N.F. Castro[131a,131e], A. Catinaccio[37], J.R. Catmore[126], T. Cavaliere[4], V. Cavaliere[30], E. Celebi[80], S. Cella[30], V. Cepaitis[55], K. Cerny[123], A.S. Cerqueira[81a], A. Cerri[73a,j], L. Cerrito[75a,75b], F. Cerutti[18a], B. Cervato[70a,70b], A. Cervelli[24b], G. Cesarini[52], S.A. Cetin[80], V. C. Chabalala[34j], P.M. Chabrillat[128], R. Chakkappai[65], S. Chakraborty[169], A. Chambers[60], J. Chan[18a], J.D. Chapman[33], E. Chapon[136], D.G. Charlton[21], C. Chauhan[132], Y. Che[112a], S. Chekanov[6], G.A. Chelkov[38,k], H. Chen[30], J. Chen[141a],

JHEP10(2026)053

J. Chen[145], M. Chen[59], S. Chen[87], S.J. Chen[112a], X. Chen[141a], X. Chen[15,l], Z. Chen[61], C.L. Cheng[146], H.C. Cheng[63a], S. Cheong[146], A. Cheplakov[38], E. Cherepanova[116], E. Cheu[7], K. Cheung[64], L. Chevalier[136], G. Chiarelli[73a], G. Chiodini[69a], A.S. Chisholm[21], J. L. Chisholm[166], A. Chitan[28b], M. Chitishvili[165], M.V. Chizhov[38,m], K. Chmiel[76a,76b], K. Choi[11], Y. Chou[140], E.Y.S. Chow[115], G. Christou[51], K.L. Chu[171], M.C. Chu[63a], Z. Chubinidze[52], J. Chudoba[132], J.J. Chwastowski[86], D. Cieri[110], K.M. Ciesla[85a], V. Cindro[93], A. Ciocio[18a], F. Cirotto[71a,71b], Z.H. Citron[171], M. Citterio[70a], D.A. Ciubotaru[28b], A. Clark[55], P.J. Clark[51], N. Clarke Hall[37], C. Clarry[158], S.E. Clawson[37], C. Clement[46a,46b], L. Clissa[24b,24a], Y. Coadou[102], M. Cobal[68a,68c], A. Coccaro[56b], M. G. Cochran Branson[140], R.F. Coelho Barrue[131a], R. Coelho Lopes De Sa[103], S. Coelli[70a], M.M. Cohen[129], L. S. Colangeli[158], B. Cole[41], P. Collado Soto[99], J. Collot[59], M.R. Coluccia[69a], I. Combes[65], P. Conde Muiño[131a,131g], L.H.J. Condren[162], M.P. Connell[34c], S.H. Connell[34c], E.I. Conroy[161], M. Contreras Cossio[11], F. Conventi[71a,n], A.M. Cooper-Sarkar[127], L. Corazzina[74a,74b], F. A. Corchia[24b,24a], A. Cordeiro Oudot Choi[140], L.D. Corpe[40], M. Corradi[74a,74b], F. Corriveau[104,o], A. Cortes-Gonzalez[156], M.J. Costa[165], F. Costanza[4], D. Costanzo[142], J. Couthures[4], G. Cowan[95], K. Cranmer[172], L. Cremer[48], D. Cremonini[24b,24a], S. Crépé-Renaudin[59], F. Crescioli[128], T. Cresta[72a,72b], M. Cristinziani[144], M. Cristoforetti[77a,77b], T. M. Critchley[55], E. Critelli[96], A. Cueto[99], H. Cui[96], Z. Cui[7], B.M. Cunnett[149], W.R. Cunningham[58], E. Cuppini[110], F. Curcio[165], J. R. Curran[51], G. D'amen[30], V. D'Amico[109], M. D'Andrea[56b,56a], G. D'anniballe[73a,73b], S. D'Auria[70a,70b], A. D'Avanzo[71a,71b], L. D'Eramo[40], A. D'Onofrio[71a,71b], M. D'Onofrio[92], M. D'uffizi[101], M.J. Da Cunha Sargedas De Sousa[56b,56a], J.V. Da Fonseca Pinto[81b], C. Da Via[101], W. Dabrowski[85a], T. Dado[37], S. Dahbi[151], T. Dai[106], D. Dal Santo[20], C. Dallapiccola[103], M. Dam[42], J.R. Dandoy[35], D. Dannheim[37], M. Danninger[145], V. Dao[148], G. Darbo[56b], F. Dattola[47], T. Davidek[134], J. Davidson[169], I. Dawson[94], K. De[8], C. De Almeida Rossi[158], N. De Biase[47], S. De Castro[24b,24a], N. De Groot[115], P. de Jong[116], H. De la Torre[117], A. De Maria[112a], S. De Miranda Rimes[81d], A. De Salvo[74a], U. De Sanctis[75a,75b], F. De Santis[69a,69b], A. De Santo[149], J.B. De Vivie De Regie[59], K.G. De Vries[116], J. Debevc[93], D.V. Dedovich[38], J. Degens[92], A.M. Deiana[44], J. Del Peso[99], L. Delagrange[27], F. Deliot[136], C.M. Delitzsch[48], A. Dell'Acqua[37], L. Dell'Asta[70a,70b], M. Della Pietra[71a,71b], D. Della Volpe[55], M. Delmastro[4], C.C. Delogu[56b,56a], P.A. Delsart[59], S. Demers[174], M. Demichev[38], H. Denizli[22a,p], M.G. Depala[92], D. Derendarz[86], L. Derin[56b,56a], F. Derue[128], P. Dervan[92,†], A. M. Desai[1], K. Desch[25], F.A. Di Bello[73a,73b], A. Di Ciaccio[75a,75b], L. Di Ciaccio[4], D. Di Croce[37], C. Di Donato[71a,71b], A. Di Girolamo[37], G. Di Gregorio[65], A. Di Luca[77a,77b], B. Di Micco[76a,76b], R. Di Nardo[76a,76b], K.F. Di Petrillo[39], M. Diamantopoulou[154], F.A. Dias[116], M.A. Diaz[138a,138b], A. R. Didenko[38], M. Didenko[165], S.D. Diefenbacher[18a], E.B. Diehl[106], S. Díez Cornell[47], C. Diez Pardos[144], C. Dimitriadi[147], A. Dimitrievska[21], A. Dimri[148], Y. Ding[61], J. Dingfelder[25], T. Dingley[127], I-M. Dinu[28b], S.J. Dittmeier[62b], F. Dittus[37], M. Divisek[134], B. Dixit[92], F. Djama[102], T. Djobava[152b], C. Doglioni[101,98], A. Dohnalova[29a], Z. Dolezal[134], K. Domijan[85a], K.M. Dona[39], M. Donadelli[81d], B. Dong[107], J. Donini[40], J. Dopke[135], A. Doria[71a], N. Dos Santos Fernandes[131a],

JHEP10(2026)053

I.A. Dos Santos Luz[81e], P. Dougan[44], M.T. Dova[90], A.T. Doyle[58], M.P. Drescher[54], E. Dreyer[171], I. Drivas-koulouris[10], M. Drnevich[118], D. Du[61], T. Du[39], T.A. du Pree[116], Z. Duan[112a], M. Dubau[4], F. Dubinin[38], M. Dubovsky[29a], E. Duchovni[171], G. Duckeck[109], P. K. Duckett[96], O.A. Ducu[28b], D. Duda[51], A. Dudarev[37], M.M. Dudek[86], E. R. Duden[27], L. Duflot[65], M. Dührssen[37], I. Duminica[28g], A.E. Dumitriu[28b], M. Dunford[62a], T. Duong[4], A. Duperrin[102], A.F. Duque Bran[40], H. Duran Yildiz[3a], A. Durglishvili[152b], G.I. Dyckes[18a], M. Dyndal[85a], B.S. Dziedzic[37], G.H. Eberwein[127], B. Eckerova[29a], J.C. Egan[96], S. Eggebrecht[54], E. Egidio Purcino De Souza[81e], G. Eigen[17], K. Einsweiler[18a], T. Ekelof[163], P.A. Ekman[98], S. El Farkh[36b], Y. El Ghazali[61], H. El Jarrari[104], A. El Moussaouy[36a], I. Elbaz[154], D. Elitez[37], M. Ellert[163], F. Ellinghaus[173], T.A. Elliot[95], J. Elmsheuser[30], M. Elsawy[83b], M. Elsing[37], D. Emeliyanov[135], Y. Enari[82], S. Epari[108], D. Ernani Martins Neto[86], F. Ernst[37], M. Escalier[65], C. Escobar[165], R. Estevam De Paula[81c], E. Etzion[154], G. Evans[131a,131b], H. Evans[67], L.S. Evans[47], S. Ezzarqtouni[36a], F. Fabbri[24b,24a], L. Fabbri[24b,24a], G. Facini[96], V. Fadeyev[137], D. Fakoudis[100], S. Falciano[74a], L.F. Falda Ulhoa Coelho[27], F. Fallavollita[110], G. Falsetti[43b,43a], J. Faltova[134], C. Fan[164], K. Y. Fan[63b], Y. Fan[14], Y. Fang[14,112c], M. Fanti[70a,70b], M. Faraj[68a,68c], Z. Farazpay[97], A. Farbin[8], A. Farilla[76a], K. Farman[151], J. N. Farr[174], M. S. Farrington[60], S.M. Farrington[135,51], F. Fassi[36e], D. Fassouliotis[9], L. Fayard[65], G. Fazzino[62b], P. Federic[134], P. Federicova[132], M. Feickert[172], L. Feligioni[102], D.E. Fellers[18a], C. Feng[113b], Y. Feng[14], Z. Feng[65], B. Fernandez Barbadillo[91], P. Fernandez Martinez[66], C. Fernandez Ruiz[33], J. Ferrando[91], A. Ferrari[163], P. Ferrari[116,115], R. Ferrari[72a], D. Ferrere[55], C. Ferretti[106], M. P. Fewell[1], D. Fiacco[74a,74b], F. Fiedler[100], P. Fiedler[133], S. Filimonov[38], M.S. Filip[28b,q], A. Filipčič[93], M. Filipig[68a,68c], E.K. Filmer[159a], F. Filthaut[115], M.C.N. Fiolhais[131a,131c,r], L. Fiorini[165], W.C. Fisher[107], T. Fitschen[101], I. Fleck[144], P. Fleischmann[106], T. Flick[173], M. Flores[34d,s], L.R. Flores Castillo[63a], M. Foll[126], F.M. Follega[77a,77b], N. Fomin[33], A. Formica[136], M. Fornasiero[149], A.C. Forti[101], N. Forti[24b,24a], E. Fortin[102], A.W. Fortman[18a], L. Foster[18a], L. Fountas[9], H. Fox[91], P. Francavilla[73a,73b], S. Francescato[60], S. Franchellucci[20], M. Franchini[24b,24a], S. Franchino[62a], D. Francis[37], L. Franco[47], L. Franconi[47], M. Franklin[60], G. Frattari[37], Y.Y. Frid[154], N. Fritzsche[37], A. Froch[55], D. Froidevaux[37], J.A. Frost[135], Y. Fu[107], S. Fuenzalida Garrido[138g], Y.C. Fujikake[137], M. Fujimoto[148], K. Y. Fung[63a], E. Furtado De Simas Filho[81e], M. Furukawa[156], M. Fuste Costa[47], P. Fuste Martin[13], J. Fuster[165], A. Gaa[54], A. Gabrielli[24b,24a], A. Gabrielli[158], G. Gagliardi[56b,56a], L.G. Gagnon[146], S. Galantzan[154], J. Gallagher[1], E.J. Gallas[127], A.L. Gallen[163], B.J. Gallop[135], K.K. Gan[120], Y. Gao[51], Z. Gao[112a], A. Garabaglu[140], F.M. Garay Walls[138a,138b], C. García[165], A. Garcia Alonso[116], A.G. Garcia Caffaro[174], J.E. García Navarro[165], M. A. Garcia Ruiz[23b], M. Garcia-Sciveres[18a], G.L. Gardner[129], R.W. Gardner[39], N. Garelli[161], R.B. Garg[146], J.M. Gargan[33], C.A. Garner[158], C.M. Garvey[34a], V. K. Gassmann[161], G. Gaudio[72a], A.J. Gavin[94], J. Gavranovic[93], I.L. Gavrilenko[131a], C. Gay[166], G. Gaycken[124], A. Gekow[120], C. Gemme[56b], M.H. Genest[59], A. D. Gentry[114], S. George[95], T. Geralis[45], A. A. Gerwin[121], P. Gessinger-Befurt[37], M. Ghani[169], K. Ghorbanian[94], A. Ghosal[144], A. Ghosh[162], A. Ghosh[7], B. Giacobbe[24b], S. Giagu[74a,74b], A. Giannini[61], S.M. Gibson[95],

JHEP10(2026)053

D.T. Gil[85b], B.J. Gilbert[41], D. Gillberg[35], G. Gilles[116], D.M. Gingrich[2,t], M.P. Giordani[68a,68c], P.F. Giraud[136], G. Giugliarelli[68a,68c], D. Giugni[70a], F. Giuli[75a,75b,u], I. Gkialas[9,v], B.C. Gladwyn[127], C. Glasman[99], M. Glazewska[20], R. M. Gleason[162], G. Glemža[47], I. Gnesi[24b,24a,w], Y. Go[30], M. Goblirsch-Kolb[37], B. Gocke[48], D. Godin[108], B. Gokturk[22a], S. Goldfarb[105], T. Golling[55], M.G.D. Gololo[34c], A. Golub[140], J.P. Gombas[107], A. Gomes[131a,131b], G. Gomes Da Silva[144], A.J. Gomez Delegido[37], R. Gonçalo[131a], A. Gongadze[152c], F. Gonnella[21], J.L. Gonski[146], R.Y. González Andana[51], S. González de la Hoz[165], M. V. Gonzalez Rodrigues[47], R. Gonzalez Suarez[163], S. Gonzalez-Sevilla[55], L. Goossens[37], B. Gorini[37], E. Gorini[69a,69b], A. Gorišek[93], T.C. Gosart[129], A.T. Goshaw[50], M.I. Gostkin[38], S. Goswami[122], C.A. Gottardo[37], S. A. Gotz[109], M. Gouighri[36b], A.G. Goussiou[140], N. Govender[34c], R. P. Grabarczyk[127], I. Grabowska-Bold[85a], K. Graham[35], E. Gramstad[126], S. Grancagnolo[69a,69b], C.M. Grant[1], P.M. Gravila[28f], F.G. Gravili[69a,69b], H.M. Gray[18a], M. Greco[110], M. J. Green[1], C. Grefe[25], A. S. Grefsrud[37], I.M. Gregor[47], K.T. Greif[162], P. Grenier[146], S.G. Grewe[110], K. Grimm[32], S. Grinstein[13,x], E. Gross[171], J. Grosse-Knetter[54], L.H. Grossman[18b], L. Guan[106], W. Guérin[89], G. Guerrieri[37], R. Guevara[126], R. Gugel[100], J.A.M. Guhit[106], A. Guida[19], E. Guilloton[169], S. Guindon[37], F. Guo[14,112c], J. Guo[141a], L. Guo[47], L. Guo[112b,y], Y. Guo[106], Y. Guo[41], A. Gupta[48], R. Gupta[130], S. Gupta[27], S. Gurbuz[25], S.S. Gurdasani[47], G. Gustavino[74a,74b], P. Gutierrez[121], L.F. Gutierrez Zagazeta[129], M. Gutsche[49], C. Gutschow[96], C. Gwenlan[127], C.B. Gwilliam[92], E.S. Haaland[126], A. Haas[118], M. Habedank[58], C. Haber[18a], R.J. Haberle[171], H.K. Hadavand[8], A. Haddad[40], A. Hadef[49], A.I. Hagan[91], J. J. Hahn[144], M. Haleem[168], J. Haley[122], G.D. Hallewell[102], J.A. Hallford[47], H. Hamdaoui[163], M. Hamer[25], S. E. D. Hammoud[65], E.J. Hampshire[95], L. Han[112a], L. Han[61], S. Han[14], K. Hanagaki[82], M. Hance[137], D.A. Hangal[41], H. Hanif[145], M.D. Hank[129], J.B. Hansen[42], P.H. Hansen[42], T. Harenberg[173], S. Harkusha[175], M.L. Harris[103], Y.T. Harris[25], J. Harrison[13], P.F. Harrison[169], M. L. E. Hart[96], N.M. Hartman[110], N.M. Hartmann[109], R. Z. Hasan[95,135], Y. Hasegawa[143], D. Hashimoto[111], F. Haslbeck[37], S. Hassan[126], R. Hauser[107], M. Haviernik[134], C.M. Hawkes[21], R.J. Hawkings[37], Y. Hayashi[156], D. Hayden[107], R.L. Hayes[116], C.P. Hays[127], J.M. Hays[94], H.S. Hayward[92], M. He[14,112c], Y. He[47], Y. He[96], V. Hedberg[98], J. Heilman[35], S. Heim[47], T. Heim[18a], J.J. Heinrich[124], L. Heinrich[110], J. Hejbal[132], M. Helbig[49], A. Held[172], S. Hellesund[17], C.M. Helling[166], F.N.E. Henry[58], H. Herde[98], Y. Hernández Jiménez[148], G. Herten[53], R. Hertenberger[109], L. Hervas[37], M.E. Hesping[100], N.P. Hessey[159a], J. Hessler[110], R. Hicks[129], M. Hidaoui[36b], N. Hidic[134], E. Hill[158], T. S. Hillersoy[17], S.J. Hillier[21], J.R. Hinds[107], F. Hinterkeuser[25], M. Hirose[125], S. Hirose[170], D. Hirschbuehl[173], B. Hiti[93], J. Hobbs[148], R. Hobincu[28e], N. Hod[171], A.M. Hodges[164], M.C. Hodgkinson[142], B.H. Hodkinson[127], A. Hoecker[37], D. D. Hofer[106], J. Hofer[165], J. Hofner[100], M. Holzbock[37], L.B.A.H. Hommels[33], V. Homsak[127], J. J. Hong[67], T.M. Hong[130], R. Honscheid[127], B.H. Hooberman[164], W.H. Hopkins[6], M. C. Hoppesch[164], Y. Horii[111], M. E. Horstmann[110], M.M. Horzela[54], S. Hou[151], M. R. Housenga[164], J. Howarth[58], J. Hoya[6], M. Hrabovsky[123], T. Hryn'ova[4], P.J. Hsu[64], S.-C. Hsu[140], T. Hsu[65], M. Hu[18a], P. Hu[63b], Q. Hu[61], S. Huang[33], X. Huang[14,112c], Y. Huang[134],

JHEP10(2026)053

Y. Huang[112b], Y. Huang[14], Z. Huang[65], Z. Hubacek[133], F. Huegging[25], T.B. Huffman[127], M. Hufnagel Maranha De Faria[81a], C. A. Hugli[47], M. Huhtinen[37], S.K. Huiberts[17], R. Hulsken[104], C. E. Hultquist[18a], D.L. Humphreys[103], N. Huseynov[12], J. Huston[107], B. Huth[37], J. Huth[60], L. Huth[47], R. Hyneman[7], G. Iacobucci[55], G. Iakovidis[30], L. Iconomidou-Fayard[65], J. P. Iddon[37], P. Iengo[71a,71b], Y. Iiyama[156], T. Iizawa[156], Y. Ikegami[82], D. Iliadis[155], N. Ilic[158], H. Imam[36a], G. Inacio Goncalves[81d], S. A. Infante Cabanas[138c], T. Ingebretsen Carlson[46a,46b], J. M. Inglis[94], G. Introzzi[72a,72b], M. Iodice[76a], V. Ippolito[74a,74b], R. K. Irwin[92], M. Ishino[156], W. Islam[172], C. Issever[19], O. N. Istaitia[65,f], S. Istin[22a,z], K. Itabashi[125], H. Ito[170], R. Iuppa[77a,77b], A. Ivina[171], F. Ivone[37], S. Izumiyama[111], V. Izzo[71a], P. Jacka[133], P. Jackson[1], P. R. Jacobson[50], P. Jain[47], K. Jakobs[53], J. Jamieson[58], W. Jang[156], S. Jankovych[116], B. K. Jashal[135], M. Javurkova[103], P. Jawahar[101], L. Jeanty[124], J. Jejelava[152a,aa], P. Jenni[53,ab], L. Jerala[93], C.E. Jessiman[35], H. Jia[166], J. Jia[148], K. Jia[146], X. Jia[110,112c], C. Jiang[51], Q. Jiang[63b], S. Jiggins[47], M. Jimenez Ortega[165], J. Jimenez Pena[13], S. Jin[112a], A. Jinaru[28b], O. Jinnouchi[139], P. Johansson[142], K.A. Johns[7], J.W. Johnson[137], F. A. Jolly[47], D.M. Jones[149], E. Jones[47], P. Jones[33], R.W.L. Jones[91], T.J. Jones[92], H.L. Joos[37], R. Joshi[120], J. Jovicevic[16], X. Ju[18a], J.J. Junggeburth[37], T. Junkermann[62a], A. Juste Rozas[13,x], M.K. Juzek[86], S. Kabana[138f], A. Kaczmarska[86], S. A. Kadir[146], M. Kado[110], H. Kagan[120], M. Kagan[146], A. Kahn[129], C. Kahra[100], T. Kaji[156], E. Kajomovitz[153], N. Kakati[171], N. Kakoty[13], S. Kandel[8], E. Kanellaki[45], N. Kanellos[10], S. Kang[50], D. Kar[34j,†], E. Karentzos[25], K. Karki[8], O. Karkout[116], S.N. Karpov[38], Z.M. Karpova[38], V. Kartvelishvili[91,152b], E. Kasimi[155], J. Katzy[47], S. Kaur[35], R. Kavak[37], K. Kawade[143], M.P. Kawale[121], C. Kawamoto[87], E.F. Kay[37], S. Kazakos[107], K. Kazakova[102], J.M. Keaveney[34a], R. Keeler[167], G.V. Kehris[60], J.S. Keller[35], J. M. Kelly[167], J.I. Kelsey[164], J.J. Kempster[149], O. Kepka[132], J. Kerr[159b], B.P. Kerridge[135], B.P. Kerševan[93], L. Keszeghova[29a], R. A. Khan[130], A. Khanov[122], M. Kholodenko[131a], T.J. Khoo[19], G. Khoriauli[168], Y. Khoulaki[36a], Y.A.R. Khwaira[128], D. Kim[6], D.W. Kim[18b], Y.K. Kim[39], N. Kimura[96], M.K. Kingston[54], F. Kirfel[25], J. Kirk[135], A.E. Kiryunin[110], S. Kita[156], O. Kivernyk[25], M. Klassen[37], C. Klein[35], L. Klein[168], M.H. Klein[44], U. Klein[92], A. Klimentov[30], P. Kluit[116], S. Kluth[110], E. Kneringer[78], T.M. Knight[158], A. Knue[48], M. Kobel[49], D. Kobylianskii[171], S.F. Koch[37], M. Kocian[146], P. Kodyš[134], D.M. Koeck[124], T. Koffas[35], K. Kojima[82], O. Kolay[49], I. Koletsou[4], T. Komarek[86], S. Kondo[156], K. Köneke[54], A.X.Y. Kong[1], T. Kono[119], N. Konstantinidis[96], P. Kontaxakis[55], B. Konya[98], R. Kopeliansky[41], S. Koperny[85a], R. Koppenhofer[53], I. Kopsalis[10], K. Korcyl[86], K. Kordas[155,ac], A. Korn[96], S. Korn[54], I. Korolkov[13], O. Kortner[110], S. Kortner[110], W.H. Kostecka[117], M. Kostov[29a], V.V. Kostyukhin[144], A. Kotsokechagia[37], A. Kotwal[50], A. Koulouris[37], A. Kourkoumeli-Charalampidi[72a,72b], O. Kovanda[124], R. Kowalewski[167], W. Kozanecki[124], G. Kramberger[93], P. Kramer[25], A. Krasznahorkay[103], A. C. Kraus[117], J.W. Kraus[173], J.A. Kremer[47], N. B. Krengel[144], T. Kresse[158], L. Kretschmann[173], J. Kretzschmar[92], P. Krieger[158], K. Krizka[21], K. Kroeninger[48], H. Kroha[110], J. Kroll[132], J. Kroll[129], K.S. Krowpman[107], U. Kruchonak[38], H. Krüger[25], N. Krumnack[79], J. Krupa[146], M.C. Kruse[50], O. Kuchinskaia[38], S. Kuday[3a], S. Kuehn[37], R. Kuesters[53], T. Kuhl[47],

JHEP10(2026)053

V. Kukhtin[38], Y. Kulchitsky[38], S. Kuleshov[138d,138b], J. Kull[1], E. V. Kumar[109], M. Kumar[34j], N. Kumari[47], P. Kumari[159b], A. Kupco[132], O. Kuprash[53], H. Kurashige[84], L.L. Kurchaninov[159a], O. Kurdysh[4], M. Kuze[139], A.K. Kvam[103], J. Kvita[123], N.G. Kyriacou[140], M. Laassiri[30], C. Lacasta[165], H. Lacker[19], D. Lacour[128], E. Ladygin[38], A. Lafarge[40], B. Laforge[128], T. Lagouri[174], F.Z. Lahbabi[36a], S. Lai[54], W. S. Lai[96], I.K. Lakomiec[54], J.E. Lambert[167], S. Lammers[67], W. Lampl[7], C. Lampoudis[155], G. Lamprinoudis[168], A.N. Lancaster[117], U. Landgraf[53], M.P.J. Landon[94], V.S. Lang[53], A.J. Lankford[162], F. Lanni[37], C. S. Lantz[164], K. Lantzsch[25], A. Lanza[72a], M. Lanzac Berrocal[165], T. Lari[70a], D. Larsen[17], L. Larson[11], F. Lasagni Manghi[24b], M. Lassnig[37], H.C. Lau[167], S.D. Lawlor[142], R. Lazaridou[162], M. Lazzaroni[70a,70b], E. T. T. Le[162], H. D. M. Le[107], E.M. Le Boulicaut[174], D.O. Le Guennec[136], L.T. Le Pottier[18a], B. Leban[24b,24a], F. Ledroit-Guillon[59], T.F. Lee[159b], L.L. Leeuw[34h], M. Lefebvre[167], C. Leggett[18a], L.M. Lehmann[116], W.A. Leight[103], W. Leinonen[115], A. Leisos[155,ad], M.A.L. Leite[81c], C.E. Leitgeb[19], R. Leitner[134], E. Lelak[134], K.J.C. Leney[44], T. Lenz[25], S. Leone[73a], C. Leonidopoulos[51], A. Leopold[147], J. LePage-Bourbonnais[35], R. Les[65], C.G. Lester[33], J. Levêque[4], L.J. Levinson[171], G. Levrini[24b,24a], M.P. Lewicki[86], C. Lewis[140], D.J. Lewis[4], L. Lewitt[142], A. Li[30], B. Li[113b], C-Q. Li[110], C. Li[106], H. Li[113b], H. Li[101], H. Li[15], H. Li[61], H. Li[113b], J. Li[141a], L. Li[141a], R. Li[174], S. Li[141b,141a], Y. Li[14], Z. Li[14,112c], Z. Li[61], S. Liang[14,112c], Z. Liang[14], M. Liberatore[136], B. Liberti[75a], G. B. Libotte[81d], K. Lie[63c], J. Lieber Marin[81e], H. Lien[67], H. Lin[106], S. F. Lin[148], L. Linden[109], R.E. Lindley[7], J.H. Lindon[37], J. Ling[60], E. Lipeles[129], A. Lipniacka[17], A. Lister[166], J.D. Little[67], B. Liu[113a], B.X. Liu[112b], D. Liu[153], D. Liu[137], E. H. L. Liu[21], H. Liu[112b], J.K.K. Liu[118], K. Liu[141b], K. Liu[141b], M. Liu[61], M.Y. Liu[61], P. Liu[113b], Q. Liu[146], S. Liu[148], X. Liu[113b], Y. Liu[112b,112c], Y. Liu[164], Y.L. Liu[113b], Y.W. Liu[61], Z. Liu[65,ae], S.L. Lloyd[94], E.M. Lobodzinska[47], P. Loch[7], E. Lodhi[158], K. Lohwasser[142], E. Loiacono[122], J. D. Lomas[21], I. Longarini[162], R. Longo[24b,24a,w], A. Lopez Solis[13], N.A. Lopez-canelas[7], N. Lorenzo Martinez[4], A.M. Lory[109], M. Losada[83b], G. Löschcke Centeno[4], X. Lou[14,112c], P.A. Love[91], H. Lu[14], M. Lu[65], S. Lu[129], Y.J. Lu[151], H.J. Lubatti[140], C. Luci[74a,74b], F.L. Lucio Alves[112a], J.A. Lue[124], F. Luehring[67], B. S. Lunday[129], O. Lundberg[147], J. Lunde[37], N.A. Luongo[6], M.S. Lutz[158], A.B. Lux[26], D. Lynn[30], R. Lysak[132], V. Lysenko[133], E. Lytken[98], V. Lyubushkin[38], T. Lyubushkina[38], M.M. Lyukova[148], H. Ma[30], K. Ma[61], L.L. Ma[113b], W. Ma[61], Y. Ma[113b], B. Maček[93], P.C. Machado De Abreu Farias[81e], D. Macina[37], R. Madar[40], T. Madula[96], J. Maeda[84], T. Maeno[30], P.T. Mafa[34f], G. Magni[65], H. Maguire[142], M. Maheshwari[33], V. Maiboroda[65], G. Maineri[70a,70b], A. Maio[131a,131b,131d], K. Maj[85a], O. Majersky[47], S. Majewski[124], A. Makita[156], N. Makovec[65], V. Maksimovic[16], B. Malaescu[128], J. Malamant[126], Pa. Malecki[86], F. Malek[59,af], M. Mali[93], D. Malito[95], A. Maloizel[5], A. Malvezzi Lopes[81d], S. Malyukov[38], J. Mamuzic[93], G. Mancini[52], M. N. Mancini[27], G. Manco[72a,72b], S.S. Mandarry[149], I. Mandić[93], L. Manhaes de Andrade Filho[81a], I.M. Maniatis[171], J. Manjarres Ramos[89], D.C. Mankad[171], A. Mann[109], T. Manoussos[100], M.N. Mantinan[39], S. Manzoni[37], L. Mao[141a], X. Mapekula[34c], A. Marantis[155], R.R. Marcelo Gregorio[1], G. Marchiori[5], C. Marcon[70a],

JHEP10(2026)053

E. Maricic[16], M. Marinescu[47], S. Marium[47], M. Marjanovic[121], A. Markhoos[53], M. Markovitch[65], M. K. Maroun[103], M. C. Marr[145], T. L. Marsault[136], G. T. Marsden[101], Z. Marshall[18a], S. Marti-Garcia[165], J. Martin[96], T.A. Martin[135], V.J. Martin[51], B. Martin dit Latour[17], S. Martin-Haugh[135], F. Martina[69a,69b], L. Martinelli[74a,74b], V.I. Martinez Outschoorn[103], P. Martinez Suarez[37], G. Martinovicova[134], V.S. Martoiu[28b], A. Martone[89], A.C. Martyniuk[96], A. Marzin[37], D. Mascione[77a,77b], L. Masetti[100], J. Masik[101], A.L. Maslennikov[38], S.L. Mason[41], P. Massarotti[71a,71b], P. Mastrandrea[73a,73b], A. Mastroberardino[43b,43a], R. Mastrofrancesco[72a,72b], T. Masubuchi[125], T.T. Mathew[124], J. Matousek[134], D.M. Mattern[48], K. Mauer[47], J. Maurer[28b], T. Maurin[58], C. Mavungu Tsava[102], A. E. May[101], E. Mayer[40], R. Mazini[34j], S.M. Mazza[137], E. Mazzeo[37], J.P. Mc Gowan[167], S.P. Mc Kee[106], C.C. McCracken[166], E.F. McDonald[105], L. F. Mcelhinney[91], J.A. Mcfayden[149], R.P. McGovern[167], R.P. Mckenzie[34j], D.J. Mclaughlin[96], S.J. McMahon[135], C.M. Mcpartland[92], R.A. McPherson[167,o], S. Mehlhase[109], A. Mehta[92], D. Melini[165], B.R. Mellado Garcia[14,ag], A.H. Melo[54], F. Meloni[47], A.M. Mendes Jacques Da Costa[101], L. Meng[91], S. Menke[110], M. Mentink[37], E. Meoni[43b,43a], G. Mercado[117], S. Merianos[155], C. Merlassino[68a,68c], C. Meroni[70a,70b], J. Metcalfe[6], A.S. Mete[6], E. Meuser[100], C. Meyer[67], J-P. Meyer[136], O. Mezhenska[29b], Y. Miao[112a], R.P. Middleton[135], M. Mihovilovic[65], L. Mijović[51], G. Mikenberg[171], M. Mikestikova[132], M. Mikuž[93], H. Mildner[100], A. Milic[37], D.W. Miller[39], E. H. Miller[146], A. Milov[171], D.A. Milstead[46a,46b], T. Min[112a], I.A. Minashvili[152b], A.I. Mincer[118], B. Mindur[85a], M. Mineev[38], L.M. Mir[13], M. Miralles Lopez[58], M. Mironova[18a], M. Missio[40], A. Mitra[169], V.A. Mitsou[165], P.S. Miyagawa[94], R. Mizuhiki[84], T. Mkrtchyan[37], M. Mlinarevic[96], T. Mlinarevic[96], M. Mlynarikova[134], L. Mlynarska[85a], C. Mo[141a], H. Möbius[47], S. Mobius[20], M. H. Mohamed Farook[114], S. Mohapatra[41], M.F. Mohd Soberi[51], S. Mohiuddin[122], G. Mokgatitswane[34j], R. Mole[21], L. Moleri[171], U. Molinatti[127], M. E. Mollerach[31], L.G. Mollier[20], L. Monaco[37,58], B. Mondal[132], S. Mondal[134], K. Mönig[47], E. Monnier[102], L. Monsonis Romero[165], A. Montella[46a,46b], M. Montella[120], F. Montereali[76a,76b], F. Monticelli[90], S. Monzani[68a,68c], M.E.E. Moors[25], A. Morancho Tarda[42], N. Morange[65], M. Moreno Llácer[165], C. Moreno Martinez[55], J.M. Moreno Perez[23b], P. Morettini[56b], S. Morgenstern[62a], M. Morii[60], M. Morinaga[156], F. Morodei[74a,74b], P. Moschovakos[37], B. Moser[53], M. Mosidze[152b], T. Moskalets[44], P. Moskvitina[115], C.J. Mosomane[34b], J. Moss[32], T. Motta Quirino[81d], A. Moussa[36d], Y. Moyal[171,ah], H. Moyano Gomez[13], E.J.W. Moyse[103], T.G. Mroz[86], S. Muanza[102], M. Mucha[25], J. Mueller[130], D. Muller[144], G.A. Mullier[163], A.J. Mullin[33], J.J. Mullin[50], A.C. Mullins[44], A.E. Mulski[60], D.P. Mungo[158], D. Munoz Perez[122], F.J. Munoz Sanchez[101], W.J. Murray[169,135], E. Musajan[61], M. Muškinja[93], C. Mwewa[47], A.J. Myers[8], G. Myers[106], M. Myska[133], B.P. Nachman[146], I.A. Nadas[28d], K. Nagai[127], K. Nagano[82], R. Nagasaka[156], J.L. Nagle[30,ai], E. Nagy[102], A.M. Nairz[37], T. Nakagawa[87], Y. Nakahama[82], K. Nakamura[82], A. Nandi[62b], H. Nanjo[125], E.A. Narayanan[44], Y. Narukawa[156], L. Nasella[70a,70b], S. Nasri[83c], C. Nass[25], G. Navarro[23a], A. Nayaz[19], S. Nechaeva[24b,24a], F. Nechansky[132], L. Nedic[127], A. Negri[72a,72b], M. Negrini[24b], C. Nellist[116], C. Nelson[104], K. Nelson[106], S. Nemecek[132], M. Nessi[37,e], M.S. Neubauer[164], J. Newell[92], P.R. Newman[21], Y.W.Y. Ng[164], B. Ngair[83b],

JHEP10(2026)053

H.D.N. Nguyen[108], J.D. Nichols[121], R. Nicolaidou[136], J. Nielsen[137], M. Niemeyer[54], J. Niermann[37], N. Nikiforou[37], I. Nikolic-Audit[128], P. Nilsson[30], G. Ninio[154], A. Nisati[74a], D. Nishimura[156], R. Nisius[110], N. Nitika[171], E.K. Nkadimeng[34b], T. Nobe[156], D. Noll[146], T. Nommensen[150], M.B. Norfolk[142], B.J. Norman[35], L.C. Nosler[18a], M. Noury[36a], J. Novak[93], T. Novak[93], P. Novotny[171], R. Novotny[133], L. Nozka[123], K. Ntekas[37], D. Ntounis[146], N.M.J. Nunes De Moura Junior[81b], A.P. O'Neill[20], J. Ocariz[128], I. Ochoa[131a], A. Odella Rodriguez[13], S. Oerdek[47], J.T. Offermann[39], A. Ogrodnik[86], A. Oh[101], C.C. Ohm[147], H. Oide[82], M.L. Ojeda[37], Y. Okumura[156], L.F. Oleiro Seabra[131a], I. Oleksiyuk[55], G. Oliveira Correa[13], D. Oliveira Damazio[30], J.L. Oliver[1], R. Omar[67], Y. Onoda[139], A. Onofre[131a,131e,aj], P.U.E. Onyisi[11], M.J. Oreglia[39], D. Orestano[76a,76b], R. Orlandini[76a,76b], R.S. Orr[158], L.M. Osojnak[41], Y. Osumi[111], G. Otero y Garzón[31], H. Otono[88], M. Ouchrif[36d], F. Ould-Saada[126], T. Ovsiannikova[140], M. Owen[58], R.E. Owen[135], S.A. Oyeniran[114], V.E. Ozcan[22a], F. Ozturk[86], N. Ozturk[8], S. Ozturk[80], H.A. Pacey[127], K. Pachal[159a], A. Pacheco Pages[13], C. Padilla Aranda[13], G. Padovano[74a,74b], S. Pagan Griso[18a], L. Pagani[75a,75b], J. Pampel[25], D.K. Panchal[11], C.E. Pandini[59], J.G. Panduro Vazquez[135], H.D. Pandya[1], H. Pang[136], P. Pani[47], G. Panizzo[68a,68c], L. Panwar[128,ak], L. Paolozzi[21], S. Parajuli[164], A. Paramonov[6], C. Paraskevopoulos[52], D. Paredes Hernandez[63b], S.R. Paredes Saenz[51], A. Pareti[72a,72b], K.R. Park[41], T.H. Park[110], F. Parodi[56b,56a], J.A. Parsons[41], J.A. Partridge[137], U. Parzefall[53], B.A. Paschen[18a], B. Pascual Dias[40], L. Pascual Dominguez[99], E. Pasqualucci[74a], S. Passaggio[56b], F. Pastore[95], P. Patel[86], U.M. Patel[50], J.R. Pater[101], T. Pauly[37], A. Paunovic[16], F. Pauwels[134], C.I. Pazos[161], M. Pedersen[126], R. Pedro[131a], O. Penc[132], C.C. Penelaud[128], S. Peng[15], G. D. Penn[174], B.S. Peralva[81d], A.P. Pereira Peixoto[140], L. Pereira Sanchez[146], D.V. Perepelitsa[30,ai], G. Perera[103], E. Perez Codina[37], M. Perganti[10], H. Pernegger[37], S. Perrella[74a,74b], K. Peters[47], R.F.Y. Peters[101], B.A. Petersen[37], T.C. Petersen[42], E. Petit[102], V. Petousis[133], A. R. Petri[70a,70b], V.A. Petrovic[96], T. Petru[134], M. Pettee[18a], A. Petukhov[80], K. Petukhova[37], R. Pezoa[138g], L. Pezzotti[24b,24a], G. Pezzullo[174], L. Pfaffenbichler[37], A. J. Pfleger[78], T. Pham[105], T.M. Pham[172], P.W. Phillips[135], G. Piacquadio[148], E. Pianori[18a], F. Piazza[124], R. Piegaia[31], D. Pietreanu[28b], A.D. Pilkington[101], T. Pilusa[34j], M. Pinamonti[68a,68c], J.L. Pinfold[2], G. Pinheiro Matos[41], B.C. Pinheiro Pereira[131a], J. Pinol Bel[13], A. E. Pinto Pinoargote[128], L. Pintucci[68a,68c], K. M. Piper[149], A. Pirttikoski[55], D.A. Pizzi[35], L. Pizzimento[63b], A. Plebani[33], M.-A. Pleier[30], V. Pleskot[134], E. Plotnikova[38], G. Poddar[94], R. Poettgen[98], L. Poggioli[128], S. Polacek[134], G. Polesello[72a], A. Poley[145], A. Polini[24b], C.S. Pollard[169], Z.B. Pollock[120], E. Pompa Pacchi[121], N. I. Pond[96], D. Ponomarenko[67], L. Pontecorvo[37], S. Popa[28a], G.A. Popeneciu[28d], A. Poreba[37], D.M. Portillo Quintero[159a], S. Pospisil[133], M. A. Postill[142], P. Postolache[28c], K. Potamianos[169], P.A. Potepa[85a], I.N. Potrap[38], C.J. Potter[33], H. Potti[150], J. Poveda[165], M.E. Pozo Astigarraga[37], R. Pozzi[37], A. Prades Ibanez[75a,75b], S.R. Pradhan[142], J. Preston[95], J. Pretel[167], D. Price[101], M. Primavera[69a], L. Primomo[68a,68c], M.A. Principe Martin[99], R. Privara[123], T. Procter[85b], M.L. Proffitt[140], N. Proklova[129], K. Prokofiev[63c], G. Proto[110], J. Proudfoot[6], M. Przybycien[85a], W.W. Przygoda[85b], A. Psallidas[45], D. Pudzha[52], P. Puhl[57],

JHEP10(2026)053

H. I. Purnell[1], D. Pyatiizbyantseva[115], J. Qian[106], R. Qian[107], D. Qichen[127], Y. Qin[13], T. Qiu[51], A. Quadt[54], M. Queitsch-Maitland[101], G. Quetant[55], R.P. Quinn[166], D. Rafanoharana[110], J.L. Rainbolt[39], S. Rajagopalan[30], E. Ramakoti[38], L. Rambelli[56b,56a], I.A. Ramirez-Berend[35], K. Ran[106,112c], S. D. Randles[92], D. S. Rankin[129], N.P. Rapheeha[34j], H. Rasheed[28b], A. Rastogi[18a], S. Rave[100], S. Ravera[56b,56a], B. Ravina[37], I. Ravinovich[171], M. Raymond[37], A.L. Read[126], N.P. Readioff[142], D.M. Rebuzzi[72a,72b], A. S. Reed[58], K. Reeves[27], D. Reikher[37], T. Reisch[55], A. Rej[48], H. Ren[61], M. Renda[28b], F. Renner[47], A.G. Rennie[58], M. Repik[55], A.L. Rescia[43b,43a], S. Resconi[70a], M. Ressegotti[56b], S. Rettie[116], W.F. Rettie[35], M. M. Revering[33], O.L. Rezanova[38], P. Reznicek[134], H. Riani[36d], N. Ribaric[37], B. Ricci[68a,68c], E. Ricci[77a,77b], R. Richter[110], E. Richter-Was[85b], M. Ridel[128], S. Ridouani[36d], P. Riedler[37], E.M. Riefel[46a,46b], J. O. Rieger[116], M. Rimoldi[34c], L. Rinaldi[24b,24a], P. Rincke[163,54], G. Ripellino[163], I. Riu[13], J.C. Rivera Vergara[167], F. Rizatdinova[122], E. Rizvi[94], B.R. Roberts[39], S.S. Roberts[137], D. Robinson[33], A. Robson[58], A. Rocchi[75a,75b], C. Roda[73a,73b], F.A. Rodriguez[117], S. Rodriguez Bosca[37], Y. Rodriguez Garcia[23a], A.M. Rodríguez Vera[117], S. Roe[37], J.T. Roemer[37], O. Røhne[126], R.A. Rojas[37], Z. Rokavec[93], C.P.A. Roland[128], A. Romaniouk[78], E. Romano[72a,72b], M. Romano[24b], N. Rompotis[92], L. Roos[128], S. Rosati[74a], L. Roscher[47], B.J. Rosser[39], E. Rossi[127], E. Rossi[71a,71b], L.P. Rossi[60], L. Rossini[53], R. Rosten[120], M. Rotaru[28b], R. Roth[37], F. A. Rothen[55], D. Rousseau[65], D. Rousso[47], S. Roy-Garand[55], A. Rozanov[102], Z. M. A. Rozario[58], Y. Rozen[153], A. Rubio Jimenez[165], V.H. Ruelas Rivera[19], T.A. Ruggeri[1], A. Ruggiero[127], A. Ruiz-Martinez[165], A. Rummler[37], G.B. Rupnik Boero[37], N.A. Rusakovich[38], S. Ruscelli[48], H.L. Russell[167], G. Russo[137], J.P. Rutherfoord[7], S. Rutherford Colmenares[118], M. Rybar[134], P. Rybczynski[85a], A. Ryzhov[44], M. A. E. Saadawy[44], F. Safai Tehrani[74a], S. Saha[1], B. Sahoo[171], B. T. Saifuddin[121], M. Saimpert[136], I. Sainz Saenz Diez[62a], G.T. Saito[81c], M. Saito[156], T. Saito[156], A. Sala[70a,70b], O. T. Salin[65], A. Salnikov[146], J. Salt[165], A. Salvador Salas[154], F. Salvatore[149], A. Salzburger[37], D. Sammel[53], E. Sampson[91], D. Sampsonidis[155,ac], D. Sampsonidou[124], M.A.A. Samy[58], J. Sánchez[165], H. Sandaker[126], C.O. Sander[47], J.A. Sandesara[172], M. Sandhoff[173], C. Sandoval[23b], L. Sanfilippo[62a], D.P.C. Sankey[135], T. Sano[87], A. Sansar[22c], A. Sansoni[52], M. Santana Queiroz[18b], L. Santi[37], C. Santoni[40], G. Santoro[43b,43a], H. Santos[131a,131b], L. Santos Pereira Trigo[47], E. Sanzani[24b,24a], K.A. Saoucha[83d], J.G. Saraiva[131a,131d], J. Sardain[7], S. Sarkar[50], O. Sasaki[82], K. Sato[160], C. Sauer[37], E. Sauvan[4], P. Savard[158,t], M. Savic[164], R. Sawada[156], C. Sawyer[135], L. Sawyer[97], A. M. Sayed[27], C. Sbarra[24b], A. Sbrizzi[24b,24a], R. Scaglioni[72a,72b], T. Scanlon[96], J. Schaarschmidt[140], U. Schäfer[100], A.C. Schaffer[65,44], D. Schaile[109], R.D. Schamberger[148], C. Scharf[19], M.M. Schefer[20], D. Scheirich[134], M. Schernau[138f], C. Scheulen[55], C. Schiavi[56b,56a], M. Schioppa[43b,43a], S. Schlenker[37], T. Schlomer[54], J. Schmeing[173], C. R. Schmidt[49], E. Schmidt[110], M. A. Schmidt[173], K. Schmieden[25], C. Schmitt[100], N. Schmitt[100], S. Schmitt[47], N.A. Schneider[109], L. Schoeffel[136], A. Schoening[62b], P.G. Scholer[35], E. Schopf[144], M. Schott[25], S. Schramm[55], T. Schroer[55], H-C. Schultz-Coulon[62a], M. Schumacher[53], B.A. Schumm[137], Ph. Schune[136], H.R. Schwartz[7], A. Schwartzman[146], T.A. Schwarz[106], Ph. Schwemling[136],

JHEP10(2026)053

R. Schwienhorst[107], F.G. Sciacca[20], A. Sciandra[30], G. Sciolla[27], S. A. Scoville[130], F. Scuri[73a], C.D. Sebastiani[37], K. Sedlaczek[117], A. Sehrawat[138b], S.C. Seidel[114], B.D. Seidlitz[41], C. Seitz[47], J.M. Seixas[81b], G. Sekhniaidze[71a], L. Selem[128], N. Semprini-Cesari[24b,24a], A. Semushin[175], V. Senthilkumar[116], L. Serin[65], M. Sessa[71a,71b], H. Severini[121], F. Sforza[56b,56a], A. Sfyrla[55], Q. Sha[14], H. Shaddix[117], A.H. Shah[33], R. Shaheen[147], J.D. Shahinian[129], M. Shamim[37], L.Y. Shan[14], M. Shapiro[18a], A. Sharma[37], A.S. Sharma[166], P. Sharma[30], K. Shaw[149], S.M. Shaw[101], D. Shemyakin[171], Q. Shen[14], D.J. Sheppard[145], P. Sherwood[96], L. Shi[112b], X. Shi[14], E.B. Shields[171], S. Shimizu[82], S. Shirabe[88], M. Shiyakova[38,al], M.J. Shochet[39], D.R. Shope[126], S. Shrestha[120,am], I. Shreyber[38], M.J. Shroff[104], P. Sicho[132], A.M. Sickles[164], E. Sideras Haddad[34j], A. C. Sidley[116], A. Sidoti[24b], F. Siegert[49], Dj. Sijacki[16], F. Sili[61], J.M. Silva[51], I. Silva Ferreira[81b], M.V. Silva Oliveira[30], S.B. Silverstein[46a], S. Simion[65], R. Simoniello[37], E.L. Simpson[101], H. Simpson[149], L.R. Simpson[6], S. Simsek[80], S. Singh[30], S. N. Singh[27], S. Sinha[47], S. Sinha[101], M. Sioli[24b,24a], K. Sioulas[9], E. Sitnikova[47], J. Sjölin[46a,46b], A. Skaf[54], E. Skorda[21], P. Skubic[121], M. Slawinska[86], I. Slazyk[17], I. Sliusar[126], V. Smakhtin[171], B.H. Smart[135], S.Yu. Smirnov[138b], Y. Smirnov[34c], O. Smirnova[98], J.L. Smith[101], M. B. Smith[35], R. Smith[146], H. Smitmanns[100], M. Smizanska[91], K. Smolek[133], P. Smolyanskiy[133], A.A. Snesarev[38], H.L. Snoek[116], R. M. Snyder[50], S. Snyder[30], R. Sobie[167,o], A. Soffer[154], C.A. Solans Sanchez[37], E.Yu. Soldatov[38], U. Soldevila[165], A.A. Solodkov[34j], S. Solomon[27], A. Soloshenko[38], O.V. Solovyanov[40], P. Sommer[49], A. Sopczak[133], A.L. Sopio[51], F. Sopkova[29b], J. D. Sorenson[114], I.R. Sotarriva Alvarez[139], V. Sothilingam[62a], O. J. Soto Sandoval[138c,138b], S. Sottocornola[67], R. Soualah[83a], D. South[47], N. Soybelman[171], S. Spagnolo[69a,69b], A.S. Spellman[124], D. Sperlich[53], B. Spisso[71a,71b], L. Splendori[102], M. Spousta[134], E.J. Staats[35], R. Stamen[62a], E. Stanecka[86], W. Stanek-Maslouska[47], M.V. Stange[49], B. Stanislaus[18a], M.M. Stanitzki[47], G.H. Stark[137], J. Stark[89], P. Staroba[132], P. Starovoitov[83d], R. Staszewski[86], C. Stauch[109], G. Stavropoulos[45], A. Stefl[37], A. Stein[100], P. Steinberg[30], B. Stelzer[145,159a], H.J. Stelzer[130], O. Stelzer[159a], H. Stenzel[57], T.J. Stevenson[149], G.A. Stewart[47], G. Stoicea[28b], M. Stolarski[131a], S. Stonjek[110], A. Straessner[49], J. Strandberg[147], S. Strandberg[46a,46b], M. Stratmann[173], M. Strauss[121], T. Strebler[102], P. Strizenec[29b], R. Ströhmer[168], D.M. Strom[124], R. Stroynowski[44], A. Strubig[46a,46b], S.A. Stucci[30], B. Stugu[17], J. Stupak[121], N.A. Styles[47], D. Su[146], S. Su[61], X. Su[61], D. Suchy[29a], A. D. Sudhakar Ponnu[54], L. Sudit[171], Y. Sue[82], K. Sugizaki[129], D.M.S. Sultan[127], L. Sultanaliyeva[25], S. Sultansoy[3b], S. Sun[172], W. Sun[14], S. Sundar Raman[166], N. Sur[98], J.P. Surdutovich[120], N. Suri Jr[174], M.R. Sutton[149], M. Svatos[132], P. N. Swallow[33], S.N. Swatman[37], M. Swiatlowski[159a], A. Swoboda[37], I. Sykora[29a], M. Sykora[134], T. Sykora[134], D. Ta[100], K. Tackmann[47,an], A. Taffard[162], R. Tafirout[159a], Y. Takubo[82], M. Talby[102], N.M. Tamir[154], A. Tanaka[156], J. Tanaka[156], R. Tanaka[65], M. Tanasini[148], Z. Tao[166], S. Tapia Araya[138g], S. Tapprogge[100], A. Tarek Abouelfadl Mohamed[37], S. Tarem[153], K. Tariq[14], G. Tarna[37], G.F. Tartarelli[70a], M. J. Tartarin[141b], P. Tas[134], M. Tasevsky[132], E. Tassi[43b,43a], A.C. Tate[164], Y. Tayalati[36e,ao], G.N. Taylor[105], W. Taylor[159b], R.J. Taylor Vara[165], A.S. Tegetmeier[89], P. Teixeira-Dias[95], J.J. Teoh[158],

JHEP10(2026)053

K. Terashi[156], J. Terron[99], S. Terzo[13], M. Testa[52], R.J. Teuscher[158,o], A. Thaler[78], T. Theveneaux-Pelzer[102], J.P. Thomas[21], E.A. Thompson[18a], P.D. Thompson[21], E. Thomson[129], R. E. Thornberry[30], T.M. Thory-Rao[21], C.N. Thotamuna Wijewardhana[148], C. Tian[61], Y. Tian[55], V. Tikhomirov[80], Yu.A. Tikhonov[38], D. Timoshyn[134], E.X.L. Ting[1], P. Tipton[174], A. Tishelman-Charny[30], K. Todome[139], S. Todorova-Nova[134], L. Toffolin[68a,68c], M. Togawa[82], J. Tojo[88], S. Tokár[29a], O. Toldaiev[67], A. J. Toler[103], G. Tolkachev[102], M. Tomoto[82], L. Tompkins[146], E. Torrence[124], H. Torres[89], D. I. Torres Arza[138g], E. Torres Reoyo[165], E. Torró Pastor[165], M. Toscani[31], C. Tosciri[39], M. Tost[11], D.R. Tovey[142], T. Trefzger[168], P.M. Tricarico[13], A. Tricoli[30], I.M. Trigger[159a], S. Trincaz-Duvoid[128], D.A. Trischuk[167], A. Tropina[38], D. Truncali[75a,75b], L. Truong[34c], M. Trzebinski[86], A. Trzupek[86], F. Tsai[148], A. Tsiamis[155], P.V. Tsiareshka[38], S. Tsigaridas[159a], A. Tsirigotis[155,ad], V. Tsiskaridze[152a], E.G. Tskhadadze[152a], H. F. Tsoi[129], Y. Tsujikawa[87], V. Tsulaia[18a], K. Tsuri[119], D. Tsybychev[148], Y. Tu[63b], A. Tudorache[28b], V. Tudorache[28b], S. B. Tuncay[127], S. Turchikhin[56b,56a], I. Turk Cakir[3a], R. Turra[70a], T. Turtuvshin[38,ap], P.M. Tuts[41], Y. Uematsu[82], F. Ukegawa[160], P.A. Ulloa Poblete[138c,138b], G. Unal[37], A. Undrus[30], J. Urban[29b], P. Urrejola[138e], G. Usai[8], R. Ushioda[157], M. Usman[108], F. Ustuner[51], Z. Uysal[80], V. Vacek[133], B. Vachon[104], A. Vaitkus[96], C. Valderanis[109], E. Valdes Santurio[46a,46b], M. Valente[37], S. Valentinetti[24b,24a], A. Valero[165], E. Valiente Moreno[165], S. Valjee[94], A. Vallier[89], J.A. Valls Ferrer[165], D. R. Van Arneman[116], R. Van Den Broucke[128], A. Van Der Graaf[48], H. Z. Van Der Schyf[34j], P. Van Gemmeren[6], M. Van Rijnbach[37], S. Van Stroud[96], I. Van Vulpen[116], P. Vana[134], M. Vanadia[75a,75b], U. M. Vande Voorde[147], W. Vandelli[37], E.R. Vandewall[146], D. Vannicola[154], R. Vari[74a], M. Varma[174], E.W. Varnes[7], C. Varni[85a], D. Varouchas[65], L. Varriale[165], K.E. Varvell[150], M.E. Vasile[28b], A. Vasileiadou[9], L. Vaslin[82], M. D. Vassilev[146], A. Vasyukov[38], L. M. Vaughan[122], R. Vavricka[134], T. Vazquez Schroeder[13], J. Veatch[32], V. Vecchio[101], M.J. Veen[103], I. Veliscek[30], I. Velkovska[93], L.M. Veloce[158], F. Veloso[131a,131c], A.G. Veltman[51], S.H. Venetianer[161], S. Veneziano[74a], A. Ventura[69a,69b], A. Verbytskyi[110], M. Verducci[73a,73b], C. Vergis[94], M. Verissimo De Araujo[81b], W. Verkerke[116], J.C. Vermeulen[116], C. Vernieri[146], M. Vessella[162], M.C. Vetterli[145,t], A. Vgenopoulos[100], N. Viaux Maira[138g,aq], L. Vicenik[133], T. Vickey[142], O.E. Vickey Boeriu[142], G.H.A. Viehhauser[127], L. Vigani[62b], M. Vigl[110], M. Villa[24b,24a], M. Villaplana Perez[165], E.M. Villhauer[39], E. Vilucchi[52], M. Vincent[165], M.G. Vincter[35], A. Visibile[116], A. Visive[116], C. Vittori[24b,24a], I. Vivarelli[24b,24a], M.I. Vivas Albornoz[47], E. Voevodina[110], F. Vogel[109], J.C. Voigt[49], P. Vokac[133], Yu. Volkotrub[85b], L. Vomberg[25], E. Von Toerne[25], B. Vormwald[37], K. Vorobev[50], M. Vos[165], K. Voss[144], M. Vozak[37], L. Vozdecky[121], N. Vranjes[16], M. Vranjes Milosavljevic[16], M. Vreeswijk[116], N.K. Vu[112a], R. Vuillermet[37], I. Vukotic[39], I. K. Vyas[35], J.F. Wack[33], A. Wada[111], S. Wada[160], C. Wagner[146], J.M. Wagner[18a], W. Wagner[173], S. Wahdan[173], H. Wahlberg[90], C. H. Waits[121], J. Walder[135], R. Walker[109], K. Walkingshaw Pass[58], W. Walkowiak[144], A. Wall[129], E.J. Wallin[98], T. Wamorkar[146], K. Wandall-Christensen[165], A. Wang[61], A.Z. Wang[137], C. Wang[47], C. Wang[11], H. Wang[18a], J. Wang[63c], P. Wang[101], P. Wang[96], R. Wang[60], R. Wang[106], R. Wang[6], S. Wang[14,ar], S.M. Wang[151],

JHEP10(2026)053

T. Wang[115], T. Wang[61], W. Wang[113c], W.T. Wang[127], X. Wang[164], X. Wang[141a], X. Wang[47], Y. Wang[148], Y. Wang[114], Z. Wang[14], Z. Wang[63b], C. Wanotayaroj[82], A. Warburton[104], A.L. Warnerbring[144], S. Waterhouse[96], A.T. Watson[21], H. Watson[51], M.F. Watson[21], E. Watton[37], G. Watts[140], B.M. Waugh[96], J. M. Webb[53], C. Weber[30], M.S. Weber[20], C. Wei[61], Y. Wei[53], A.R. Weidberg[127], E.J. Weik[118], J. Weingarten[48], C. Weiser[53], C.J. Wells[47], P.S. Wells[37], T. Wenaus[30], T. Wengler[37], N.S. Wenke[110], N. Wermes[25], D. Werner[47], M. Wessels[62a], A.M. Wharton[91], A. White[8], A.S. White[37], M.J. White[1], D. Whiteson[162], W. Wiedenmann[172], M. Wielers[135], R. Wierda[147], C. Wiglesworth[42], H.G. Wilkens[37], J. J. H. Wilkinson[33], S. Williams[33], S. Willocq[103], D.J. Wilson[101], P.J. Windischhofer[39], F.I. Winkel[31], F. Winklmeier[124], B.T. Winter[53], M. Wittgen[146], M. Wobisch[97], T. Wojtkowski[59], Z. Wolffs[116], J. Wollrath[37], M.W. Wolter[86], H. Wolters[131a,131c], M.C. Wong[137], E.L. Woodward[41], S.D. Worm[47], B.K. Wosiek[86], K. A. Wozniak[55], K.W. Woźniak[86], S. Wozniewski[54], K. Wraight[58], C. Wu[158], J. Wu[156], M. Wu[112b], M. Wu[115], S. Wu[14,ar], S.L. Wu[172], X. Wu[61], Y. Wu[61], Y.Q. Wu[158], Z. Wu[102], Z. Wu[112a], J. Wuerzinger[110], T.R. Wyatt[101], B.M. Wynne[51], S. Xella[42], L. Xia[112a], M. Xie[61], A. Xiong[124], I. Xiotidis[37], D. Xu[14], H. Xu[61], L. Xu[61], R. Xu[129], T. Xu[106], W. Xu[112a], Y. Xu[140], Z. Xu[51], R. Xue[130], B. Yabsley[150], S. Yacoob[11], Y. Yamaguchi[82], E. Yamashita[156], H. Yamauchi[160], T. Yamazaki[18a], Y. Yamazaki[84], F. Yan[2], S. Yan[58], Z. Yan[103], C. Yang[18a], H.J. Yang[141a], H.T. Yang[61], S. Yang[61], X. Yang[37], X. Yang[14], Y. Yang[156], Y. Yang[61], W-M. Yao[18a], C. L. Yardley[149], J. Ye[14], S. Ye[30], X. Ye[106], I. Yeletskikh[38], B. Yeo[18b], M.R. Yexley[96], T. P. Yildirim[127], K. Yorita[156], C. Young[146], C.J.S. Young[37], I.N.L. Young[58], N.D. Young[124], D. Yu[141b,5], Y. Yu[61], J. Yuan[14,112c,ar], M. Yuan[106], R. Yuan[141b], L. Yue[96], M. Zaazoua[61], B. Zabinski[86], I. Zahir[36a], Q.U.A. Zahoor[51], A. Zaio[56b,56a], Z.K. Zak[86], T. Zakareishvili[165], S. Zambito[55], J. Zang[156], R. Zanzottera[70a,70b], O. Zaplatilek[133], I. Zatocilova[53], E. Zaya[147], C. Zeitnitz[173], H. Zeng[14], D.T. Zenger Jr[27], T. Ženiš[29a], S. Zenz[94], W. Zhan[61], B. Zhang[169], D.F. Zhang[142], G. Zhang[14,ar], J. Zhang[113b], J. Zhang[6], L. Zhang[61], L. Zhang[112a], P. Zhang[14,112c], R. Zhang[112a], S. Zhang[14], Y. Zhang[140], Y. Zhang[96], Y. Zhang[61], Y. Zhang[112a], Z. Zhang[149], Z. Zhang[101], Z. Zhang[18a], Z. Zhang[113b], Z. Zhang[65], H. Zhao[140], T. Zhao[113b], Y. Zhao[35], Z. Zhao[61], Z. Zhao[61], A. Zhemchugov[38], J. Zheng[112a], K. Zheng[164], L. Zheng[113b], X. Zheng[61], Z. Zheng[146], D. Zhong[164], B. Zhou[106], B. Zhou[141b,141a], N. Zhou[141a], Y. Zhou[15], Y. Zhou[112a], Y. Zhou[7], Z. Zhou[61], J. Zhu[106], X. Zhu[141b], Y. Zhu[141a], X. Zhuang[14], K. Zhukov[67], P. Ziakas[4], N.I. Zimine[38], J. Zinsser[62b], M. Ziolkowski[144], L. Živković[16], A. Zoccoli[24b,24a], K. Zoch[37], A. Zografos[37], T.G. Zorbas[142], L. Zwalinski[37]

[1] *Department of Physics, University of Adelaide, Adelaide, Australia*
[2] *Department of Physics, University of Alberta, Edmonton AB, Canada*
[3a] *Department of Physics, Ankara University, Ankara, Türkiye*
[3b] *Division of Physics, TOBB University of Economics and Technology, Ankara, Türkiye*
[4] *LAPP, Université Savoie Mont Blanc, CNRS/IN2P3, Annecy, France*
[5] *APC, Université Paris Cité, CNRS/IN2P3, Paris, France*
[6] *High Energy Physics Division, Argonne National Laboratory, Argonne IL, U.S.A.*
[7] *Department of Physics, University of Arizona, Tucson AZ, U.S.A.*
[8] *Department of Physics, University of Texas at Arlington, Arlington TX, U.S.A.*

JHEP10(2026)053

[9] Physics Department, National and Kapodistrian University of Athens, Athens, Greece
[10] Physics Department, National Technical University of Athens, Zografou, Greece
[11] Department of Physics, University of Texas at Austin, Austin TX, U.S.A.
[12] Institute of Physics, Azerbaijan Academy of Sciences, Baku, Azerbaijan
[13] Institut de Física d'Altes Energies (IFAE), Barcelona Institute of Science and Technology, Barcelona, Spain
[14] Institute of High Energy Physics, Chinese Academy of Sciences, Beijing, China
[15] Physics Department, Tsinghua University, Beijing, China
[16] Institute of Physics, University of Belgrade, Belgrade, Serbia
[17] Department for Physics and Technology, University of Bergen, Bergen, Norway
[18a] Physics Division, Lawrence Berkeley National Laboratory, Berkeley CA, U.S.A.
[18b] University of California, Berkeley CA, U.S.A.
[19] Institut für Physik, Humboldt Universität zu Berlin, Berlin, Germany
[20] Albert Einstein Center for Fundamental Physics and Laboratory for High Energy Physics, University of Bern, Bern, Switzerland
[21] School of Physics and Astronomy, University of Birmingham, Birmingham, U.K.
[22a] Department of Physics, Bogazici University, Istanbul, Türkiye
[22b] Department of Physics Engineering, Gaziantep University, Gaziantep, Türkiye
[22c] Department of Physics, Istanbul University, Istanbul, Türkiye
[23a] Facultad de Ciencias y Centro de Investigaciónes, Universidad Antonio Nariño, Bogotá, Colombia
[23b] Departamento de Física, Universidad Nacional de Colombia, Bogotá, Colombia
[24a] Dipartimento di Fisica e Astronomia A. Righi, Università di Bologna, Bologna, Italy
[24b] INFN Sezione di Bologna, Italy
[25] Physikalisches Institut, Universität Bonn, Bonn, Germany
[26] Department of Physics, Boston University, Boston MA, U.S.A.
[27] Department of Physics, Brandeis University, Waltham MA, U.S.A.
[28a] Transilvania University of Brasov, Brasov, Romania
[28b] Horia Hulubei National Institute of Physics and Nuclear Engineering, Bucharest, Romania
[28c] Department of Physics, Alexandru Ioan Cuza University of Iasi, Iasi, Romania
[28d] National Institute for Research and Development of Isotopic and Molecular Technologies, Physics Department, Cluj-Napoca, Romania
[28e] National University of Science and Technology Politechnica, Bucharest, Romania
[28f] West University in Timisoara, Timisoara, Romania
[28g] Faculty of Physics, University of Bucharest, Bucharest, Romania
[29a] Faculty of Mathematics, Physics and Informatics, Comenius University, Bratislava, Slovak Republic
[29b] Department of Subnuclear Physics, Institute of Experimental Physics of the Slovak Academy of Sciences, Kosice, Slovak Republic
[30] Physics Department, Brookhaven National Laboratory, Upton NY, U.S.A.
[31] Universidad de Buenos Aires, Facultad de Ciencias Exactas y Naturales, Departamento de Física, y CONICET, Instituto de Física de Buenos Aires (IFIBA), Buenos Aires, Argentina
[32] California State University, CA, U.S.A.
[33] Cavendish Laboratory, University of Cambridge, Cambridge, U.K.
[34a] Department of Physics, University of Cape Town, Cape Town, South Africa
[34b] iThemba Labs, Western Cape, South Africa
[34c] Department of Mechanical Engineering Science, University of Johannesburg, Johannesburg, South Africa
[34d] National Institute of Physics, University of the Philippines Diliman (Philippines), Philippines
[34e] Department of Physics, Stellenbosch University, Matieland, South Africa
[34f] University of KwaZulu-Natal, School of Agriculture and Science, Mathematics, Westville, South Africa
[34g] University of South Africa, Department of Physics, Pretoria, South Africa
[34h] University of Pretoria, Department of Mechanical and Aeronautical Engineering, Pretoria, South Africa
[34i] University of Zululand, KwaDlangezwa, South Africa
[34j] School of Physics, University of the Witwatersrand, Johannesburg, South Africa
[35] Department of Physics, Carleton University, Ottawa ON, Canada

JHEP10(2026)053

[36a] Faculté des Sciences Ain Chock, Université Hassan II de Casablanca, Morocco
[36b] Faculté des Sciences, Université Ibn-Tofail, Kénitra, Morocco
[36c] Faculté des Sciences Semlalia, Université Cadi Ayyad, LPHEA-Marrakech, Morocco
[36d] LPMR, Faculté des Sciences, Université Mohamed Premier, Oujda, Morocco
[36e] Faculté des sciences, Université Mohammed V, Rabat, Morocco
[36f] Institute of Applied Physics, Mohammed VI Polytechnic University, Ben Guerir, Morocco
[37] CERN, Geneva, Switzerland
[38] Affiliated with an international laboratory covered by a cooperation agreement with CERN
[39] Enrico Fermi Institute, University of Chicago, Chicago IL, U.S.A.
[40] LPC, Université Clermont Auvergne, CNRS/IN2P3, Clermont-Ferrand, France
[41] Nevis Laboratory, Columbia University, Irvington NY, U.S.A.
[42] Niels Bohr Institute, University of Copenhagen, Copenhagen, Denmark
[43a] Dipartimento di Fisica, Università della Calabria, Rende, Italy
[43b] INFN Gruppo Collegato di Cosenza, Laboratori Nazionali di Frascati, Italy
[44] Physics Department, Southern Methodist University, Dallas TX, U.S.A.
[45] National Centre for Scientific Research "Demokritos", Agia Paraskevi, Greece
[46a] Department of Physics, Stockholm University, Sweden
[46b] Oskar Klein Centre, Stockholm, Sweden
[47] Deutsches Elektronen-Synchrotron DESY, Hamburg and Zeuthen, Germany
[48] Fakultät Physik, Technische Universität Dortmund, Dortmund, Germany
[49] Institut für Kern- und Teilchenphysik, Technische Universität Dresden, Dresden, Germany
[50] Department of Physics, Duke University, Durham NC, U.S.A.
[51] SUPA — School of Physics and Astronomy, University of Edinburgh, Edinburgh, U.K.
[52] INFN e Laboratori Nazionali di Frascati, Frascati, Italy
[53] Physikalisches Institut, Albert-Ludwigs-Universität Freiburg, Freiburg, Germany
[54] II. Physikalisches Institut, Georg-August-Universität Göttingen, Göttingen, Germany
[55] Département de Physique Nucléaire et Corpusculaire, Université de Genève, Genève, Switzerland
[56a] Dipartimento di Fisica, Università di Genova, Genova, Italy
[56b] INFN Sezione di Genova, Italy
[57] II. Physikalisches Institut, Justus-Liebig-Universität Giessen, Giessen, Germany
[58] SUPA — School of Physics and Astronomy, University of Glasgow, Glasgow, U.K.
[59] LPSC, Université Grenoble Alpes, CNRS/IN2P3, Grenoble INP, Grenoble, France
[60] Laboratory for Particle Physics and Cosmology, Harvard University, Cambridge MA, U.S.A.
[61] Department of Modern Physics and State Key Laboratory of Particle Detection and Electronics, University of Science and Technology of China, Hefei, China
[62a] Kirchhoff-Institut für Physik, Ruprecht-Karls-Universität Heidelberg, Heidelberg, Germany
[62b] Physikalisches Institut, Ruprecht-Karls-Universität Heidelberg, Heidelberg, Germany
[63a] Department of Physics, Chinese University of Hong Kong, Shatin, N.T., Hong Kong, China
[63b] Department of Physics, University of Hong Kong, Hong Kong, China
[63c] Department of Physics and Institute for Advanced Study, Hong Kong University of Science and Technology, Clear Water Bay, Kowloon, Hong Kong, China
[64] Department of Physics, National Tsing Hua University, Hsinchu, Taiwan
[65] IJCLab, Université Paris-Saclay, CNRS/IN2P3, 91405, Orsay, France
[66] Centro Nacional de Microelectrónica (IMB-CNM-CSIC), Barcelona, Spain
[67] Department of Physics, Indiana University, Bloomington IN, U.S.A.
[68a] INFN Gruppo Collegato di Udine, Sezione di Trieste, Udine, Italy
[68b] ICTP, Trieste, Italy
[68c] Dipartimento Politecnico di Ingegneria e Architettura, Università di Udine, Udine, Italy
[69a] INFN Sezione di Lecce, Italy
[69b] Dipartimento di Matematica e Fisica, Università del Salento, Lecce, Italy
[70a] INFN Sezione di Milano, Italy
[70b] Dipartimento di Fisica, Università di Milano, Milano, Italy
[71a] INFN Sezione di Napoli, Italy

JHEP10(2026)053

[71b] *Dipartimento di Fisica, Università di Napoli, Napoli, Italy*
[72a] *INFN Sezione di Pavia, Italy*
[72b] *Dipartimento di Fisica, Università di Pavia, Pavia, Italy*
[73a] *INFN Sezione di Pisa, Italy*
[73b] *Dipartimento di Fisica E. Fermi, Università di Pisa, Pisa, Italy*
[74a] *INFN Sezione di Roma, Italy*
[74b] *Dipartimento di Fisica, Sapienza Università di Roma, Roma, Italy*
[75a] *INFN Sezione di Roma Tor Vergata, Italy*
[75b] *Dipartimento di Fisica, Università di Roma Tor Vergata, Roma, Italy*
[76a] *INFN Sezione di Roma Tre, Italy*
[76b] *Dipartimento di Matematica e Fisica, Università Roma Tre, Roma, Italy*
[77a] *INFN-TIFPA, Italy*
[77b] *Università degli Studi di Trento, Trento, Italy*
[78] *Universität Innsbruck, Department of Astro and Particle Physics, Innsbruck, Austria*
[79] *Department of Physics and Astronomy, Iowa State University, Ames IA, U.S.A.*
[80] *Istinye University, Sariyer, Istanbul, Türkiye*
[81a] *Departamento de Engenharia Elétrica, Universidade Federal de Juiz de Fora (UFJF), Juiz de Fora, Brazil*
[81b] *Universidade Federal do Rio De Janeiro COPPE/EE/IF, Rio de Janeiro, Brazil*
[81c] *Instituto de Física, Universidade de São Paulo, São Paulo, Brazil*
[81d] *Rio de Janeiro State University, Rio de Janeiro, Brazil*
[81e] *Federal University of Bahia, Bahia, Brazil*
[82] *KEK, High Energy Accelerator Research Organization, Tsukuba, Japan*
[83a] *Khalifa University of Science and Technology, Abu Dhabi, United Arab Emirates*
[83b] *New York University Abu Dhabi, Abu Dhabi, United Arab Emirates*
[83c] *United Arab Emirates University, Al Ain, United Arab Emirates*
[83d] *University of Sharjah, Sharjah, United Arab Emirates*
[84] *Graduate School of Science, Kobe University, Kobe, Japan*
[85a] *AGH University of Krakow, Faculty of Physics and Applied Computer Science, Krakow, Poland*
[85b] *Marian Smoluchowski Institute of Physics, Jagiellonian University, Krakow, Poland*
[86] *Institute of Nuclear Physics Polish Academy of Sciences, Krakow, Poland*
[87] *Faculty of Science, Kyoto University, Kyoto, Japan*
[88] *Research Center for Advanced Particle Physics and Department of Physics, Kyushu University, Fukuoka, Japan*
[89] *L2IT, Université de Toulouse, CNRS/IN2P3, UPS, Toulouse, France*
[90] *Instituto de Física La Plata, Universidad Nacional de La Plata and CONICET, La Plata, Argentina*
[91] *Physics Department, Lancaster University, Lancaster, U.K.*
[92] *Oliver Lodge Laboratory, University of Liverpool, Liverpool, U.K.*
[93] *Department of Experimental Particle Physics, Jožef Stefan Institute and Department of Physics, University of Ljubljana, Ljubljana, Slovenia*
[94] *Department of Physics and Astronomy, Queen Mary University of London, London, U.K.*
[95] *Department of Physics, Royal Holloway University of London, Egham, U.K.*
[96] *Department of Physics and Astronomy, University College London, London, U.K.*
[97] *Louisiana Tech University, Ruston LA, U.S.A.*
[98] *Fysiska institutionen, Lunds universitet, Lund, Sweden*
[99] *Departamento de Física Teorica C-15 and CIAFF, Universidad Autónoma de Madrid, Madrid, Spain*
[100] *Institut für Physik, Universität Mainz, Mainz, Germany*
[101] *School of Physics and Astronomy, University of Manchester, Manchester, U.K.*
[102] *CPPM, Aix-Marseille Université, CNRS/IN2P3, Marseille, France*
[103] *Department of Physics, University of Massachusetts, Amherst MA, U.S.A.*
[104] *Department of Physics, McGill University, Montreal QC, Canada*
[105] *School of Physics, University of Melbourne, Victoria, Australia*
[106] *Department of Physics, University of Michigan, Ann Arbor MI, U.S.A.*
[107] *Department of Physics and Astronomy, Michigan State University, East Lansing MI, U.S.A.*

JHEP10(2026)053

[108] Group of Particle Physics, University of Montreal, Montreal QC, Canada
[109] Fakultät für Physik, Ludwig-Maximilians-Universität München, München, Germany
[110] Max-Planck-Institut für Physik (Werner-Heisenberg-Institut), München, Germany
[111] Graduate School of Science and Kobayashi-Maskawa Institute, Nagoya University, Nagoya, Japan
[112a] Department of Physics, Nanjing University, Nanjing, China
[112b] School of Science, Shenzhen Campus of Sun Yat-sen University, China
[112c] University of Chinese Academy of Science (UCAS), Beijing, China
[113a] School of Physics, Nankai University, Tianjin, China
[113b] Institute of Frontier and Interdisciplinary Science and Key Laboratory of Particle Physics and Particle Irradiation (MOE), Shandong University, Qingdao, China
[113c] School of Physics, Zhengzhou University, China
[114] Department of Physics and Astronomy, University of New Mexico, Albuquerque NM, U.S.A.
[115] Institute for Mathematics, Astrophysics and Particle Physics, Radboud University/Nikhef, Nijmegen, Netherlands
[116] Nikhef National Institute for Subatomic Physics and University of Amsterdam, Amsterdam, Netherlands
[117] Department of Physics, Northern Illinois University, DeKalb IL, U.S.A.
[118] Department of Physics, New York University, New York NY, U.S.A.
[119] Ochanomizu University, Otsuka, Bunkyo-ku, Tokyo, Japan
[120] Ohio State University, Columbus OH, U.S.A.
[121] Homer L. Dodge Department of Physics and Astronomy, University of Oklahoma, Norman OK, U.S.A.
[122] Department of Physics, Oklahoma State University, Stillwater OK, U.S.A.
[123] Palacký University, Joint Laboratory of Optics, Olomouc, Czech Republic
[124] Institute for Fundamental Science, University of Oregon, Eugene, OR, U.S.A.
[125] Graduate School of Science, University of Osaka, Osaka, Japan
[126] Department of Physics, University of Oslo, Oslo, Norway
[127] Department of Physics, Oxford University, Oxford, U.K.
[128] LPNHE, Sorbonne Université, Université Paris Cité, CNRS/IN2P3, Paris, France
[129] Department of Physics, University of Pennsylvania, Philadelphia PA, U.S.A.
[130] Department of Physics and Astronomy, University of Pittsburgh, Pittsburgh PA, U.S.A.
[131a] Laboratório de Instrumentação e Física Experimental de Partículas — LIP, Lisboa, Portugal
[131b] Departamento de Física, Faculdade de Ciências, Universidade de Lisboa, Lisboa, Portugal
[131c] Departamento de Física, Universidade de Coimbra, Coimbra, Portugal
[131d] Centro de Física Nuclear da Universidade de Lisboa, Lisboa, Portugal
[131e] Departamento de Física, Escola de Ciências, Universidade do Minho, Braga, Portugal
[131f] Departamento de Física Teórica y del Cosmos, Universidad de Granada, Granada (Spain), Spain
[131g] Departamento de Física, Instituto Superior Técnico, Universidade de Lisboa, Lisboa, Portugal
[132] Institute of Physics of the Czech Academy of Sciences, Prague, Czech Republic
[133] Czech Technical University in Prague, Prague, Czech Republic
[134] Charles University, Faculty of Mathematics and Physics, Prague, Czech Republic
[135] Particle Physics Department, Rutherford Appleton Laboratory, Didcot, U.K.
[136] IRFU, CEA, Université Paris-Saclay, Gif-sur-Yvette, France
[137] Santa Cruz Institute for Particle Physics, University of California Santa Cruz, Santa Cruz CA, U.S.A.
[138a] Departamento de Física, Pontificia Universidad Católica de Chile, Santiago, Chile
[138b] Millennium Institute for Subatomic physics at high energy frontier (SAPHIR), Santiago, Chile
[138c] Instituto de Investigación Multidisciplinario en Ciencia y Tecnología, y Departamento de Física, Universidad de La Serena, Chile
[138d] Universidad Andres Bello, Department of Physics, Santiago, Chile
[138e] Universidad San Sebastian, Recoleta, Chile
[138f] Instituto de Alta Investigación, Universidad de Tarapacá, Arica, Chile
[138g] Departamento de Física, Universidad Técnica Federico Santa María, Valparaíso, Chile
[139] Department of Physics, Institute of Science, Tokyo, Japan
[140] Department of Physics, University of Washington, Seattle WA, U.S.A.

JHEP10(2026)053

[141a] State Key Laboratory of Dark Matter Physics, School of Physics and Astronomy, Shanghai Jiao Tong University, Key Laboratory for Particle Astrophysics and Cosmology (MOE), SKLPPC, Shanghai, China
[141b] State Key Laboratory of Dark Matter Physics, Tsung-Dao Lee Institute, Shanghai Jiao Tong University, Shanghai, China
[142] Department of Physics and Astronomy, University of Sheffield, Sheffield, U.K.
[143] Department of Physics, Shinshu University, Nagano, Japan
[144] Department Physik, Universität Siegen, Siegen, Germany
[145] Department of Physics, Simon Fraser University, Burnaby BC, Canada
[146] SLAC National Accelerator Laboratory, Stanford CA, U.S.A.
[147] Department of Physics, Royal Institute of Technology, Stockholm, Sweden
[148] Departments of Physics and Astronomy, Stony Brook University, Stony Brook NY, U.S.A.
[149] Department of Physics and Astronomy, University of Sussex, Brighton, U.K.
[150] School of Physics, University of Sydney, Sydney, Australia
[151] Institute of Physics, Academia Sinica, Taipei, Taiwan
[152a] E. Andronikashvili Institute of Physics, Iv. Javakhishvili Tbilisi State University, Tbilisi, Georgia
[152b] High Energy Physics Institute, Tbilisi State University, Tbilisi, Georgia
[152c] University of Georgia, Tbilisi, Georgia
[153] Department of Physics, Technion, Israel Institute of Technology, Haifa, Israel
[154] Raymond and Beverly Sackler School of Physics and Astronomy, Tel Aviv University, Tel Aviv, Israel
[155] Department of Physics, Aristotle University of Thessaloniki, Thessaloniki, Greece
[156] International Center for Elementary Particle Physics and Department of Physics, University of Tokyo, Tokyo, Japan
[157] Graduate School of Science and Technology, Tokyo Metropolitan University, Tokyo, Japan
[158] Department of Physics, University of Toronto, Toronto ON, Canada
[159a] TRIUMF, Vancouver BC, Canada
[159b] Department of Physics and Astronomy, York University, Toronto ON, Canada
[160] Division of Physics and Tomonaga Center for the History of the Universe, Faculty of Pure and Applied Sciences, University of Tsukuba, Tsukuba, Japan
[161] Department of Physics and Astronomy, Tufts University, Medford MA, U.S.A.
[162] Department of Physics and Astronomy, University of California Irvine, Irvine CA, U.S.A.
[163] Department of Physics and Astronomy, University of Uppsala, Uppsala, Sweden
[164] Department of Physics, University of Illinois, Urbana IL, U.S.A.
[165] Instituto de Física Corpuscular (IFIC), Centro Mixto Universidad de Valencia — CSIC, Valencia, Spain
[166] Department of Physics, University of British Columbia, Vancouver BC, Canada
[167] Department of Physics and Astronomy, University of Victoria, Victoria BC, Canada
[168] Fakultät für Physik und Astronomie, Julius-Maximilians-Universität Würzburg, Würzburg, Germany
[169] Department of Physics, University of Warwick, Coventry, U.K.
[170] Waseda University, Tokyo, Japan
[171] Department of Particle Physics and Astrophysics, Weizmann Institute of Science, Rehovot, Israel
[172] Department of Physics, University of Wisconsin, Madison WI, U.S.A.
[173] Fakultät für Mathematik und Naturwissenschaften, Fachgruppe Physik, Bergische Universität Wuppertal, Wuppertal, Germany
[174] Department of Physics, Yale University, New Haven CT, U.S.A.
[175] Yerevan Physics Institute, Yerevan, Armenia

[a] Also at Department of Physics, King's College London, London, U.K.
[b] Also at Institute of Physics, Azerbaijan Academy of Sciences, Baku, Azerbaijan
[c] Also at Imam Mohammad Ibn Saud Islamic University, Saudi Arabia
[d] Also at Department of Physics, University of Thessaly, Greece
[e] Also at Département de Physique Nucléaire et Corpusculaire, Université de Genève, Genève, Switzerland
[f] Also at An-Najah National University, Nablus, Palestine
[g] Also at Department of Physics, University of Fribourg, Fribourg, Switzerland
[h] Also at Department of Physics, Westmont College, Santa Barbara, U.S.A.

JHEP10(2026)053

[i] Also at Departament de Fisica de la Universitat Autonoma de Barcelona, Barcelona, Spain
[j] Also at University of Siena, Italy
[k] Also at Affiliated with an institute formerly covered by a cooperation agreement with CERN
[l] Also at The Collaborative Innovation Center of Quantum Matter (CICQM), Beijing, China
[m] Also at Faculty of Physics, Sofia University, 'St. Kliment Ohridski', Sofia, Bulgaria
[n] Also at Università di Napoli Parthenope, Napoli, Italy
[o] Also at Institute of Particle Physics (IPP), Canada
[p] Also at Department of Physics, Bolu Abant Izzet Baysal University, Bolu, Türkiye
[q] Also at Faculty of Physics, University of Bucharest, Romania
[r] Also at Borough of Manhattan Community College, City University of New York, New York NY, U.S.A.
[s] Also at National Institute of Physics, University of the Philippines Diliman (Philippines), Philippines
[t] Also at TRIUMF, Vancouver BC, Canada
[u] Also at Universita degli Studi Link, Italy
[v] Also at Department of Financial and Management Engineering, University of the Aegean, Chios, Greece
[w] Also at University and INFN Torino, Torino, Italy
[x] Also at Institucio Catalana de Recerca i Estudis Avancats, ICREA, Barcelona, Spain
[y] Also at Henan University, China
[z] Also at Yeditepe University, Physics Department, Istanbul, Türkiye
[aa] Also at Institute of Theoretical Physics, Ilia State University, Tbilisi, Georgia
[ab] Also at CERN, Geneva, Switzerland
[ac] Also at Center for Interdisciplinary Research and Innovation (CIRI-AUTH), Thessaloniki, Greece
[ad] Also at Hellenic Open University, Patras, Greece
[ae] Also at Department of Modern Physics and State Key Laboratory of Particle Detection and Electronics, University of Science and Technology of China, Hefei, China
[af] Also at Department of Physics, Stellenbosch University, South Africa
[ag] Also at School of Physics, University of the Witwatersrand, Johannesburg, South Africa
[ah] Also at Department of Physics, Ben Gurion University of the Negev, Beer Sheva, Israel
[ai] Also at University of Colorado Boulder, Department of Physics, Colorado, U.S.A.
[aj] Also at Centre of Physics of the Universities of Minho and Porto (CF-UM-UP), Portugal
[ak] Also at Indian Institute of Technology (IIT), Jodhpur, India
[al] Also at Institute for Nuclear Research and Nuclear Energy (INRNE) of the Bulgarian Academy of Sciences, Sofia, Bulgaria
[am] Also at Washington College, Chestertown, MD, U.S.A.
[an] Also at Institut für Experimentalphysik, Universität Hamburg, Hamburg, Germany
[ao] Also at Institute of Applied Physics, Mohammed VI Polytechnic University, Ben Guerir, Morocco
[ap] Also at Institute of Physics and Technology, Mongolian Academy of Sciences, Ulaanbaatar, Mongolia
[aq] Also at Millennium Institute for Subatomic physics at high energy frontier (SAPHIR), Santiago, Chile
[ar] Also at University of Chinese Academy of Sciences (UCAS), Beijing, China
[†] Deceased

JHEP10(2026)053